From the Department of Microbiology, Tumor and Cell Biology
Karolinska Institutet, Stockholm, Sweden

RESPONSIVE NANOSTRUCTURED MATERIALS FOR BIOANALYTE DETECTION AND TRIGGERED ANTIMICROBIAL THERAPY

Padryk Merkl

Karolinska Institutet

Stockholm 2022

All previously published papers were reproduced with permission from the publisher.
Published by Karolinska Institutet
Printed by Universitetsservice US-AB, 2022

Typeset by the author using LaTeX

ISBN 978-91-8016-603-4
Cover illustration: artistic rendition by Padryk Merkl of a flame-made nanoaggregate with illustrations to represent photothermal and photoluminescent properties.

RESPONSIVE NANOSTRUCTURED MATERIALS FOR BIOANALYTE DETECTION AND TRIGGERED ANTIMICROBIAL THERAPY

THESIS FOR DOCTORAL DEGREE (Ph.D.)

By

Padryk Merkl

This thesis will be defended in public in Cesar lecture hall, Berzelius väg 3, 17165 Stockholm, Friday the 20th of May 2022 starting at 09:00.

Principal supervisor:
Dr. Georgios A. Sotiriou, Principal Researcher
Karolinska Institutet
Department of Microbiology, Tumor and Cell Biology

Co-supervisor:
Professor Birgitta Henriques-Normark
Karolinska Institutet
Department of Microbiology, Tumor and Cell Biology

Opponent:
Professor Nicole Pamme
Stockholm University
Department of Materials and Environmental Chemistry

Examination board:
Docent Maria Messing
Lund University
Department of Solid State Physics

Professor Andreas Dahlin
Chalmers University of Technology
Department of Chemistry and Chemical Engineering

Professor Daniel Aili
Linköping University
Department of Physics Chemistry and Biology

Popular Science Summary of the Thesis

In order to treat a disease, the crucial first step is to determine what the disease is. In the modern age, many different diseases are known and specific treatments for them available, so information on exactly what is present in the patient's body and the impact of the disease on bodily functions is critically important. If you try and treat one disease with another disease's cure it can have serious consequences. At a research level using model systems to understand exactly what is happening in the human body can give us important insights into what the disease is doing and potentially open up new treatments. This first paragraph essentially provides the motivation for the projects covered by the "bioanalyte detection" in the title.

Although we now have so many different ways to treat diseases we are also becoming more aware of areas where our treatments are lacking or where problems are emerging with existing treatments. These problems can be a loss of efficacy or due to side effects causing unwanted consequences alongside their desired effect. One cause for such problems can be that although the treatment might achieve the target effect it is "always-on", so it circulates around the body and attacks the patient's healthy processes. Another problem can occur if the treatment is at levels insufficient to outright kill the disease or other potentially disease-causing bystanders and so can allow these elements to "train" themselves against the treatment. This process can, over time, lead to the treatment becoming less effective or even ineffective. A potential solution to this is to only apply the therapy when and where it is needed. Such that it can be activated by a local signal and therefore apply its effect at a defined time and place. This describes the approach and motivation for the project covered by "triggered antimicrobial therapy" in the title.

Lastly, we come to the technology which is applied here to achieve these effects. The field of nanotechnology describes the use of structures on the same length scale as proteins and viruses. They thereby lie somewhere in between the realm of atoms and molecules and the larger-scale structures of cells which make up our bodies. This size allows them to not only navigate within our bodies but also to interact with smaller entities such as molecules and proteins around them in a sensitive manner. They can also have unique properties due to their size, this can be due to interactions between particles which are not found in larger-scale structures or due to interactions within a particle and its environment. These aspects can be applied to design novel and effective treatments and detection strategies. This potential of nanotechnology explains the desire to apply "responsive nanostructured materials", as the title puts it, to develop new systems.

Over the course of this thesis, I will be describing my work applying nanotechnology to develop a treatment which can be switched on and off by light in Paper I and in order to sense biologically relevant analytes (Paper II, Paper III, Paper IV). In Paper I an easily produced surface is developed which can convert light of a tissue transparent colour into heat. This means that the light can be applied through thin tissue layers and is less damaging to tissues than other colours. The local temperature increase produced is applied to kill bacteria which are growing in a biofilm structure which is typically challenging to treat with antibiotics. In this biofilm structure, bacteria are bound together and to a surface by sticky molecular ropes. This glue-like structure brings the bacteria into a tight community and is the reason why bacteria are difficult to treat as a biofilm. But the surface developed in Paper I was nonetheless able to kill the bacteria in a lab setting. Paper II concerns the development of a pH-responsive surface which can be "read" by light. Bacteria are grown on the surface again in the challenging biofilm structure but in this project, the intention was to understand the area between the biofilm and the surface that it grows on. The surface we developed measures changes in acidity caused by the growth of bacteria in this biofilm structure.

In Paper III we continued the development of a sensor for the detection of the molecule hydrogen peroxide. This same molecule can be found in some household cleaning bleaches but it is also found at much lower levels in the human body. The sensor uses light to detect hydrogen peroxide levels produced by both bacteria and human cells as a way to communicate and defend against other "foreign" cells. In this paper, we take this developed sensor further and improve its robustness so that it can find application in a more complex medium and broaden its applicability. Finally, Paper IV is a manuscript describing the development of a colour-change based sensor for the detection of ammonia. Ammonia is also found in the human body at very low levels. The body has intricate systems to control ammonia levels and keep them within healthy ranges, if these systems fail the increase in ammonia can be hard to notice (no clear symptoms) and be potentially fatal. So in Paper IV work is described developing an easy to produce sensor with the aim to improve access to blood ammonia measurements.

Abstract

Inorganic nanomaterials are attractive candidates for biomedicine as they can offer unique material properties and good stability while also offering the benefits of high-throughput synthetic techniques such as flame spray pyrolysis. In this thesis, work will be presented describing novel inorganic nanoparticle systems for biomedical applications. The works is presented in four papers of which three are published in peer-reviewed scientific journals.

The first project in Paper I presents a surface treatment to address biofilm formation, which is thought to be the major cause of implant-associated infections. A near-infrared (near-IR) activated plasmonic nanoparticle system with photothermal properties is developed which utilises the inter-particle coupling of spherical silver nanoparticles. This inter-particle coupling produces a strong plasmonic extinction with a wavelength dependence on the spacing between neighbouring spherical silver nanoparticles. Therefore by using a silica dielectric spacer to control the average spacing between spherical silver nanoparticles in the synthesised nanoaggregates the optical and photothermal behaviour of the nanoaggregates can be tuned into the near-IR. The effectiveness of these nanoaggregates for the photothermal eradication of biofilms formed on catheter mimicking surfaces was evaluated. Nanoaggregates were directly deposited onto silicone substrates and entirely encased in a second layer of silicone. Biofilms of *Escherichia coli* and *Staphylococcus aureus* were grown on the silicone surface and near-IR light was used to activate the photothermal response of the nanoaggregates with complete eradication of biofilms achieved in a temperature-dependent manner.

Application of nanomaterials to biofilms was further continued in Paper II, a characteristic of biofilms is their dense nature as they are embedded in a glue-like self-produced extracellular matrix which also attaches them to the substrate on which they grow. This can promote the formation of heterogeneous microenvironments, with concentration gradients of parameters such as oxygen, nutrients and pH readily occurring between the substrate-attached interface and the liquid in which they are grown. An understanding of the pH of these interfacial microenvironments and a high-throughput compatible measurement system is desirable to help guide the development of targeted anti-biofilm systems. In Paper II a novel all-inorganic system based on calcium phosphate nanoparticles doped with europium is presented which displays pH-dependent luminescence as a deposited film. The growth of bacterial biofilms of different species on these nanoparticle coatings allows the measurement of the acidic microenvironments which they produce in an ordinary well-plate luminescence spectrometer.

Bacterial bioanalyte detection can be challenging due to the complex growth media which bacteria may require and the dynamic changes to the optical properties of the medium as the bacteria grow. Moreover, the developed detection mechanism should be resistant to bacterial degradation, therefore the development of robust sensors for such applications is essential. In Paper III the development of a dual-emission ratiometric luminescence sensor for the detection of hydrogen peroxide from bacterial cultures is described. The sensing system consists of a reference emission from Y_2O_3:Tb^{3+} nanoparticles which are decorated with CeO_2:Eu^{3+} nanoparticles providing the hydrogen peroxide sensitive emission. This system was applied for the determination of hydrogen peroxide production levels by the known hydrogen peroxide producing bacterium and major human pathogen *Streptococcus pneumoniae*.

Finally the manuscript Paper IV applies inorganic nanomaterials for the detection of ammonia (here used to refer to total NH_3 and NH_4^+ levels) which is an important diagnostic bioanalyte. Ammonia production by urease producing gut bacteria is a major contributor to blood ammonia levels and must be effectively detoxified by the liver for excretion by the kidneys. Overproduction of ammonia or failure of the liver or kidney can lead to high levels of ammonia which are neurotoxic. However, the symptoms of this hyperammonemia are diffuse ranging from mild confusion to coma and death. Therefore a readily available system for the measurement of ammonia levels is highly desirable. In Paper IV a plasmonic silver nanoparticle-based system is described for the detection of ammonia. The system relies on the reactivity of the ClO^- with both ammonia and silver nanoparticles. If no ammonia is present upon addition of ClO^- to the silver nanoparticles a strong decrease in their plasmonic colour is observed. However, in the presence of ammonia, the ClO^- is removed and therefore no colour change is observed. This system was able to detect ammonia levels around the 50 µM limit defined as hyperammonemia.

Scientific papers included in the thesis

I. **Padryk Merkl**, Shuzhi Zhou, Apostolos Zaganiaris, Mariam Shahata, Athina Eleftheraki, Thomas Thersleff and Georgios A. Sotiriou
Plasmonic coupling in silver nanoparticle aggregates and their polymer composite films for near-infrared photothermal biofilm eradication
ACS Applied Nano Materials 2021; 4; 5330-5339

II. **Padryk Merkl**, Marie-Stéphanie Aschtgen, Birgitta Henriques-Normark and Georgios A. Sotiriou
Biofilm interfacial acidity evaluation by pH-responsive luminescent nanoparticle films
Biosensors and Bioelectronics 2021; 171; 112732

III. Dorian Henning,**Padryk Merkl**, Changhun Yun, Federico Iovino, Ling Xie, Eleftherios Mouzourakis, Constantinos Moularas, Yiannis Deligiannakis, Birgitta Henriques-Normark, Klaus Leifer and Georgios A. Sotiriou
Luminescent CeO_2:Eu^{3+} nanocrystals for robust in situ H_2O_2 real-time detection in bacterial cell cultures
Biosensors and Bioelectronics 2019; 132; 286-293

IV. **Padryk Merkl** and Georgios A. Sotiriou
Ammonia sensing by silver nanoparticles for point of care diagnostic applications
Manuscript

Other scientific papers

- Federico Iovino, **Padryk Merkl**, Anastasia Spyrogianni, Birgitta Henriques-Normark and Georgios A. Sotiriou
  Silica-coated phosphorescent nanoprobes for selective cell targeting and dynamic bioimaging of pathogen–host cell interactions
  Chemical Communications 2020; 56; 6989-6992

- Vasiliki Tsikourkitoudi, Jens Karlsson, **Padryk Merkl**, Edmund Loh, Birgitta Henriques-Normark and Georgios A. Sotiriou
  Flame-made calcium phosphate nanoparticles with high drug loading for delivery of biologics
  Molecules 2020; 25; 1747

- Karthik Subramanian, Federico Iovino, Vasiliki Tsikourkitoudi, **Padryk Merkl**, Sultan Ahmed, Samuel B. Berry, Marie-Stéphanie Aschtgen, Mattias Svensson, Peter Bergman, Georgios A. Sotiriou and Birgitta Henriques-Normark
  Mannose receptor-derived peptides neutralize pore-forming toxins and reduce inflammation and development of pneumococcal disease
  EMBO Molecular Medicine 2020; 12; el2695

- **Padryk Merkl**, Siwen Long, Gerald M. McInerney and Georgios A. Sotiriou
  Antiviral activity of silver, copper oxide and zinc oxide nanoparticle coatings against SARS-CoV-2
  Nanomaterials 2021; 11; 1312

- Nele J. Hempel, **Padryk Merkl**, Shno Asad, Matthias M. Knopp, Ragna Berthelsen, Christel A.S. Bergström, Alexandra Teleki, Georgios A. Sotiriou and Korbinian Löbmann
  Utilizing laser activation of photothermal plasmonic nanoparticles to induce on-demand drug amorphization inside a tablet
  Molecular Pharmaceutics 2021; 18; 2254-2262

- Nele J. Hempel, **Padryk Merkl**, Matthias M. Knopp, Ragna Berthelsen, Alexandra Teleki, Georgios A. Sotiriou and Korbinian Löbmann
  The influence of drug–polymer solubility on laser-induced in situ drug amorphization using photothermal plasmonic nanoparticles
  Pharmaceutics 2021; 13; 917
- Nele J. Hempel, **Padryk Merkl**, Matthias M. Knopp, Ragna Berthelsen, Alexandra Teleki, Anders K. Hansen, Georgios A. Sotiriou and Korbinian Löbmann
  The Effect of the molecular weight of polyvinylpyrrolidone and the model drug on laser-induced in situ amorphization
  Molecular Pharmaceutics 2021; 26; 4035

Contents

List of abbreviations

BET	Brunauer-Emmet-Teller
CFU	colony forming units
DLS	dynamic light scattering
DNA	deoxyribonucleic acid
eDNA	extracellular DNA
EDS	energy dispersive X-ray scattering
EELS	electron energy loss spectroscopy
EPS	extracellular polymeric substance
EPR	electron paramagnetic resonance spectroscopy
EU	European Union
FSP	flame spray pyrolysis
FTIR	Fourier transform infrared
HMDSO	hexamethyldisiloxane
IR	infrared
MRI	magnetic resonance imaging
OD600	optical density at 600 nm
PDMS	polydimethylsiloxane
SEM	scanning electron microscopy
SPIONS	superparamagnetic iron oxide nanoparticles
STEM	scanning transmission electron microscopy
TEM	transmission electron microscopy
UV	ultraviolet
XPS	X-ray photoelectron spectroscopy
XRD	X-ray diffraction

1 Introduction

Nanostructured materials are present in everyday life across a wide range of applications, from consumer cosmetics to paints and tyres.[1] Over the past years, potential medical and biomedical uses of inorganic nanoscale materials have shown promise with applications as diagnostic sensors, research tools and therapeutic agents.[2,3] The advantages which such structures exhibit arise due to their size, typically from 1-100 nm, which allows them to have unique material properties such as, high sensitivity to their surroundings, high loading of drugs and access to challenging biological targets.[4] The size of the nanostructure can give rise to behaviours not found in bulk materials of the same composition such as plasmon resonances which give rise to intense colours useful for sensing and therapeutics.[5] Moreover, in comparison to a single solid object, if a given mass is distributed across many tiny objects the surface area will be much larger. This surface area is important for the sensitivity of inorganic nanostructures for diagnostics, their intrinsic application as therapeutics and their loading capacity as these processes typically occur at the interface between the inorganic particle and the medium it is in. Lastly their size, charge and potential for targeting modifications can allow them to pass through biological barriers to access challenging therapeutic or diagnostic sites.[6] This allows nanotechnology to provide new approaches to help tackle difficult medical challenges.[3,7,8]

One such medical challenge is bacterial infections which account for a significant number of hospitalised patients. Even in cases where the initial cause of hospitalisation was not bacterial infection, subsequent nosocomial infection is frequent.[9] As the occurrence of such infections being caused by resistant or multi-resistant bacterial strains increases the challenge of successfully treating them becomes ever greater.[10] One form of bacterial growth with properties allowing it to exhibit high antibiotic tolerance is the biofilm. This form of growth is characterised by bacterial adhesion to a surface as a microcolony and encapsulation in a self-produced extracellular matrix.[11] Due partly to the dense nature of the bacterial growth and protective properties of the extracellular polymeric substance, these structures typically exhibit higher antibiotic

tolerance compared with free-floating, planktonic bacteria. The close-packing of bacteria also enables easy transfer of genetic information between bacteria and therefore the frequency of exchange of antibiotic resistance can also be higher.[12] From a diagnostic perspective, these infections can be difficult to diagnose and identify accurately as the bacteria are highly localised and therefore a sample taken at an easily accessible site, such as a blood sample, may not reveal the infection.[13] Biofilms are thought to account for the majority of human bacterial infections and are especially frequent on implant surfaces.[14] These abiotic interfaces can allow bacterial biofilms to grow and thereafter disseminate throughout the body. Due to the difficulty in treatment and diagnosis such infections are often only identified by implant failure and subsequent removal of the implant can be required for effective treatment.[15]

Owing to to this limited selection of existing treatments for bacterial infections, there is a clear need for novel strategies to prevent or eliminate bacterial biofilms on implant surfaces. In order to tackle this problem surface modification of implants has been explored. In this approach the fundamental aim is to modify the surface of the implant such that the biofilm cannot begin to form or is eradicated without the need for invasive intervention.[12] This can be achieved for instance by applying a topographic effect by nanopatterning or by modification of the surface with an antimicrobial agent thereby disfavouring the initial attachment of bacteria to the surface, which is an important first step in biofilm formation.[16] Alternative strategies include the development of surfaces which respond to the generation of a characteristic biofilm microenvironment by releasing an antimicrobial agent, thereby providing an automated triggered antimicrobial delivery system to eradicate biofilms in the early stages of their formation. Techniques to target formed biofilms include the development of molecules or nanocarriers which are designed to degrade and/or penetrate the bacterial biofilm and effectively deliver an antimicrobial agent into the established biofilm.[17] Alternatively, more physical or mechanical means have been developed, in these systems aspects such as pressure through ultrasound waves or temperature by photothermal therapy are exploited to locally induce an environment capable of disrupting or eradicating the biofilm.[18] Photothermal therapy is an attractive prospect due to the entirely non-contact nature of the treatment and the potential for *in situ* implementation. Many complex geometric nanostructures with excellent photothermal properties have been developed.[19] However, a key challenge of photothermal therapy for bacterial biofilm removal is the realisation of efficient photothermal agents which can also be easily applied to an implant surface and translated to larger-scale production. Therefore synthetically simple and flexible approaches are critical as will be further explored in this thesis and in Paper I.

An additional strategy discussed previously is triggered antimicrobial delivery. Due to the dense nature of biofilms and their surface attachment, there can be large gradients of substances such as nutrients, water, oxygen, pH and toxic compounds or ions within the biofilm. By leveraging an understanding of exactly what local microenvironment a biofilm forms on a device close to the device-biofilm interface a surface can be designed to spontaneously react to the formation of this characteristic microenvironment and release an antimicrobial cargo.[17] The most popular trigger for such surfaces is the low pH which some bacterial biofilms can form under certain conditions at their surface-attached interface. However, a prerequisite for the design of such surfaces is a good understanding of the relevant local pH, this has been measured using techniques such as electrochemistry, and fluorescent dyes in conjunction with confocal fluorescence microscopy.[20,21] The invasive nature of microelectrodes used for electrochemical pH determination and the specialised equipment and low throughput of confocal fluorescence microscopy present some disadvantages. An alternative strategy for measurement of the interfacial biofilm pH microenvironment will be further explored here and is presented in Paper II.

The detection of bacterial bioanalytes from bacteria growing in a planktonic state can also be valuable. *Streptoccocus pnuemoniae* is a gram-positive bacterium and a significant human pathogen which can infect the upper respiratory tract. Like many bacteria, *S. pneumoniae* has evolved key mechanisms which allow it to both evade the host immune response and combat other bacterial species with which it may be competing.[22] One such mechanism of *S. pneumoniae* is the production and release of hydrogen peroxide into its environment.[23] Aside from bacterial hydrogen peroxide production the ability to accurately determine hydrogen peroxide levels is attractive for enzymatic assays which frequently apply detection of hydrogen peroxide for final analyte quantification. Moreover, hydrogen peroxide is produced by the human immune response as a signalling method to promote inflammation and combat foreign cells.[24] Therefore the development of sensors capable of accurately quantifying hydrogen peroxide levels from the complex environments used to culture cells is highly desirable. In Paper III work describing the further development of a luminescent hydrogen peroxide sensor to improve its capacity to operate in relevant biological settings will be described.

Bioanalyte detection can also be critical from a broader patient health perspective, to give the clinical staff the best understanding of patient condition and aid in diagnosis. While for some bioanalytes the range of acceptable values can be relatively large, other bioanalytes can cause serious consequences even at low levels and must be tightly

regulated in a healthy body. This is true for ammonia, used here and throughout the thesis to refer to total ammonia including non-ionic NH_3 and ionic NH_4^+, which in a healthy human must be kept below 50 µM.[25] Due to the toxicity of ammonia, there has been intense interest in developing ammonia sensors, these can make use of a number of properties such as the pH, electrochemistry and reactivity of ammonia.[26] Due to the size and charge of ammonia, selectivity in sensors is often attained by the use of a barrier or membrane with relatively high permeability to ammonia.[27] An alternative common strategy is to exploit the volatile nature of the non-ionic NH_3 form to drive the sample ammonia into the gas phase and subsequently perform detection.[28] Ammonia detection can also be performed by chemical reaction, whereby the ammonia reacts with specifically designed reagents to provide a coloured product, allowing colorimetric ammonia detection.[29] Typically these detection strategies require well-equipped clinical laboratories and specialised staff to perform them forming an obstacle to their application in resource-limited point-of-care settings. The development of a paper-based low-cost ammonia sensor is presented here and in Paper IV.

Critical to all nanomaterials enabled strategies is their synthesis. Such procedures can be broadly classified into "bottom-up" processes such as crystallisation and "top-down" as in lithography, referring respectively to the gradual addition or removal of material from a larger object until the correct nanoscale dimensions have been attained. The number and range of nano synthetic procedures have expanded greatly with approaches such as "wet" synthetic chemistry, biologically generated materials and aerosol-based inorganic synthesis. In this thesis a critical aspect in the choice of synthetic method is the scalability of the process, the aerosol synthesis technique employed here for nanoparticle preparation is flame spray pyrolysis (FSP).[30] This process involves the atomisation of an organic solution containing inorganic precursor materials. A pilot flame is used to ignite the atomised spray causing the organic components to combust and the resultant high temperature vaporises the inorganic precursor materials which subsequently form nanoaggregate structures. Such aerosol synthesis procedures are applied for the tonne/h scale synthesis of dry nanoparticle powders or the direct deposition of nanomaterials onto even thermally fragile substrates.[31,32] One important limitation of this synthesis method is that the nanoparticles to be produced must be compatible with the high temperatures and oxidising nature of the flame process. Therefore, materials produced are typically metal oxides or more complex metal salts such as metal carbonates and phosphates. Metallic nanoparticles can be formed in reducing flames or of sufficiently noble metals such as Au and Ag by conventional FSP.[33]

2 Background

2.1 Nanomaterials and nanomedicine

Nanomaterials today can be found in a wide range of products from medical devices to the automotive industry, they can be inorganic nanoparticles, organic polymers or biologically derived materials.[34] In order to provide a focus more relevant to the thesis, the discussion will be mainly focused on inorganic nanoparticles. Silica can be found in commercial rubbers, cosmetic products, alloys and even under E551 as a food additive.[35–38] The antimicrobial properties of nanosilver have found applications in medical products, packaging and textile products including face masks.[39,40] Titanium dioxide and zinc oxide nanoparticles are applied in paints and cosmetics such as sunscreen as they exhibit strong absorption of ultra-violet (UV) light while retaining stability and demonstrating photo-catalytic behaviour which can allow for self-cleaning and antimicrobial properties.

The field of nanomedicine specifically deals with applications of nanotechnology to medicine and inorganic nanoparticles find applications here too.[2,3,41] A large portion of these applications concern the development of coatings for implants and biomedical devices. Hydroxyapatite nanoparticles are applied to commercially available titanium implants as coatings to improve osseointegration.[42] Silver nanoparticles can be found in some urinary catheters and other implant coatings as antimicrobial agents.[43] The field of dentistry makes prolific use of inorganic nanomaterials as coatings, dental fillers and toothpaste.[44]

Aside from these coating technologies applications of nanomaterials in medicine and biomedicine are prolific in the scientific literature. Plasmonic nanomaterials such as Au, Ag, Cu and TiN capitalise on their strong interaction with electromagnetic radiation to provide highly sensitive diagnostic readouts or potent photothermal therapeutic effects.[45] Iron oxide nanoparticles designed as superparamagnetic nanoparticles (SPIONS) have been extensively explored as magnetic resonance imaging contrast agents,

and their properties of magnetic hyperthermia are applied for the treatment of cancer and bacterial infection.[46] The properties of SPIONS have also prompted the development of a promising new *in vivo* imaging modality, magnetic particle imaging.[47] The fields of *in vivo* and *in vitro* imaging also benefit from frequent advances in luminescent nanoparticle development, including the use of rare-earth doped nanophosphors and quantum dots which can have luminescence excitation and emission from the UV to the near-infrared (near-IR).[48,49]

Inorganic nanoparticles also contribute significantly to the field of drug delivery and targeting. Therapeutic agents delivered by such systems can be traditional small molecule drugs or larger biologics including peptides, proteins and oligonucleotides.[50] Such systems either incorporate the drug into the structure of the nanoparticle, as seen in the case of many calcium phosphate-based delivery systems[51] or load the molecule onto the surface of the nanoparticle by exploiting physicochemical interactions such as electrostatics and direct chemical conjugation.[52,53] These systems offer several advantages as due to their size, charge and the density of therapeutic agents they can be trafficked differently compared with the free agent. By the addition of a targeting moiety or property, e.g. an antibody or pH-sensitive dissolution, such systems may selectively yield higher local concentrations at the desired location.[54]

Surprisingly given this broad range of developed nanomedical strategies the number of approved clinical treatments, outside of dentistry and implant coatings, are still relatively limited. Perhaps the most successful group of inorganic nanoparticles are SPIONS which found clinical application as MRI contrast agents under the brand names Feridex® (AMAG pharmaceuticals), Resovist® (Bayer Healthcare) and Ferrotran® (SPL Medical). However, to the best of the author's knowledge, Feridex® and Resovist® have been discontinued and Ferrotran® is only available in the Netherlands. An alternative application of SPIONS for magnetic hyperthermia ablation of glioblastoma tumours is available in Germany with approval across the European Union (EU) under the brand name NanoTherm® (MagForce). Recently a hafnium oxide based system as a radioenhancer for cancer radiotherapy was granted EU market approval under the brand name Hensify® (Nanobiotrix).[3]

Apart from the MRI imaging diagnostics referred to above, inorganic nanotechnology has produced other *ex vivo* diagnostic tools. Perhaps most well-known is the application in lateral flow assays, such as some pregnancy tests, which can leverage the plasmonic properties of gold nanoparticles conjugated to an antibody to produce a clear optical signal visible to the naked eye.[55] More advanced systems for clinical diagnostic laboratories are also on the market such as the plasmonic gold enabled Verigene® (Lu-

minex) system for pathogen identification and easy analyte purification by magnetic nanoparticle enabled separation in the Magtration® (Precision System Science Co., Ltd).[56,57] Nanomaterial applications to gas-phase sensors have also enjoyed success for instance with the development of a methanol sensor Spark M-20 (Alivion) with a sensing component consisting of Pd-doped SnO_2 nanoparticles made by flame spray pyrolysis (FSP).[58]

2.1.1 Plasmonic properties

The plasmonic properties of noble metals such as Au and Ag are frequently harnessed for biomedical applications. These properties arise due to surface plasmons which are collective oscillations of electrons usually found at the metal-dielectric interface. The greatly enhanced interactions with the electric field of electromagnetic radiation generated by the localised surface plasmon resonance of nanostructures (as schematically depicted in Figure 1) result in strong absorbance signatures.[59,60] The most popular plasmonic materials are Au and Ag due to their low chemical activity and visible light plasmonic properties. Cu and Al have also been investigated due to their reduced cost, however, the surface reactivities of these metals make their application in biological settings challenging. Alloys of these metals such as gold-silver alloys have also been used as efficient plasmonic elements which can make use of the chemical inertness of gold and the plasmon efficiency and reduced cost of silver. Other less traditional plasmonic materials have also been investigated, particularly for near-IR applications, such as TiN.[61]

Plasmonic nanomaterials can also be further optimised by considering their morphology, with sharp edges, small radius cones and core-shell structures giving rise to greatly enhanced localised surface plasmons.[62,63] Moreover, the interactions between nanoparticles can significantly impact the plasmon resonance and tuning of this inter-particle spacing can be used to optimise the strength of the plasmon resonance at the desired wavelength. Thus nanostructured materials can couple their inherently higher surface area with strong localised surface plasmon resonance to outperform larger-scale materials on two fronts.[64] Although many applications make inherent use of the absorbance and scattering properties of plasmonic nanoparticles for the development of optical systems they can also couple to other radiative processes such as fluorescence and Raman scattering to enhance the signal strengths which can be achieved.[65,66]

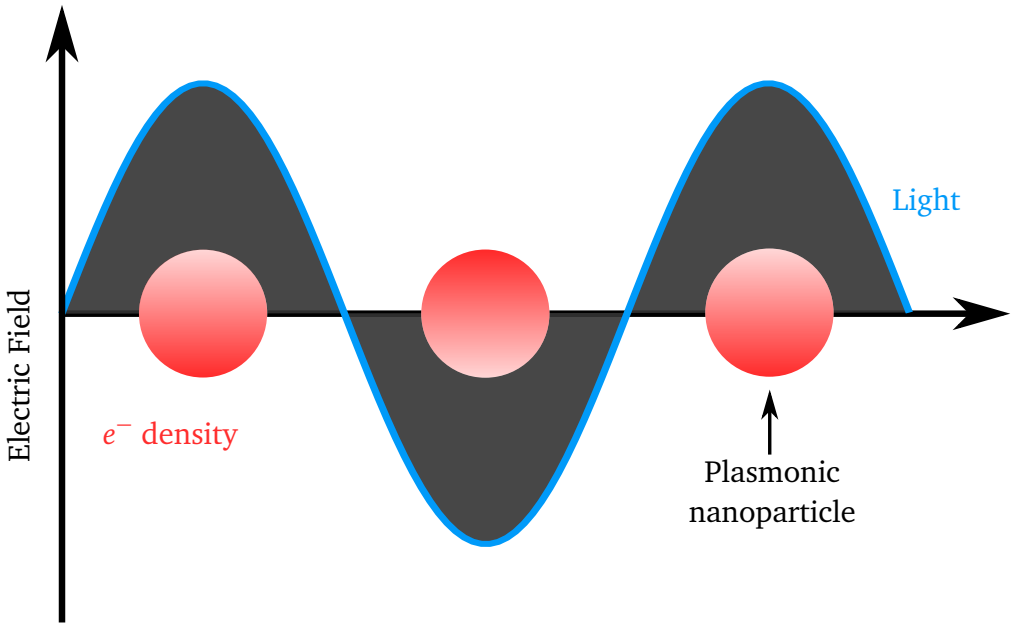

Figure 1: Schematic depiction of the interaction occurring between light and the conduction band electron density of plasmonic nanoparticles which give rise to the surface plasmon resonance phenomenon and the strong light absorption of plasmonic nanostructures.

2.1.2 Luminescent properties

Photoluminescent inorganic nanomaterials find many applications in nanomedicine, particularly for imaging, sensing and diagnostics. The characteristic property of these materials is the emission of light upon photoexcitation. The photoluminescent properties of these materials can be broadly divided according to the energy relaxation processes occurring after excitation.[67] These processes can occur quickly, known as fluorescence, yielding light emission on the nanosecond timescale. Phosphorescence is the term applied to slower emission, due to the passage of the electron into a long-lived triplet state with timescales from milliseconds to minutes.[68] Due to the loss of energy during the decay process, the wavelength of emitted light is typically longer than the excitation wavelength termed down-conversion, although more complicated schemes making use of multiple excitation processes can allow for emission at shorter wavelengths than the excitation in up-conversion processes.[69] These differences are schematically illustrated in Figure 2.

The two most prominent classes of inorganic photoluminescent nanomaterials are quantum dots (QDs) and nanophosphors. Semiconducting QDs give rise to luminescence emission by the recombination of an electron-hole pair after excitation by electromagnetic radiation. This property is inherently emergent from the confinement of the excited state to the nanometre scale particle, giving rise to an atom-like elec-

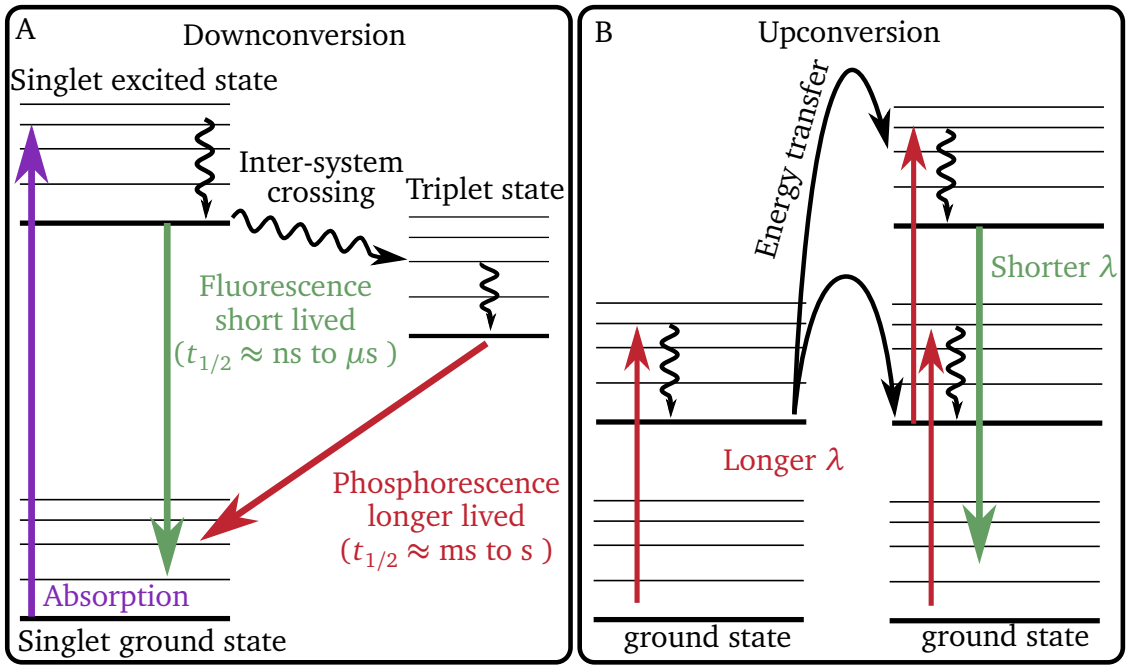

Figure 2: Simplified Jablonski diagrams illustrating A) the essential differences between phosphorescence and fluorescence phenomena with the example of a downconversion system and B) illustrating a possible up-conversion scheme with the sensitiser on the left and emitter on the right. The colours other than black are intended to reflect trends in the wavelengths of light, going in order from shortest wavelength (highest energy) to longest wavelength: purple, green and red.

tronic structure. The wavelengths of luminescence emission from these QDs can be tuned by controlling their size, typically in the sub 10 nm range. This narrow range of sizes means that in order to achieve narrow emission bands the synthetic procedure must yield sufficiently monodisperse nanoparticles.[70] These nanomaterials are found in commercial electronic products, however, the reliance on toxic heavy metals has hampered their application to nanomedicine with significant research activity being directed towards the development of non-toxic QDs such as carbon QDs.[71,72]

Nanophosphors are nanomaterials with phosphorescent photoluminescence. Inorganic nanophosphors are typically made up of or doped with lanthanide elements which provide the phosphorescent properties. Luminescence emission in these materials can occur by direct excitation of the lanthanide ion or by excitation of the host lattice in which the lanthanide ions are doped and subsequent energy transfer to the lanthanide ion.[48] The emission wavelengths of these materials are therefore principally determined by the choice of lanthanide ion, although it can also be influenced to a lesser extent by the electronic configuration in the vicinity of the lanthanide ion.[73,74] The luminescence emission intensity and spectral profile of the emission, however, can be greatly influenced by the symmetry of the lattice site in which the lanthanide ion finds

itself. Particularly Eu^{3+} finds applications as a tool to evaluate changes to local lattice symmetry due to the strong dependence of its pseudo electric dipole transitions and relative stability of the magnetic dipole dependent transitions. [75]

The design of up-conversion luminescence nanophosphors, undergoing multi-photon excitation processes, enables the use of longer excitation wavelengths, which are biologically less damaging and more penetrating. [76] Moreover, the emitted lower wavelength radiation can be harnessed by other photoactive materials located close to the nanophosphor such as catalysts and photodynamic therapy agents. [77] However, by their very nature, up-conversion luminescent nanophosphors typically yield lower quantum yields than their down-conversion counterparts.

Nanophosphors find important biological and medicinal applications as bioimaging agents and sensors with a key characteristic being their photostability. [78] A key issue for many fluorescent dyes is that over time, under illumination their emission fades in a process known as photobleaching, nanophosphors, however, have been shown to exhibit excellent photostability under relevant imaging conditions. [79] In addition, the longer time scales of nanophosphors allows for time-gating to filter out background auto-fluorescence to improve the signal to noise ratio. [80] This has been taken to an extreme with persistent luminescent nanophosphors, in which the excitation takes place before the addition of the particles to the sample, removing, therefore, the excitation source for any background fluorescence emission. [81] However, as in the case of QDs, nanophosphors are currently confined to *in vitro* and animal *in vivo* experiments.

2.1.3 Optical detection mechanisms

Both plasmonic properties and luminescent properties find important applications in sensing. Analyte dependent spectral changes are often harnessed in order to provide the sensor response. [82] The exact nature and the advantages of these different spectral responses can be an important consideration when considering potential applications in the target environment, some examples of such spectral changes are illustrated in Figure 3. Perhaps the simplest optical sensor, shown in Figure 3A, correlates a change in the intensity of the optical process to the analyte concentration. Many colorimetric assays are based on this principle, whereby a coloured dye is produced in an analyte dependent fashion. [83] In carefully controlled environments these can be highly effective, however, in more dynamic environments changes to the optical properties of the medium can seriously affect the readout leading to inaccurate results. [84]

If these dynamic changes could be measured then the output of the single peak sensor

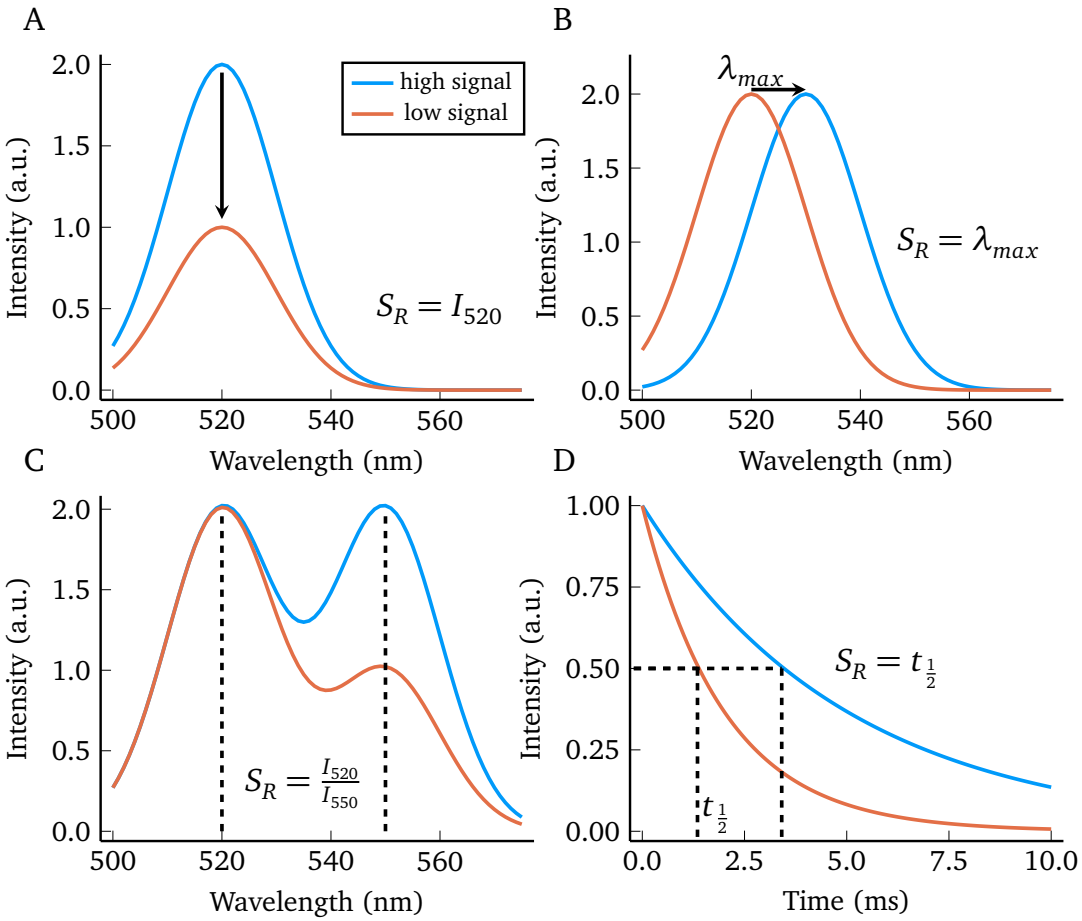

Figure 3: Schematic examples of different optical sensing mechanisms with S_R indicating the analyte dependent sensor response. A) shows a simple relationship between peak intensity at 520 nm (I_{520}) and analyte, B) demonstrates the use of analyte dependent shift in the peak maximum (λ_{max}) C) illustrates a ratiometric sensor response between two close-lying peaks and D) provides an example of using lifetime measurements for analyte sensing where $t_{\frac{1}{2}}$ denotes the halflife of the luminescence emission.

could be corrected for them. An attractive improvement to do this is to equip the sensor with a reference signal. This can be achieved for instance by loading an analyte sensitive fluorescent dye on the surface of a luminescent nanoparticle with stable emission. Therefore instead of correlating the change in intensity alone, the relative change in intensities between the two peaks can be correlated to the analyte illustrated in Figure 3C. Here it is beneficial to choose two spectrally close peaks, which are still sufficiently well resolved, this helps to ensure that any interfering changes to the optical properties of the medium influence both spectral peaks equally.[84,85]

Due to the dependence of the maximum absorbance wavelength of localised surface plasmon resonance peaks on the refractive index of the nanoparticle's surroundings, a common optical output when applied for analyte detection is a shift in the spectral

peak position as shown in Figure 3B.[86] An alternative example is in assays which can be designed such that a plasmonic nanoparticle's aggregation state is altered and therefore the absorbance maximum wavelength.[87] This method can also be tolerant to some dynamic changes to the optical properties of the medium such as increased scattering and has effectively been applied for naked-eye detection. The last example, presented in Figure 3D, involves the lifetime of the luminescence emitter.[88] In some conditions, such as low oxygen environments, the lifetimes of excited states can be altered. These optical sensors are also quite robust to changes in potentially interfering properties of the analyte medium. A limitation to their application is that particularly for short-lived states the experimental apparatus required can be specialised and not readily available.

2.2 Flame spray pyrolysis

Throughout this thesis, all intentionally generated nanoparticles have been produced by the aerosol synthesis technique: flame spray pyrolysis. The technique was initially derived from established flame aerosol technology used to produce at the tons/h scale nanoparticles such as carbon black, TiO_2, fumed silica and Al_2O_3 in a market worth more than $15 billion per year.[89] A key aspect of this established technology for the synthesis of ceramic nanomaterials is that the precursor is fed into the flame as a vapour, e.g. $SiCl_4$ and $TiCl_4$.[90] This limits the accessible materials to those with a suitable vapour precursor and provides additional risks due to the reactive nature of the precursors. FSP distinguishes itself in that a liquid precursor is used and the combustion of the organic and inorganic compounds provides the majority of the enthalpy needed for particle synthesis.[91] A third related flame aerosol synthesis technique exists allowing the use of aqueous solutions, which rely on an external heat source such as a hydrogen flame to provide the majority of the combustion enthalpy.[92]

The FSP reactor design as developed by Mädler et al. involves the pressure-assisted dispersion of an organic precursor with dissolved inorganic components into a fine droplet spray and subsequent ignition by a pre-mixed methane-oxygen flame.[30,93] The basic aspects of synthesis in this nozzle design are schematically depicted in Figure 4. The components of the precursor-solvent should be chosen such that their highly exothermic combustion is able to yield a metal vapour in the flame of above 2000 K.[94] The turbulent high-velocity nature of the flame leads to high air entrainment and therefore also rapid cooling, the high-temperature residence times are therefore extremely short (in the millisecond timescale).[95] This prevents the excessive growth of the nanoparti-

cles after formation from the metal vapour, while the high temperatures can produce homogeneous crystalline nanoparticles. The rapid cooling can even yield metastable crystalline phases such as monoclinic Y_2O_3 and Maghemite. [96,97] Subsequently, the dry nanoparticle powder can be collected by vacuum filtration on a suitable filter medium such as glass fibre or deposited by thermophoresis on a water-cooled substrate. [98,99]

The mechanism by which particle formation occurs is an important consideration and dependent on the precursors used. The desired formation route occurs when the precursor is completely combusted and the metal component goes into the gas phase, from which upon cooling primary particles form by coalescence and sintering and subsequently fractal-like aggregates of the primary particles form. [30,100] It should be noted also that there is some debate around the terminology of aggregates and agglomerates with inconsistencies and contradicting definitions highlighted in a review by Nichols et al. [101] In the present text aggregate is preferentially used and should be understood to refer to firmly bound clusters of primary particles. Whether all FSP produced particles form as such nanoaggregates and do not also include more loosely bound structures, such as agglomerates, likely depends on the exact material properties.

The primary particle size of these nanoaggregates is largely determined by two crucial considerations in FSP, the high-temperature residence time and vapour phase metal concentration. These can most easily be regulated by controlling the concentration of dissolved metal in the precursor, the flow rate of the precursor solution and the flow rate of the oxygen used for dispersion of the precursor. [102,103] Constraining cooling and combustion by reducing air-entrainment also yields larger nanoparticles and can be controlled by placing a suitable tube around the flame. [95,104]

Under certain conditions (e.g. if the melting temperature of the metal precursor is greater than the solvent boiling point) less desirable particle formation routes can occur by precipitation of the metal precursor, incomplete evaporation or combustion, of the droplets to yield inhomogeneous micron-sized particles, the so-called droplet-to-particle route. [92,105,106] In order to improve the homogeneity of synthesised nanopowders a mixture of two solvents, one with a significantly lower boiling point than the other can lead to beneficial microexplosions in the droplets which can reduce the frequency of the droplet-to-particle formation route. [107,108]

Multi-material nanoparticles can also be formed by FSP, usually by one of three mechanisms. By dissolving multiple metal precursors into the same precursor solution multi-material nanoparticles can be formed, the structure of which depends largely on the concentrations of the components and metals used. Doping of a crystalline lattice of

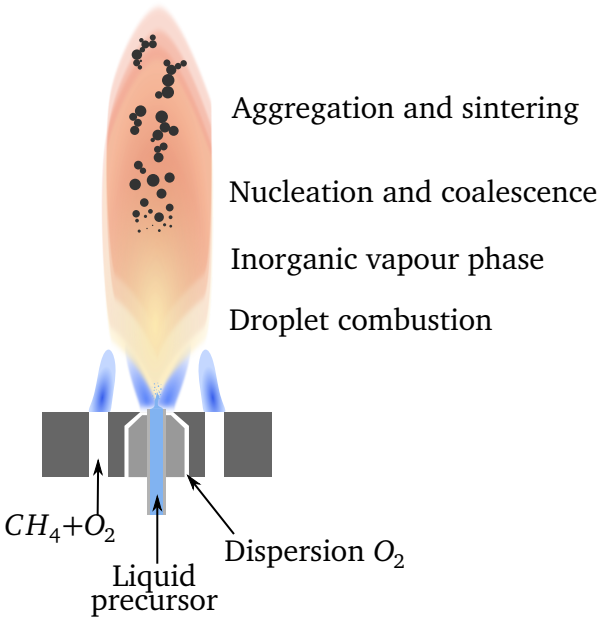

Figure 4: Diagram of the FSP reactor showing core components and basic processes which lead to nanoparticle formation. A liquid precursor, consisting of the desired metal dissolved in a combustible organic solvent, is flown through a capillary with the help of a syringe pump. Concentric to the tip of the capillary is a high-velocity flow of dispersion O_2 which forms a spray of the precursor. Supporting flamelets in an annular configuration ignite the spray, the precursor droplets combust and the inorganic phase is forced into the vapour phase. As the flame temperatures decrease particles begin to form by nucleation and grow by coalescence and sintering, as the flame temperature decreases further primary particle aggregation into fractal-like aggregates occurs.

Y_2O_3 with Eu^{3+} (denoted henceforth Y_2O_3:Eu^{3+}) can be achieved in this way, or the formation of Ag-Au alloyed nanoparticles demonstrating the formation of single-phase nanoparticles.[97,109] Alternatively, phase separation of the materials can occur, yielding either mixed nanoparticles with different material sub-domains or well-separated nanoparticles which have aggregated together.[110] In order to avoid phase mixing of materials inside a particle a dual flame setup can be used as shown in Figure 5A. In this case the nanoparticle formation occurs separately for the two materials and the flames are oriented such that the formed nanoparticles meet at a point where they can be well-mixed and the temperature is sufficiently high for aggregation to occur.[111] Applied for instance for the synthesis of separated $BaCO_3$ and Al_2O_3 nanoparticles which are nonetheless present in the same nanoaggregate structures.[112] Silica coatings can also be formed *in situ* on nanoparticles by confining the flame within quartz tubes and injecting at a suitable height a flow of silica precursor vapour, depicted in Figure 5B. This has been used for example for the formation of hermetic silica coatings to passivate TiO_2 nanoparticles or to prevent silver ion release from Ag nanoparticles.[104,113]

Coatings of nanoparticles synthesised by FSP can also be formed on substrates by direct deposition illustrated in Figure 5C. In this process a, typically water-cooled, substrate is placed above the flame with deposition of nanoparticles occurring directly from the flame by thermophoresis and collision.[98,99] This process has been used to deposit multi-layer coatings with different materials and due to the water-cooling can even be applied for the deposition on thermally more fragile materials such as polymers.[114,115] The deposited coatings, exhibit very high porosity up to 98 %, although this allows for excellent sensitivity for instance in sensing applications, it also renders the coatings somewhat fragile. In order to stabilise the coatings *in situ* annealing can be performed by impinging a particle-free flame onto the substrate.[116] Alternatively, an impinging flame containing metal precursor can be directly applied to the substrate and has been used to synthesise stable, highly-porous coatings in a single step.[117]

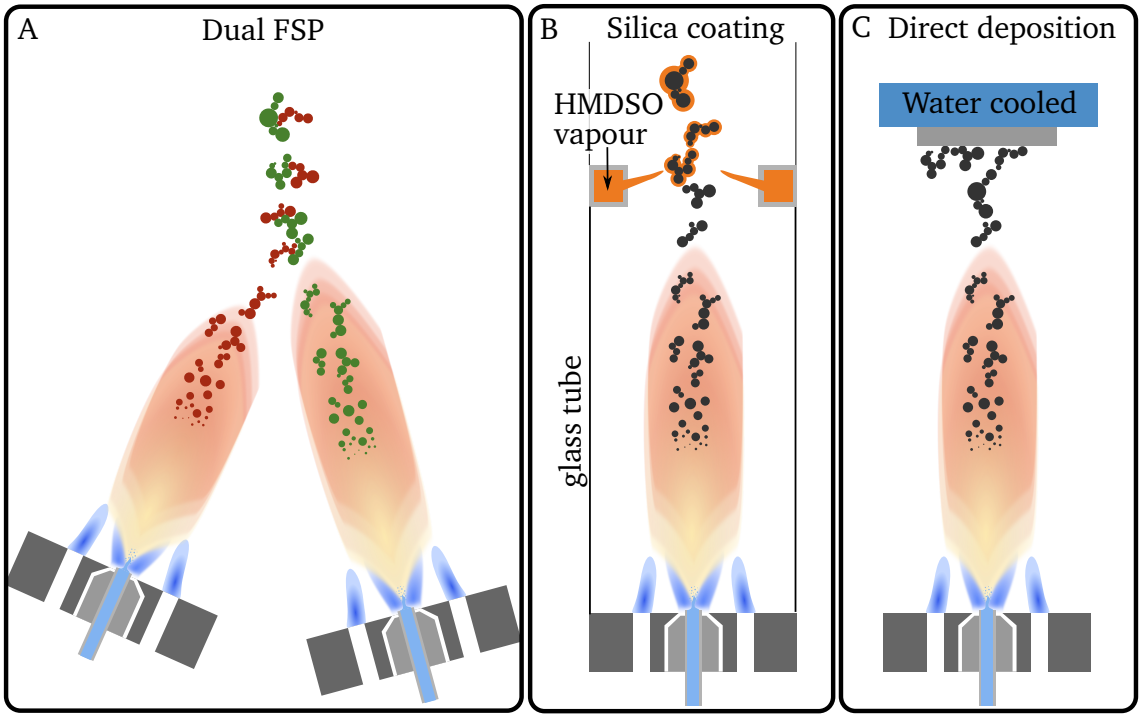

Figure 5: Diagram depicting the three modifications of the standard FSP shown in Figure 4. A) Dual FSP involves the orientation of two FSP nozzles such that their aerosolised nanoparticle products are able to inter-mix while maintaining segregated phases. B) The silica coating reactor involves injecting vapour of hexamethyldisiloxane (HMDSO) above the flame into the hot-aerosol of the formed nanoparticles. The HMDSO combusts and the nanoparticles become hermetically coated in a thin silica layer. C) Direct deposition allows the deposition of nanoparticles directly onto a water-cooled substrate by ballistic and thermophoretic processes. This allows the direct single-step synthesis of functional nanocoatings.

FSP has therefore been shown to be a flexible synthesis technique, not only for the large scale production of homogeneous nanoaggregates but also with the potential for customisation to achieve complex, controlled multi-phase and multi-material aggregates

as dry powders or highly porous coatings. Over the past 20 years, the development of FSP as a synthesis method for inorganic nanoparticles has been proceeding at a rapid pace, with applications in catalysis, energy storage, nanomedicine and many more. The successes have led to the formation of a number of companies based around the technology for example TurboBeads GmbH provides FSP produced magnetic beads for sample purification, ParteQ GmbH provide lab-scale FSP reactors, Hemotune AG develops FSP produced magnetic nanoparticle-based dialysis technology, Anavo medical develops a surgical nanoglue based on FSP made nanoparticle ionic networks, and Alivion AG develops gas-phase sensors which use FSP deposited nanoparticle films as the sensing element. [31]

2.3 Bacterial infections

The intention of this section is to give a brief introduction to bacteria and the infections they can cause in humans with emphasis on providing important background information for nanomedicine and the papers included in this thesis. Bacterial infections are an important sub-category of medical microbiology and can cause serious consequences for overall health, including limb loss and death. Although some respite was offered in the early 20th century due to the discovery of antibiotics, the rise of antibiotic resistance is an urgent problem. [118,119] The number of deaths due to antimicrobial resistant infections was predicted in a 2016 study to surpass 10 million by 2050, in contrast to the 8.2 million annual deaths caused by cancer. [120] The ever-increasing density of the human population, interconnectedness of the world and intensity of agriculture is thought to only contribute to this problem. [121,122]

Bacteria are prokaryotic microorganisms which therefore lack a defined nucleus and membrane-bound organelles. The ribosomes, deoxyribonucleic acid (DNA) and other critical components are therefore spread out in the bacterial cytoplasm. Bacteria are smaller than eukaryotic cells typically with volumes $< 3\,\mu m^3$. This volume can be in the form of 3 typical shapes and their intermediates: spheres (cocci), cylinders (rods) and spirals (spirochaetes). [123] Bacteria are bounded by a cell wall which is traditionally classified into two sub-groups gram-positive and gram-negative. This naming is derived from the Gram staining procedure developed in 1884, crystal violet dye applied to the bacteria can be washed away from gram-negative bacteria. Whereas a thick outer peptidoglycan layer retains the dye in gram-positive bacteria and they therefore appear as positively stained by microscopy. Thus this difference in naming reflects critical differences between the structures of the bacterial cell wall which has

an enormous influence on antibiotic efficacy and the interaction of bacteria with their surroundings (e.g. immune response, temperature, attachment).[124]

Although bacteria can cause disease it is rare for bacteria or any microbiological organism to exist in a purely pathogenic capacity like in the cases of *Bacillus anthracis* and *Rabies lyssavirus*.[124] Instead, most disease-causing bacteria are opportunistic pathogens and can co-exist as commensal bacteria in their particular biological niche only causing disease when transferred to a new location.[125] For instance *Staphylococcus aureus* is a facultative anaerobic gram-positive coccus which can exist as a commensal in the skin, respiratory tract and female lower reproductive tract, but if provided with for instance a wound site can become a serious infection and lead to sepsis. *S. pneumoniae* is a gram-positive aerotolerant anaerobe which can reside asymptomatically in the respiratory tract of carriers, but when transmitted to hosts with a weakened immune system due to age, medication or other illnesses, can become pathogenic and cause conditions such as pneumonia and meningitis. *Pseudomonas aeruginosa* is a ubiquitous gram-negative rod that is found in water, soil, human skin, the human gut and many other locations such as hospital surfaces. *P. aeruginosa* can infect a large number of sites for instance: it is a common cause of pneumonia in cystic fibrosis patients, causes severe burn wound infections and is often found in urinary tract infections. *Klebsiella pneumoniae* is a rod-shaped gram-negative facultative anaerobe which naturally occurs in the soil and is also frequently found in the mouth, skin and intestinal flora. Nosocomial infection is again thought to be a major mode of transmission, with elderly individuals being a key demographic, causing a wide range of diseases such as pneumonia, urinary tract infections and wound infection. *Escherichia coli* is another rod-shaped gram-negative facultative anaerobe and exists to a large degree as a harmless commensal in the microbiota of the gut. However, virulent strains can cause serious disease such as enterohemorrhagic *E. coli* which can cause life-threatening hemolytic uremic syndrome. *E. coli* is also a common cause of urinary tract infections, termed uropathogenic *E. coli*.[124]

Bacteria often share a biological niche and there can be intense competition between bacterial species. To achieve this bacteria have developed numerous systems of biological weaponry.[126] *P. aeruginosa* has a particularly large arsenal, including the redox-active toxin pyocyanin, which also gives rise to the characteristic green colour of *P. aeruginosa*. Alternatively R and F pyocin are protein molecules with a more mechanical mode of action, forcing apart the cell wall akin to phage entry and causing lysis.[127,128] Both, *S. pneumoniae* and *S. aureus* are found in the nasopharynx and have evolved weapons to try and gain a competitive advantage in their shared niche. For in-

stance, *S. pneumoniae* is a potent producer of hydrogen peroxide which has been shown to inhibit the growth of *S. aureus*.[129] Moreover, the complex relationship between hydrogen peroxide and the immune system results in hydrogen peroxide production by *S. pneumoniae* having an immune-suppressive character.[130]

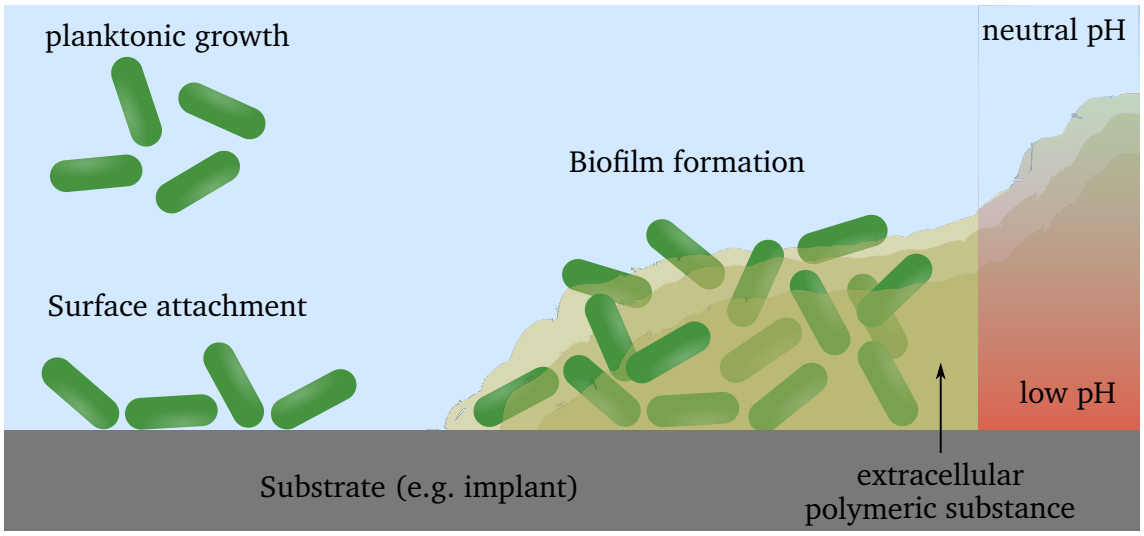

Figure 6: Highlighting the differences in planktonic and biofilm growth. In planktonic growth free-floating bacteria grow in the medium and are therefore easily accessed, however, by using charge, surface properties such as lipophilicity and specific attachment elements (like adhesins) bacteria can attach to a surface. As they grow on the surface they can begin to excrete an extracellular polymeric substance which encases them and reinforces their surface attachment while protecting them from many stress factors such as shear forces and antibiotics. The dense nature of this growth can lead to the build-up of gradients within the biofilm, as shown in the case of pH, where the biofilm-substrate interface can be at a significantly more acidic pH than the liquid facing surface.

The bacterial biofilm as shown in Figure 6 is a mode of growth in which cells are embedded in a self-produced extracellular polymeric substance (EPS) and attached to a surface, distinct from the free-floating planktonic bacterial growth often performed in laboratory cultures.[131] Biofilms grow throughout nature as a highly successful form of growth, as seen in microbial mats on the beds of fast-flowing rivers and problematic biofouling of industrial processes.[132,133] They also form persistent infections in humans both on tissue and implant surfaces.[14] These highly complex structures encase bacteria in a self-produced extracellular matrix which provides a scaffold to grow in, protecting the bacteria from external stresses such as shear forces of moving liquids or desiccation if the biofilm finds itself temporarily in a dry environment. The EPS is a highly hydrated structure and is the origin of most of the biomass of the biofilm, components of the EPS include polysaccharides, proteins and extracellular DNA (eDNA).[11] Bacteria produce specialised biomolecules to modulate the EPS such as the increase in rigidity conferred by the eDNA cross-linking cationic exopolysaccharide Pel of the

potent biofilm former *P. aeruginosa*.[134] Although dense the biofilm is not a static or impassable body, bacteria continuously remodel the structure and nutrient channels can be formed. Moreover, essential to biofilm virulence is the sensing of nutrient availability and dissemination of bacteria from the biofilm in favourable conditions. This behaviour is enabled by EPS degrading enzymes which allow the bacterial release to colonise new sites.[135]

Although often studied as a mono-culture biofilm in laboratories, natural biofilms are rarely composed of a single species and can also integrate bacterial and fungal species into a single biofilm. The different bacterial cells can adopt very different roles and effectively cooperate.[136] Such multi-species cooperative biofilms can have much-increased resistance to treatment compared with the individual mono-species biofilms.[137] Even in a biofilm composed of a single strain, the bacteria can adopt heterogeneous roles, for instance, some bacteria may go into a more dormant state, lowering their metabolic activity to allow them to survive in harsher environments and becoming providing an opportunity for regrowth when the stress is reduced. These cells are termed persister cells and contribute to the stress tolerance of the biofilm.[138] The dense EPS also provides a diffusion-limited environment, therefore, bacterial enzymes secreted into their surroundings do not diffuse easily away and can be used for effective nutrient recovery.[11] The lack of clearance can also build up steep concentration gradients of oxygen, nutrients and pH.[139] All linked to the metabolic activity of the bacteria, in particular for species capable of fermentation the anaerobic environment can lead to a sharp decrease in pH.[140]

Antimicrobial efficacy is also typically reduced against bacteria growing in a biofilm. This can, in part, be due to decreased local concentrations due to diffusion compared with planktonic culture, however, other factors can also play an important role. The EPS is able to bind to many cationic antimicrobials and metal ions such as copper. Antimicrobials that rely on an oxidative mechanism can be effectively quenched by reaction to EPS components.[141,142] The high enzyme concentrations of the biofilm can also cause antimicrobial degradation. The presence of slow-growing persister cells can also hinder antibiotics such as vancomycin which require active metabolism. These mechanisms can cause sufficiently low effective local concentrations of the antimicrobial that selection for antimicrobial-resistant bacteria can occur.[11] Additionally, the proximity of cells and physical spatial stability of their environment can promote horizontal gene transfer of resistance promoting genes.[143,144] These factors cause biofilms to often have significantly lower susceptibility to antibiotics compared with planktonic bacterial cultures. For instance, *S. aureus* biofilms have been shown to be up to 1000

fold more tolerant to some antibiotics than the planktonic cells.[145] These unique features of the biofilm help to explain the significant role of biofilms in infections with some estimates suggesting as many as 80% of bacterial infections could be in the form of biofilms.[14] These challenging aspects of the biofilm structure further highlight the need to develop additional novel treatment strategies, such as local temperature or pressure manipulation, which can circumvent the biofilm defences.

2.4 Photothermal nanomaterials in the near-IR

Photothermal nanomaterials convert incident electromagnetic radiation into heat. Such materials find uses in applications such as energy harvesting from sunlight, but they have also been shown to hold promise for nanomedicine.[146,147] Temperature is usually a closely controlled parameter in mammals, and the input of local heat can be enough to induce cell apoptosis at temperatures exceeding 42 °C.[148] This has been applied to the photothermal ablation of cancer. Although bacteria cannot regulate their temperature as efficiently as mammals, human disease-causing bacteria are adapted to survive within the normal ranges of human body temperature and can be susceptible to even moderately high temperatures. Therefore, photothermal nanomaterials can be applied for both killing eukaryotic and prokaryotic cells.[146,149]

The specificity of photothermal treatments relies on the co-location of the photothermal device with the site of infection or disease. The source of heat should be the photothermal agent and the temperature is, therefore, highest in the immediate vicinity and equilibrates to ambient temperature with distance. Therefore the physical location of the photothermal agent is important.[150] Approaches to achieve this co-localisation can consist of targeting by functionalisation of a nanoparticle to achieve selective delivery, injection into the local site or in the case of implants applying the coating to the implant prior to implantation. Targeted delivery is seen as a promising approach for anti-cancer treatments, whereas the tendency of biofilms to form on implant surfaces makes photothermal implant functionalisation attractive for anti-biofilm surfaces.[151]

Since light is a key component of the therapy, the interaction of light with biological tissue is a key issue since in order for the photothermal material to be effective the intensity of light at the material's location must be sufficient. This absorption of light is highly wavelength dependent as shown in Figure 7, in the visible region between 400 and 700 nm there is strong absorption by tissue, especially by blood.[152] The first so-called near-IR window occurs between 650 and 900 nm, where there is a minimum in the absorption spectrum.[153] The second near-IR window occurs between 1000

and 1350 nm.[154] By using these wavelengths of light the tissue absorption can be minimised and the light can therefore penetrate deeper to more effectively access the embedded photothermal device.[155]

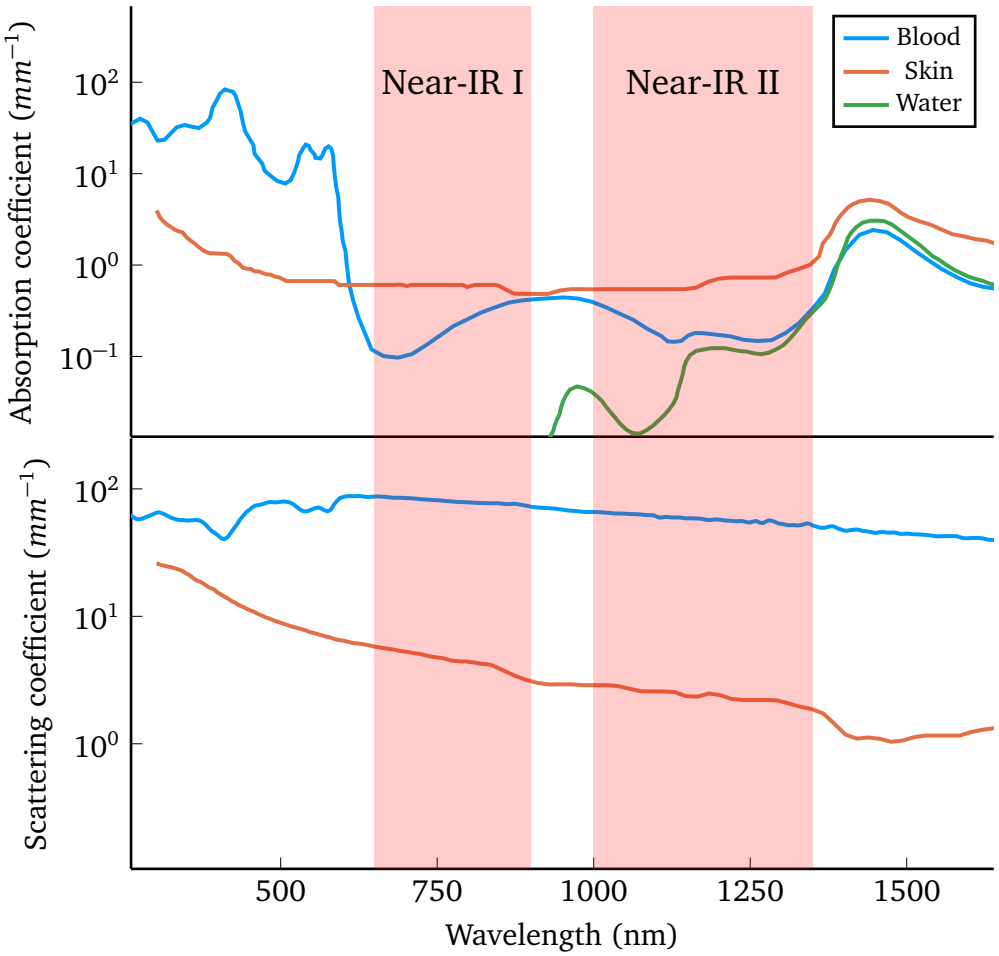

Figure 7: Re-plotted data of scattering and absorption coefficients of skin,[156] blood[152] and water[152]. Demonstrating the favourable decreases in absorbance leading to the two near-IR windows, overlayed as red shading, in which light can penetrate deeper. These near-IR wavelength ranges, therefore, provide attractive potential for *in vivo* measurements and treatments.

The design and synthesis of nanomaterials which achieve this near-IR photothermal activity has been greatly developed and inorganic nanomaterials play a significant role in this field. By tuning oxygen vacancies in molybdenum trioxide photothermal properties of the material could be tuned which have been applied as antibacterial and anticancer treatments.[157] However, it should be noted that this material is not only photothermal but also produced reactive oxygen species thereby acting as a dual photothermal/photodynamic agent. Inorganic nanosheets of metal dichalcogenides have also been developed with photothermal properties such as MoS_2 and Bi_2S_3 particularly for anti-tumour treatments.[158–160] However, plasmonic nanomaterials are undoubt-

edly the most popular class of inorganic photothermal agents for the near-IR.[161,162] Silver has excellent photothermal properties, however, the peak of plasmon resonance absorbance is typically at 400 nm for unmodified spherical silver nanoparticles.[163] Therefore modifications applying silver must tune the absorbance to yield effective near-IR activity. Moreover, the chemical instability and toxicity of silver nanoparticles can limit their applicability.[115,164] Gold has many attractive properties for use in such nanoparticles, for instance, it has low toxicity and high chemical stability. Moreover, the plasmon resonance of spherical gold colloidal suspensions is typically between 500 and 600 nm and near-IR photothermal behaviour is, therefore, more accessible.[165] A more recently developed material for photothermal plasmonics consists of titanium nitride nanoparticles which have good activity in the near-IR and were demonstrated for killing cancer cells.[61,166]

Careful tuning of plasmon resonance absorbance wavelength into the near-IR can be achieved by synthesising complex structures such as nanoshells,[167] nanostars,[168] nanocubes[169] and nanocages.[170] Controlling properties of the nanomaterials such as their aspect ratio, size and interparticle coupling can also be used to tune the near-IR photothermal activity of the nanomaterials.[171,172] Given that in a recent clinical study applying gold nanoshells for the photothermal ablation of prostate tumours 1-2 g of nanoparticles were required per patient (body mass-dependent dosing of 7.5 mL/kg of a 4.5 mg/mL gold nanoshell suspension) a clear emphasis on scalable synthesis techniques and readily available precursor materials should be applied.[173]

Therefore, the FSP enabled synthesis of nanoparticles with controlled interparticle plasmonic coupling to yield efficient near-IR absorbance remains an attractive prospect. This has been realised for spherical gold and silver nanoparticle powder synthesis using FSP coating reactor methods to apply a thin silica coating around the primary gold or silver nanoparticles thereby limiting the interparticle distances within a nanoaggregate.[174,175] In Paper I an alternative method is described for the direct deposition of near-IR photothermal coatings using the standard FSP reactor and co-oxidation of the silica interparticle spacer.

Of particular relevance to this thesis is the application of such surfaces to the near-IR photothermal treatment of bacterial and more specifically biofilm infections. Gold nanomaterials for such applications have been explored. For instance, Khantamat et al. demonstrated the functionalisation of a model urinary catheter with gold nanoshells and subsequent ability to photothermally kill *Enterococcus faecalis* biofilms.[176] However, silver has been applied only to a lesser extent with two articles by D'Agostino et al. demonstrating the synthesis and antibacterial effect of silver nanotriangles on

biofilms of *E. coli* and *S. aureus* and subsequent larger-scale surface application.[177,178] Magnetic Fe_3O_4 coated silver nanoparticles with near-IR photothermal activity have also been realised but only demonstrated to be effective against planktonic *E. coli*.[179] The application of near-IR photothermal spherical silver nanoparticle coatings against formed biofilms of *E. coli* and *S. aureus* will be demonstrated in Paper I.

2.5 Biofilm pH sensing

As described in 2.3 biofilms can develop low pH microenvironments which can contribute to substrate decay and the knowledge surrounding this acidic phenomenon can be used to design smart surfaces. Such surfaces release antimicrobial components upon biofilm formation due to the generation of this characteristic low pH microenvironment. Therefore accurate information on the pH microenvironment which different bacterial biofilms can form is essential. Approaches to do this have been developed utilising confocal microscopy, microelectrodes and pH-sensitive surfaces which will be described here.

Accurate determination of pH in solution is often performed by electrochemical methods utilising electrodes or micro-electrodes. This has also been applied for biofilm microenvironment pH determination using microelectrodes attached to a translational stage. Measurements have been demonstrated in dental biofilms formed in patients, with local pH measurements after 7 days of incubation demonstrating pH microenvironments of below pH 5 after the addition of glucose.[180] The effect of sucrose and chlorhexidine on biofilm pH was also evaluated on *in vivo* formed dental biofilm by micro-electrode measurement with pH values of below pH 4.5 attained in the presence of only sucrose and pH 5.9 in the highest chlorhexidine concentration.[181] Although clearly effective methods to determine pH the disruptive nature of the measurement technique raises some concerns about the relevance of the measurement and the methods are also low-throughput.[182]

Fluorescent dyes and particles labelled with fluorescent dyes have also been successfully applied to evaluate biofilm pH. The complete 3D pH distribution of *E. coli* and mixed-species wastewater biofilms was evaluated using core-shell silica nanoparticles with a cy5 rich core and a fluorescein rich outer shell. Thereby a ratiometric pH-dependent sensor could be developed due to the stable cy5 emission and the pH-dependent fluorescein. By employing confocal microscopy a topographic map of the biofilm microenvironment could be obtained.[183] A similar system was demonstrated with mesoporous silica loading with rhodamine B and fluorescein.[184] Alternatively,

the fluorescent dye C-SNARF-4 exhibiting ratiometric pH-dependent emission has also been applied for the three-dimensional mapping of pH microenvironments of *in vivo* formed dental biofilms.[183] In both cases, local pH values of below pH 5 were recorded. A combined measurement and treatment strategy was developed by Albright et al. by producing coatings containing the pH-sensitive fluorescent dye SNARF-1 and gentamicin or polymyxin B. Imaging of the fluorescence provided pH information and pH-dependent release of the antimicrobial yielded antibacterial activity.[185] All of these techniques utilise confocal fluorescence microscopy to measure the local biofilm microenvironment which is ill-suited to high-throughput screening and the reliance on fluorescent dyes can cause unwanted photobleaching over time potentially affecting the measurement.[48]

2.6 Hydrogen peroxide sensing

Hydrogen peroxide is a small reactive oxygen species with strong oxidative activity and therefore generally limited stability in biological media. An important producer of hydrogen peroxide in the human body is the enzyme superoxide dismutase where hydrogen peroxide is produced as an important intermediary in the clearance of toxic superoxide species.[186] Itself hydrogen peroxide is also toxic to cells due to its oxidative activity and levels must be carefully controlled generally by the enzymatic activity of catalases.[187] Although often a by-product of other processes hydrogen peroxide can also be deliberately produced as illustrated in Figure 8 and expanded over the coming paragraphs.

Biological systems can use elevated hydrogen peroxide levels for a range of purposes including production by the host immune system as part of the defence mechanism against infection and to modulate inflammation. Bacteria produce hydrogen peroxide for signalling and interbacterial warfare or host-immune modulation.[188,189] For instance, in the case of *S. pnuemoniae* conversion of pyruvate to acetyl phosphate and hydrogen peroxide is used to generate high hydrogen peroxide levels to help out-compete other bacteria in the upper respiratory tract.[190,191] Moreover, hydrogen peroxide finds many interesting biomedical applications as a common readout for enzyme-linked assays which commonly consume or produce hydrogen peroxide as a part of their readout.[192,193] Given the biological importance of this molecule the ability to rapidly, accurately and sensitively detect relevant concentrations in complex media is desirable.

Nano-enabled electrochemical sensors have been developed for the detection of hydro-

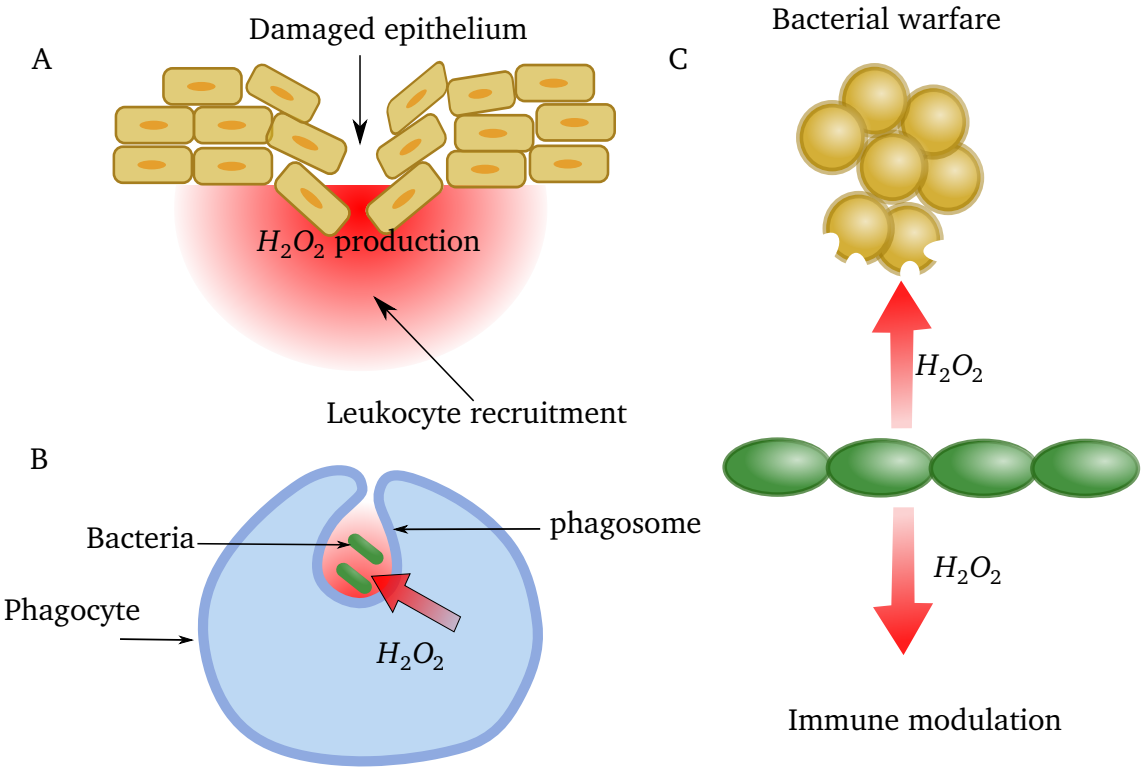

Figure 8: Illustration of some of the roles hydrogen peroxide production can have both as part of the immune system and bacterial survival. At the site of inflammation, hydrogen peroxide release can lead to recruitment of immune cells such as leukocytes, upon arrival antioxidants are secreted and thereby hydrogen peroxide dependent immune signalling can occur as illustrated in A). In B) hydrogen peroxide secretion is illustrated as an important component of the hostile environments which phagocytes can produce in their phagosomes to kill bacteria. Two important roles of bacterial hydrogen peroxide are illustrated in C): as a chemical agent to inhibit the growth of a competing bacterial species (e.g. *S. pneumoniae* (green) inhibition of *S. aureus* (golden)) and for immune modulation whereby hydrogen peroxide production can be used to interfere with immunological signalling pathways.

gen peroxide. These systems can be broadly categorised into three categories: chemiresistive, conductometric and field-effect transistor systems.[194] Chemiresistive sensors rely on a change in resistance of a sensor film to detect analyte concentration, in the case of hydrogen peroxide this is typically caused by a direct reaction with the sensor. For instance, SnO_2 nanostructured films with surface adsorbed oxygen displayed a hydrogen peroxide dependent electron loss and consequent increase in resistance with a linear range from 0.5 to 20 mM.[195] Conductometric sensors measure an overall change in the conductivity of the solution due to analyte dependent creation or consumption of ions, for instance, hydrogen peroxide reaction with iodide ions with a measurement range from 0.005 to 0.3 mM.[196] Lastly, field-effect transistors exploit the dependence of current flow on the surface charge to detect their analyte as in the case of ZnO nanorods with a linear range from 0.05 to 70 mM.[197] The role of nano-

materials in these cases is mainly to increase the surface area and thereby to lower the limits of detection. All of these methods require contact between the measurement system and the sensor, with the potential for increased contamination. Moreover, these methods are poorly suited to the higher throughput of well-plate systems commonly used in biological assays.

An alternative form of sensing which can avoid these problems is optical sensing. Inorganic nanomaterials for optical hydrogen peroxide sensing have emerged as important technologies in this field. Such systems can be based on chemically modified quantum dots as in the case of glutathione-capped CdTe with detection in the range of 0.1 to 10 mM.[198] Fluorescent N-doped silicon quantum dots which were quenched with silver nanoparticles were applied, utilising the hydrogen peroxide oxidation of the silver to recover the fluorescent properties, yielding a limit of detection of 1.5 µM.[199] The ability of cerium dioxide nanoparticles to catalytically reduce hydrogen peroxide has also led to wide interest in their application for hydrogen peroxide measurement. For instance, the affinity of cerium dioxide nanoparticles for hydrogen peroxide over DNA was made use of in a sensor designed by Biwu et al.[200] In the sensor design, the DNA was fluorescently tagged such that when it was adsorbed on the cerium dioxide surface the fluorescence of the DNA was quenched. The presence of hydrogen peroxide displaced the DNA and therefore its fluorescence properties were restored with the detection of hydrogen peroxide down to 0.13 µM.[200]

Luminescent cerium phosphate doped with terbium has been used for hydrogen peroxide sensing due to hydrogen peroxide-induced luminescence quenching with a limit of detection at 1.03 µM.[201] Similarly, cerium dioxide nanoparticles doped with europium have also been used, with detection down to 0.15 µM.[202] The luminescence emission of these nanoparticle systems originates from the lanthanide ion (Tb^{3+} and Eu^{3+}), but their excitation occurs due to the Ce-O charge transfer absorbance in the UV.[203] The proposed sensing mechanism suggests that due to the oxidation of the cerium dioxide there is an increase in the Ce-O coordination number and therefore a decrease in the Ce-O charge transfer absorbance which also lowers the emission from the lanthanide ions.[204,205] Although excellent limits of detection were achieved with such a system, due to the reliance on a decrease in luminescence intensity of a single peak the sensors lack robustness to some potential forms of sample interference.[84] For instance, in the case of bacterial growth in a medium, the scattering of light is greatly enhanced compared with the sterile medium which could appear as an increase in hydrogen peroxide concentration. Therefore, the realisation of a ratiometric sensing system could greatly improve the robustness as will be described in Paper III.

2.7 Biological ammonia sensing

Ammonia is another biologically important small molecule with carefully controlled levels in the human body linked to a broad range of metabolic functions, it is therefore also an interesting bioanalyte for detection. Ammonia can be found both in the basic NH_3 and the conjugate acid NH_4^+, although with a pK_a in human plasma at 37 °C of 9.01 the ionised NH_4^+ form is predominant (approximately 98%) at physiological pH. [206,207] Unless indicated the term ammonia is used here to refer to the total content of both NH_3 and NH_4^+. A significant contribution to blood ammonia levels is due to bacterial ammonia production in the gut, where urease activity produces carbon dioxide and ammonia from urea. [208] Another significant ammonia source are the kidneys through hydrolysis of glutamine. Levels of blood ammonia are carefully controlled to a large extent by regulatory mechanisms in the liver which incorporate ammonia in urea for excretion by the kidneys. [207] Alternatively, ammonia can also be removed by extrahepatic tissue by incorporation into glutamine for subsequent processing by the kidneys to ammonia and ultimately conversion to urea by the liver for subsequent excretion by the kidneys. These intricate regulation mechanisms, illustrated in Figure 9, exist due to the toxicity which ammonia can present. Ammonia can traffic through the blood-brain barrier and cause neuro-toxicity potentially leading to coma and death. Plasma ammonia levels should be below 50 µM in adults and 100 µM in newborn babies, ammonia levels greater than these are considered hyperammonaemia. Visual diagnosis can be challenging as patients can present with symptoms from mild cognitive and behavioural changes to coma. [209] Thus there is a clear need for readily available point-of-care diagnostic devices for the determination of blood ammonia levels.

Due to the volatile nature of the non-ionic NH_3 breath ammonia analysis may appear an attractive strategy. However, ammonia clearance by the lungs is minute in comparison to other clearance mechanisms. [210] In addition, exhaled breath ammonia is influenced by the urease activity of the resident microbiota of the oral cavity and therefore may not accurately represent blood ammonia levels. [211] Therefore, although in well-controlled settings a breath ammonia sensor may present a valid option for continuous monitoring, such as during hemodialysis, in poorly controlled point-of-care applications direct blood ammonia concentration determination may present a better option. At the time of writing to the best of the author's knowledge, there exists only one commercially available point-of-care ammonia analyser the PocketChem™ BA Blood Ammonia Meter (Arkray). The blood sample is first alkalised to convert ammonia present to volatile non-ionic NH_3 which by gas phase diffusion can pass through a membrane and cause a colour change in a bromocresol green indicator strip. The colour of the strip is mea-

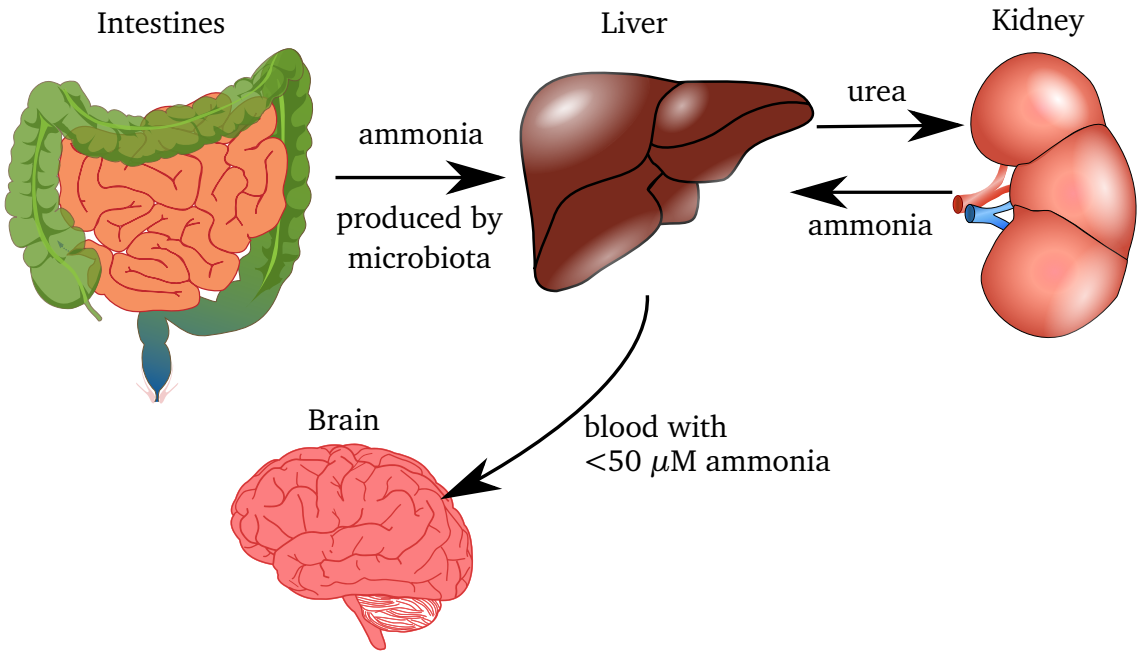

Figure 9: Schematic diagram of major ammonia metabolic routes in the human body. Significant quantities of ammonia are produced by the resident microbiota of the intestine by urease action. The ammonia enters the bloodstream by diffusion and is transported by the portal vein to the liver where ammonia is converted to urea to be secreted by the kidneys. The kidneys also break down glutamine produced in the muscles which releases ammonia. In some disease states, for instance, liver cirrhosis, the regulation of ammonia may fail leading to high ammonia levels ($> 50\,\mu M$) reaching the brain and leading to neurotoxicity.

sured by the PocketChem meter and correlated to an ammonia concentration.[28] An alternative gas-phase sensor for blood ammonia concentration measurement has been developed, relying again on the conversion of ammonia to volatile non-ionic NH_3 and applying a fuel cell which generates a current in the presence of ammonia.[26] In principle, it seems that many of the other gas-phase sensors should also be compatible with such a measurement approach.[212]

Clinical ammonia determination is typically done in liquid with glutamate dehydrogenase enzymatic assays with spectroscopic readout. This has also been expanded to a paper-based enzymatic assay by Sheini with detection down to $35\,\mu M$.[213] Direct electrochemical determination of blood ammonia has also been demonstrated by Branelly et al. in 15 minutes with a limit of detection in serum of $25\,\mu M$.[214] Selective membranes have also been applied for ammonia detection, for instance by the application of selective polymerosomes with encapsulated fluorescent dyes.[215] Alternatively, perfluorosulfonic acid polymers have been used to allow for the separation of ammonia from whole blood and subsequent detection using a modified version of the well-known Berthelot reaction.[27,216] Although ammonia levels can be effectively

determined in clinical laboratories and point-of-care systems do exist the development of a cheap disposable system which does not rely on a custom readout device remains an attractive proposition as will be explored in Paper IV.

3 Research aims

The overall aims of this thesis were to develop translatable nanotechnological strategies for the treatment of established biofilms and the development of novel sensors for the measurement of bioanalyte concentrations relevant to disease.

More specifically, the aims were:

- To develop a near-IR photothermal spherical silver nanoparticle based approach capable of killing established biofilms on a catheter mimicking surface (Paper I).
- To synthesise a luminescent pH sensitive surface capable of measuring the pH at the interface of the biofilm and the surface it is growing on (Paper II).
- To further improve luminescent cerium dioxide sensors for the robust detection of hydrogen peroxide produced by bacteria in complex media (Paper III).
- To detect ammonia concentration in physiologically relevant ranges optically in a fashion compatible with naked-eye detection and with the potential for point-of-care application (Paper IV).

4 Methodological considerations

In this chapter considerations regarding the choice of methodologies applied across the work described in this thesis will be discussed. Rather than a discussion of each separate work similar methods across the papers will be combined and discussed together. Detailed materials and methods sections can be found in the individual publications.

4.1 Regarding synthesis and characterisation

An important initial consideration valid for all publications in this thesis regards the synthesis technique: flame spray pyrolysis. The main advantages of this synthesis technique are scalability and reproducibility of the generated dry nano-powders. However, the nanoparticles or more descriptively termed fractal-like nanoaggregates generated by this technique are, typically, confined to metal oxides and metal salts such as phosphates. Post-synthetic modifications can be applied to alter the nanomaterials, however, this inevitably impacts the main two advantages of scalability and reproducibility.

Moreover, aerosol assembly of these nanoaggregates defines their aggregate structure. Therefore, the FSP production of single non-aggregated nanoparticles is poorly feasible. Even if size-selection is applied to the aerosol, resulting in significantly lower yields, the primary particle sizes would be challenging to select for as the nanoaggregate size will dominate. Therefore although primary particle sizes can be below 5 nm the nanoaggregate size can be upwards of 100 nm. However, despite these limitations, FSP remains a highly attractive synthesis method. Synthesis of a wide range of elemental compositions can easily be performed. Control of the oxidation state and primary particle size can be performed directly in the flame by controlling process parameters such as gas flow rates, precursor flow rate and precursor composition. Meta-stable phases can be accessed in the steep flame temperature gradients. The fractal-like nanoaggregate geometry can give rise to unique properties, and the exposed surface area of the nanoparticles need not differ greatly from equivalent dispersed particles. The high

exposed surface area is therefore maintained and available for applications such as sensing and drug loading. Finally, FSP allows for the production of dry nanopowders in a scalable fashion or their direct aerosol deposition onto substrates. Therefore FSP remains a highly attractive synthesis technique. [31,32,89,91]

A critical aspect of characterisation is size determination, over the course of the papers described in this thesis determination of nanoparticle size has been performed with scanning transmission electron microscopy (STEM), transmission electron microscopy (TEM), scanning electron microscopy (SEM), dynamic light scattering (DLS), powder X-ray diffraction (XRD) and specific surface area measurements by application of Brunauer-Emmet-Teller theory (BET) to N_2 adsorption measurements. SEM involves scanning a beam of highly focused electrons across a sample and detecting the scattered or emitted electrons, back-scattered electrons provide information on topology and atomic mass since heavier elements scatter more. Secondary electrons are inelastically scattered from the sample and due to the lower energy, those detected arise close to the material surface, providing greater topological information than back-scattered electrons which can be detected from deeper into the material. TEM involves focusing a broader beam of electrons onto a sample and re-focusing the transmitted electrons onto a detector to form an image. Electrons which are scattered by the sample cannot be re-focused onto the image providing information about the sample, scattering is greater for higher density, thickness and atomic mass. An important consideration is that the overall sample thickness must be sufficiently thin so that electrons can be transmitted. STEM is a modification of TEM in which, rather than illuminating the whole image, the beam is focused to a point and scanned across the sample. Therefore the scattered electrons or generated X-rays from each point can be measured separately allowing for additional spectroscopic information to be derived while retaining spatial information.

Provided the sample shows sufficient contrast STEM, TEM and SEM can perhaps give the most realistic understanding of the particle sizes as they are able to image both the primary particles and the nanoaggregates. Moreover, SEM, STEM and TEM can provide information on the size distributions. BET determined specific surface areas can also be correlated to a primary particle size assuming particular particle geometry and density distributions (e.g. spherical and uniformly dense). Finally, the only solution-phase measurement of size performed in this thesis is DLS. This technique determines hydrodynamic diameter by measuring particle diffusion using scattering of laser light. This technique, therefore, measures on the level of the entire nanoaggregate and moreover, is susceptible to solution-phase aggregation. All these techniques mea-

sure distinct aspects of nanoparticle size and careful consideration of the determined sizes is important for a good understanding of the nanoparticle properties.

XRD allows for the analysis of the crystalline structure of materials. An X-ray beam is used to irradiate the sample at an angle, due to the short wavelength of X-rays they can be diffracted by the atoms present in the sample. If there is a periodic arrangement of atoms in the sample, as in a crystalline material, then constructive interference can occur at particular detection angles. The exact angles at which this interference occurs is determined by the wavelength of the X-rays (usually kept constant) and the periodic spacing of the atoms. Therefore by measuring the angles at which constructive interference occurs information on the crystal planes of the crystalline lattice can be derived. By analysis of the angle and pattern of the diffraction peaks observed and comparison with a database of known materials crystal phase composition can be determined. Subsequent analysis by whole powder pattern fitting such as Rietveld refinement can provide detailed information such as relative phase concentrations and the average size of the crystallites in the sample. Where applicable, particle composition was further assessed by vibrational spectroscopy using Fourier-transform infrared spectroscopy (FTIR). This technique utilises the absorbance of photons resonant to molecular bond vibrations of certain allowed vibrational modes. In this way, vibrational frequencies of molecules can be determined which are characteristic of the particular molecular bonds involved. Thus the presence and quantity of infrared active chemical species can be determined as applied in Paper II.

Elemental analysis has been performed using energy-dispersive X-ray spectroscopy (EDS) in SEM and STEM. In this technique core-level electrons of an atom are excited to higher energy levels, subsequent relaxation processes may result in X-ray emission. Due to the discrete characteristic spacing of core energy levels of elements the wavelengths of X-ray emission can identify the element they originate from. However, the infrequent nature of this process of X-ray generation means that EDS spatial resolution must often be decreased to allow for reasonable measurement times and signal to noise levels in EDS spectra can be low. A complementary technique for elemental analysis is electron energy loss spectroscopy (EELS), performed in Paper I using STEM by Thomas Thersleff. EELS analyses transmitted electron energies for inelastic losses due to the atomic core or outer energy level electron excitation. EDS has higher sensitivity to heavier elements, whereas EELS is more suited for light element identification. The computational data fusion of EELS and EDS developed by Thersleff et al. allows for remarkable enhancements in signal to noise but is still a highly specialised technique requiring advanced instrumentation and all collection and analysis was performed by

Thomas Thersleff in Paper I.[217] The STEM and EDS data collection and analysis in Paper III were performed by Ling Xie and Klaus Leifer.

Detailed chemical and elemental information can be obtained from X-ray photoelectron spectroscopy (XPS) and electron paramagnetic resonance (EPR) spectroscopy as applied in Paper III. XPS involves X-ray bombardment of a sample and measurement of emitted electron energies which can be related to the electronic energy levels from which they originate. Thus XPS can provide elemental information, and at higher spectral resolution XPS can also provide information on subtle shifts in energy levels which can be linked to, for instance, the oxidation states and bonding of the elements. EPR spectroscopy relies on energy level splitting of the spin quantum number in unpaired electrons (paramagnetic materials) when a magnetic field is applied, this provides a ground-level and excited state which can cause photon absorption allowing precise determination of the energy difference between the split energy levels. The variables determining the magnitude of the energy level splitting are the magnetic field strength and the "g-factor" or dimensionless magnetic moment of the electron. The g-factor can be strongly influenced by the electronic environment of the electron and can therefore provide important information on the bonding environment of the electron. The XPS and EPR measurements and analysis presented in Paper III were performed by Eleftherios Mouzourakis, Constantinos Moularas and Yiannis Deligiannakis.

The optical extinction measurements consist of passing a beam of light with a defined bandwidth through a sample and recording the intensity for comparison against a reference intensity to determine how much of the incident beam passed through. However, the processes giving rise to a difference in measured transmission intensity need not only arise due to the absorption of light by the sample. If scattering processes occur then some of the light intensity can be redirected, and not detected, without being absorbed. Therefore, quantification of absorbance requires separate measurements of both total scattered and absorbed light. With molecular solutions and small nanoparticles, the contribution of the scattering to the extinction measurement is typically small and therefore the extinction is sometimes considered to be equivalent to the absorbance.

Photoluminescence measurements have been performed in Paper II and Paper III with a luminescence spectrometer. In order to characterise the emission wavelengths of a system, a beam of light with a controlled wavelength illuminates the sample and the wavelengths of emitted light are recorded. Excitation wavelengths can be assessed by scanning the wavelengths of a broadband light source across the sample and recording the emission of either a single wavelength or the entire emission spectrum. Importantly

for phosphorescence measurements, a pulsed light source can be used allowing for control over a delay between the excitation pulse and emission measurement. This can be used to remove the fast-decaying autofluorescence background and retain the slow-decaying phosphorescence signal thereby improving the signal to noise ratio. Wide-field fluorescence microscopy has also been applied, in which case the excitation beam and the emission from a sample are passed through optical filters and dichroic mirrors to select for the desired wavelengths before impinging on the sample or detection camera respectively.

Supporting simulations to better understand the interparticle coupling of silver nanoaggregates were performed. The prerequisite for this is three-dimensional models of representative nanoaggregate structures. Models have been developed to generate such nanoaggregates using for instance finite element modelling to recreate flame processes. However, simpler less computationally intense packages have also been developed which are able to recreate the nanoaggregate morphologies. FracVal developed by Morán and others is one such package and was used here to generate the fractal nanoaggregates. [218] These nanoaggregates were then loaded into R and processed by the coupled dipole approximation package cda developed by Baptiste Augié to simulate their extinction spectra. [219,220]

4.2 Considerations regarding bacterial work

In this section, I will briefly discuss the choice of bacterial species and strains as well as growth conditions. The growth of bacteria has been assessed principally by two methods optical scattering at 600 nm (OD600) and colony-forming units (CFU). OD600 measurements provide an easy and quick method to determine the approximate number of bacteria in a culture and were used here principally to normalise bacterial starting dose rather than quantify an effect. This measurement relies on live bacteria being intact scattering bodies, whereas upon death they should lyse and therefore scattering should decrease. This, therefore, does not give any information on whether the bacteria are still metabolically active or capable of reproducing. In addition, differently sized bacteria and clumped bacteria can scatter light differently leading to differences in their OD600 even if the bacterial concentration is similar. To assess the number of bacteria capable of reproducing the bacteria are spread onto a solid surface containing a growth medium. This allows them to grow but only supports minimal opportunity for movement, if the bacteria are capable of dividing then they will produce a cluster of bacteria around them which will eventually form a macroscopically visible colony. By spreading

the bacteria from liquid culture out at a sufficiently low density the number of such macroscopic colonies can be counted and related to the number of live bacteria (CFU counting). Live/dead staining was also applied for the assessment of bacterial viability, the method used here relied on two dyes which greatly enhance their fluorescence upon DNA binding: propidium iodide (red emission) and SYTO 9 (green emission). SYTO 9 is membrane permeable and so can pass into cells, bind to nucleic acids and provide a green fluorescent signal. Propidium iodide is less membrane-permeable and so can only traverse damaged membranes of dead, or dying cells. Propidium iodide can displace bound SYTO 9, therefore under appropriate fluorescence illumination, live cells with intact membranes appear green and dead or dying cells (with damaged membranes) appear red.

Biofilm formation was assessed by determining the number of bacteria or the biomass they produced which is adherent to a surface. In order to do this after incubation to allow for bacterial growth, the substrates were rinsed, with the intention of displacing loosely attached bacteria. This rinsing step is important as the intensity of it influences bacterial removal and can be a source of great variability between experiments and laboratories. Quantification of remaining bacteria was performed by CFU counting and measurement of remaining biomass by crystal violet staining.

As discussed in 2.3 naturally occurring biofilms are typically multi-species phenomena, however, for ease of reproducibility and interpretation mono-species biofilms are often performed in laboratory settings. This was also the case for the projects described here. Moreover, biofilms grown here were performed in static conditions, whereas particularly in the case of urinary catheter implants shear stresses could be expected. This decision was made due to the additional complexity of biofilm growth under flow conditions.

An additional important consideration is the choice of bacteria. Catheters were chosen as an example application in Paper I, as such two bacterial species commonly associated with catheter infections were chosen: *S. aureus* (ATCC 25923) and *E. coli* (HVM52). Both strains are clinical isolates and in particular, HVM52 was isolated from a catheter-associated urinary tract infection and therefore has high relevance. In Paper II pathogenic bacteria which are known to form different biofilm pH were selected with *E. coli* (strains HVM52 and DH5α) known to produce highly acidic biofilms and *P. aeruginosa* (PA01) known to produce less acidic biofilms. *K. pneumoniae* (iA565) was also included as it is a frequent cause of nosocomial infections, a facultative anaerobe and known to be a potent biofilm former.

Ethical Considerations

Scientific research involving the use of clinical samples or data requires a thorough consideration of the benefits and potential risks in terms of both privacy and potential harm to the patient. Moreover, animal experiments require careful consideration of whether the methodology is appropriate and necessary, whether there is any other possible non-animal alternative, how to minimise the number of animals and their suffering and whether the results it will yield are sufficiently valuable. The projects presented in this thesis did not involve patient samples or animal work and as such no ethical permits were required.

5 Results and discussion

In this chapter, the main findings of the papers included in this thesis will be briefly presented and discussed.

Paper I: Plasmonic coupling in silver nanoparticle aggregates and their polymer composite films for near-infrared photothermal biofilm eradication

The main aims of Paper I (summarised in Figure 10) were to demonstrate the facile synthesis of spherical silver nanoparticles with controlled extinction and photothermal properties reaching into the near-IR. As a demonstration of a potential application, the nanoparticles were deposited on a substrate to render it photothermal and used for the eradication of established biofilms. Spherical silver nanoparticles were synthesised by FSP supported on silica, during the aggregation process the silica acts as a spacer between the silver nanoparticles and limits sintering and coalescence. Therefore the silica acts as a dielectric glue which holds the silver nanoparticles apart. By carefully varying the silica content the spacing between the silver nanoparticles can be controlled. In this way, the interparticle plasmonic coupling is controlled to shift the extinction into the near-IR. The extinction of deposited films and liquid solutions was measured by UV-Visible spectroscopy, and with 25 wt% of silica the extinction peak was located at just above 400 nm as can be expected for well-separated spherical silver nanoparticles. However, as the silica wt% was decreased to 6 wt%, 4 wt% and 2 wt% a clear second peak was observed at higher wavelengths with a tail extending into the near-IR region.

As described previously multiple phenomena can affect the extinction spectra of plasmonic nanoparticles such as the size of the nanoparticles. Measurements by XRD of the crystallite size showed that between 4 and 6 wt% silica there was only a difference of 0.3 nm and by TEM the difference in primary particle diameter was 0.9 nm. Sim-

ulations of extinction spectra from fractal-like nanoaggregates with varying primary particle sizes were performed, based on these simulations and previous literature it was determined that the small changes in primary particle size alone would not give rise to the large shifts in extinction spectra observed. However, shifts of only a couple of nanometers in the inter-particle distance were sufficient to produce large spectral shifts in the simulated extinction spectra. Changes in inter-particle distances with increasing silica wt% can be observed in the TEM images, however, accurate quantification of inter-particle distance is challenging due to the dense nature of nanoaggregates and since TEM images are two-dimensional representations of the three-dimensional nanoaggregates. The differences in inter-particle distances between the silica wt% were determined in order to perform an approximate comparison and a trend towards increasing inter-particle distances was observed with changes on the order of 1 nm between 4 and 6 wt%. Considering, therefore, the comparison between simulation and experimental data together with previous studies the spectral shift in extinction was mainly ascribed to changes in inter-particle distance. Elemental mapping was also performed to confirm that indeed the silica was located between spherical silver nanoparticles and therefore appears to act as a dielectric spacer.

Photothermal behaviour relies on a light source to provide the energy for heat generation, therefore, the choice of optimally tuned extinction is dependent also on the wavelength of the light source. In this study, high extinction at 808 nm was desired as this was the centre wavelength of the near-IR laser used, and therefore the 2 wt% silica condition was most suited. However, high extinction does not necessarily guarantee good photothermal activity and therefore all silica wt% were also evaluated with trends consistent with the extinction data. In these dry conditions, 2 wt% silica reached the highest temperature of over 100 °C and was therefore chosen for further experiments.

The application to demonstrate the effectiveness of the photothermal behaviour was chosen to be biofilms on catheters. An immediate potential confounding factor would be the antibacterial action of the silver nanoparticles themselves. Moreover, silver can be cytotoxic and concerns exist regarding the clearance of these nanomaterials in the human body. Therefore the photothermal nanoaggregates were directly deposited from FSP on a layer of spin-coated polydimethylsiloxane (PDMS), which is the same material used for many catheters and subsequently completely encased in PDMS by spin-coating an additional PDMS layer on top. Although this did affect the extinction profiles of the films, similar near-IR extinction values at 808 nm were maintained after encasing in PDMS. No silver ion release was detected by silver ion selective electrode measurements.

Biofilms were then formed on the PDMS surfaces and irradiated with 808 nm laser light at an intensity of 1.4 Wcm^{-2} for different periods of time. After 300 s and 600 s no CFUs were retrieved from biofilms of *E. coli* and *S. aureus* respectively. This corresponds to final temperatures of the liquid at 300 s and 600 s of almost 70 °C. Although these temperatures are substantially higher than what would likely be desirable in a clinical setting it nonetheless demonstrates the powerful photothermal capacity of the deposited nanoaggregates. Paper I therefore demonstrates the facile synthesis of near-IR photothermally active plasmonic nanoaggregates of spherical silver nanoparticles and their direct aerosol deposition.

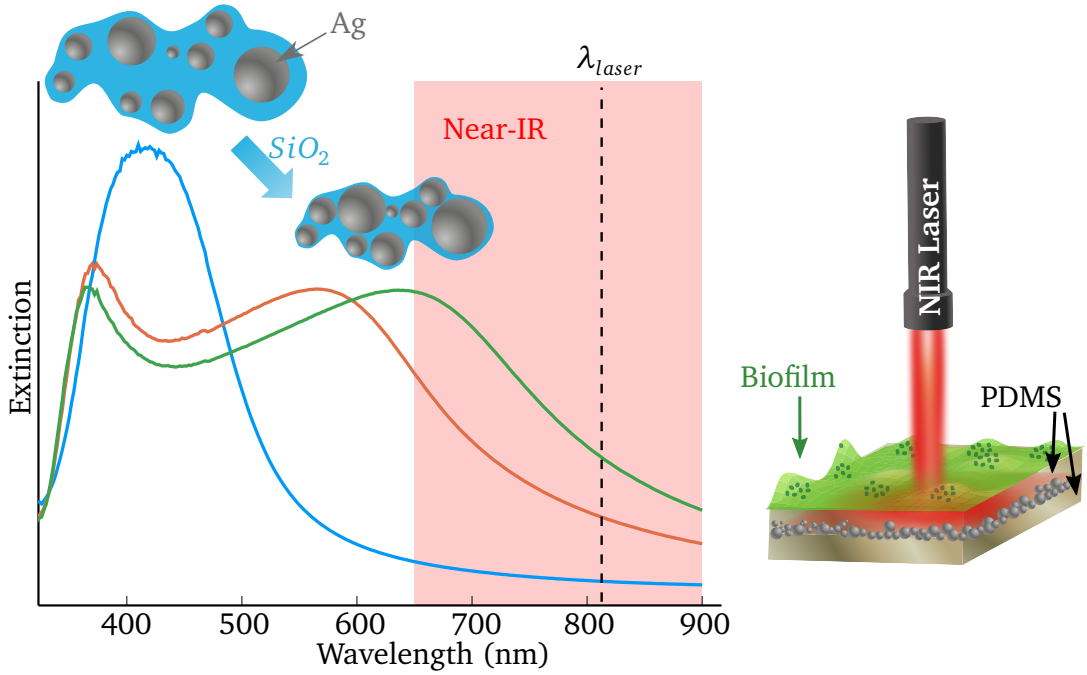

Figure 10: Overview of the content of Paper I demonstrating the tuning of the extinction of the silver nanoaggregates by using silica as a dielectric spacer to control the average interparticle distance between primary silver nanoparticles. Having tuned the extinction into the near-IR these silver nanoaggregates were deposited as a coating encased between two layers of PDMS. Biofilms were then grown on this PDMS catheter mimicking surface and the temperature increase due to near-IR irradiation used to eradicate the formed biofilms.

Paper II: Biofilm interfacial acidity evaluation by pH-responsive luminescent nanoparticle films

Paper II describes the synthesis of pH-sensitive luminescent films of calcium phosphate nanoparticles for the measurement of biofilm interfacial pH as schematically depicted in Figure 11. The initial aim of this project was inspired by Paper III, and intended to deposit films capitalising on the pH-dependent solubility of calcium phosphate doped with europium (CaP:Eu^{3+}) and the pH-independent solubility of a reference signal (e.g. Y_2O_3:Tb^{3+}) to generate a ratiometric pH-sensitive surface. However, initial experiments of CaP:Eu^{3+} films revealed an interesting pH-dependent spectral feature. The emission spectrum of CaP:Eu^{3+} consists of two spectrally resolved major peaks, one at approximately 590 nm and the other at 614 nm. When immersed in an acetate buffer at pH 5.5 the peak at 614 nm strongly reduces in intensity, whereas the peak at 590 nm undergoes no major decrease. However, in a pH 7 buffer or ultra-pure water, both peaks at 614 nm and 590 nm remain stable. Therefore a ratiometric sensor response was obtained with only CaP:Eu^{3+}. Moreover, the two peaks are located spectrally close to each other, and therefore any change in absorbance of the medium in which they are immersed due to scattering phenomena is likely to affect both peaks equally.

The luminescence excitation of the CaP:Eu^{3+} nanoparticle films is performed at 252 nm and therefore excites lattice charge transfer bands of the CaP which subsequently transfer the energy to excite the Eu^{3+}. It, therefore, follows that if the particles dissolve this energy transfer process from the lattice to the Eu^{3+} should stop. The ratiometric shift should therefore be understood to be a more subtle process. The peak at 590 nm is due to a magnetic dipole transition which is relatively insensitive to changes in site symmetry, however, the peak at 614 nm is an electric dipole transition which is highly sensitive to the symmetry of the Eu^{3+}.[75] An asymmetry ratio ($A_R = \frac{I_{614}}{I_{590}}$) is often used to compare this effect with a higher asymmetry in the Eu^{3+} site leading to a higher A_R. Thus at lower pH there appears to be some rearrangement in the lattice symmetry around the Eu^{3+} ion. This, therefore, enables the CaP:Eu^{3+} to be an all-inorganic ratiometric pH sensor.

A more detailed analysis of the synthesised nanoparticle composition reveals by XRD the presence of crystalline hydroxyapatite and a very minor lime phase. By FTIR peaks are detected corresponding to PO_4^{3-} but also CO_3^-, indicating that the hydroxyapatite formed is likely carbonated hydroxyapatite. The presence of CO_3^- can be explained as a likely consequence of the Ca/P ratio used in the precursor, in order to promote the formation of crystalline hydroxyapatite an excess of Ca was added at a Ca/P ratio

of 2.19 (stoichiometric hydroxyapatite has a Ca/P of 1.67). The CO_3^- can therefore act as a counter-ion for the excess of Ca^{2+}. The CO_3^- is also suggested as the likely cause of the changes in A_R at pH 5.5. A decrease in Ca/P ratio in the precursor of the CaP coatings yields coatings with a decreased A_R and also a decreased CO_3^- content. Moreover, a clear decrease in CO_3^- content was observed after the CaP coatings were incubated in pH 5.5 buffer whereas no such change was observed in ultra-pure water. It is therefore suggested that at pH 5.5 lattice rearrangements can occur releasing the CO_3^- from the lattice and increasing the symmetry of the Eu^{3+} lattice site causing the change in asymmetry ratio.

Since the target application was bacterial growth, calibration of the sensor was performed in bacterial growth medium (modified M9) at 37 °C from pH 4 to pH 7 for up to 48 hours. Although even at a pH of 7 some gradual change in A_R was observed over the 48 hour period, at lower pHs the A_R converged to stable values. Growth medium was replaced with fresh medium after 8 and 24 hours. The relationship between pH and A_R is non-linear and therefore interpolation was used to establish a relationship across the pH range 4 to 7. The CaP films were subsequently incubated in the presence of bacteria capable of forming biofilms on their surface in a buffered M9 minimal medium at a pH of 6.75 and the luminescence of the films was monitored to determine the pH which the biofilm produced. The pHs determined for the biofilms of *E. coli* and *P. aeruginosa* of close to pH 4 and pH 6.5 respectively were in good agreement with values previously determined by confocal microscopy.[183,221]

Some limitations are apparent for this sensor, no detailed assessment of interfering agents was performed, however, it is reasonable to expect properties of the medium such as the ionic concentration and in particular the Ca^{2+} and PO_4^{3-} concentrations to play an important role in the solubility and therefore perhaps also lattice restructuring of the CaP films. Therefore calibration should be performed in the desired growth medium and at the desired measurement time points. Moreover, the release of Ca^{2+} and PO_4^{3-} into the medium at low pHs can be observed and potential influence on pH and bacterial growth should be considered. In addition, the A_R was not recovered when the pH of the medium was increased, the pH values measured are therefore the minimum values attained. However, provided these caveats are considered the developed CaP:Eu^{3+} can be used for biofilm pH determination. Moreover, the system is compatible with the well-plate style format commonly used to achieve higher throughput in biological applications providing a significant advantage over confocal microscopy.

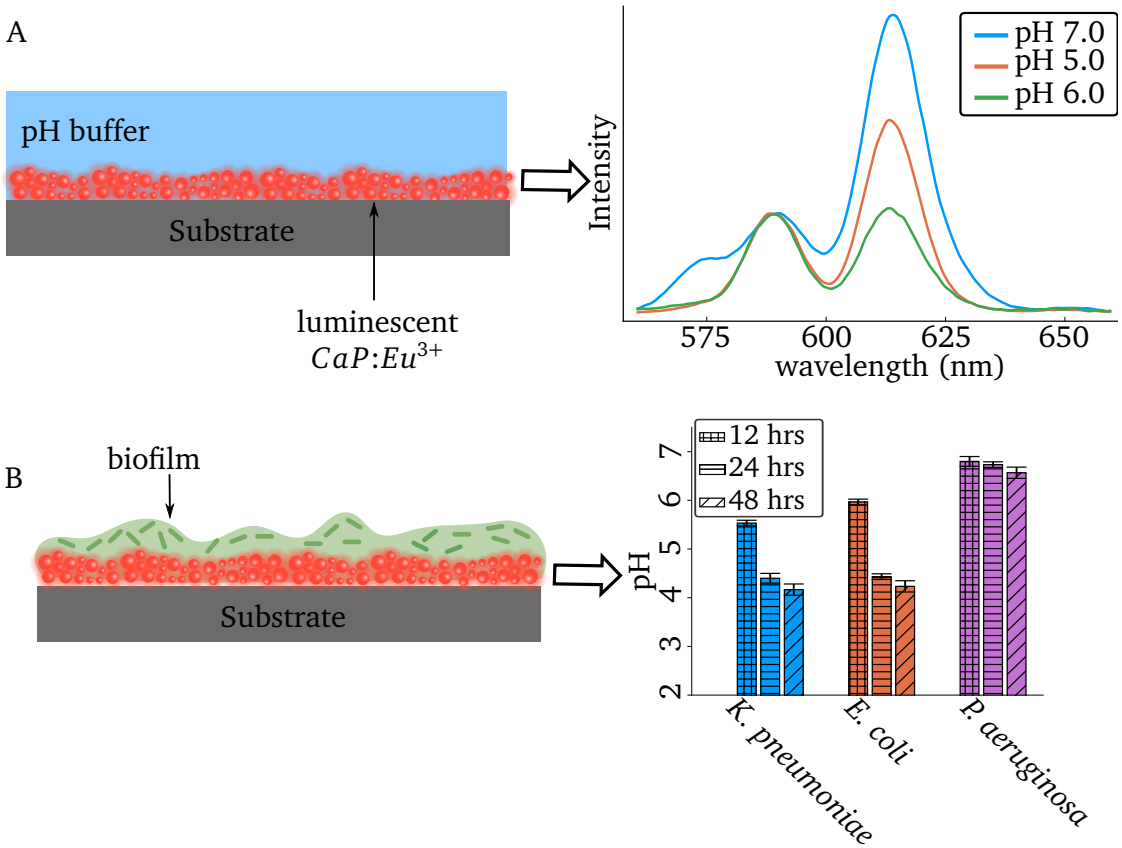

Figure 11: Graphical summary of the work in Paper II. Initially, the synthesised films were subjected to various pH buffers in order to understand the pH dependence of the luminescence emission, as shown in A), with a ratiometric sensor response observed. Biofilms were then grown on the surface of the CaP:Eu^{3+} films as shown in B), with the luminescence emission of the films over 48 hours correlated to the biofilm pH.

Paper III: Luminescent CeO_2:Eu^{3+} nanocrystals for robust in situ H_2O_2 real-time detection in bacterial cell cultures

In Paper III the core hydrogen peroxide sensing capabilities previously developed of CeO_2:Eu^{3+} are further developed to allow for more robust hydrogen peroxide detection from complex media such as bacterial cell cultures. The essence of the previously developed system was that the luminescence emission of CeO_2:Eu^{3+} became quenched in a hydrogen peroxide concentration-dependent manner. The readout was therefore purely a decrease in luminescence intensity and as described previously could be vulnerable to absorbance changes in the medium appearing as hydrogen peroxide concentration changes. Therefore in order to generate a robust signal, several approaches were taken. During bacterial growth changes to the optical properties of the medium occur. By

depositing CeO_2:Eu^{3+} onto optically transparent glass coverslips measurements could be performed through the glass without the luminescence emission or excitation beam passing through the potentially scattering bacterial growth medium.

An alternative method is to develop a ratiometric sensor response by providing an additional reference luminescent signal, therefore changes in absorbance due to the relatively broadband scattering processes of bacterial growth should affect both the reference signal and the sensor signal to a similar degree. The reference signal is produced by Y_2O_3:Tb^{3+} which does not show hydrogen peroxide dependent luminescent changes. Both Y_2O_3:Tb^{3+} and CeO_2:Eu^{3+} can be excited at the same wavelength but Y_2O_3:Tb^{3+} exhibits emission at 545 nm and CeO_2:Eu^{3+} at 590 nm. This, however, poses a synthetic challenge in a single flame as the CeO_2:Eu^{3+} and Y_2O_3:Tb^{3+} phases should exist separately and inter-mixing of the dopants between the two lattices is undesirable. The sensitivity of the hydrogen peroxide sensing capabilities of CeO_2:Eu^{3+} is also dependent on the nanoparticle size, with a smaller primary nanoparticle size allowing for higher sensitivity. Therefore a dual-flame synthesis was performed to allow the separate formation of the Y_2O_3:Tb^{3+} and CeO_2:Eu^{3+} nanoparticles, while the angle of the flame was controlled such that the high-temperature aerosols collided and allowed nanoscale mixing and firm adhesion between the two nanoparticle compositions. A schematic summary of this sensing system is provided in Figure 12.

Measurement of the luminescence emission at different hydrogen peroxide concentrations confirmed the hydrogen peroxide sensing capabilities of CeO_2:Eu^{3+} were retained with the additional stable Y_2O_3:Tb^{3+} reference signal. Calibration with known hydrogen peroxide concentrations was then performed in C+Y bacterial growth medium and three strains of *S. pneumoniae* were grown in the presence of the dual emission ratiometric CeO_2:Eu^{3+}/Y_2O_3:Tb^{3+} and the luminescence emission measured. Two of the strains of *S. pneumoniae* generated elevated levels of hydrogen peroxide (strains BHN 31 and BHN 32) whereas the third strain which was genetically modified to lack the hydrogen peroxide producing spxB gene showed no hydrogen peroxide generation (BHN 123). These values were in good agreement with the previous enzymatic measurement of hydrogen peroxide production in the literature by these same strains.

Some aspects of the sensor design should be considered for its successful application. The wavelength of light used for excitation of the CeO_2:Eu^{3+}/Y_2O_3:Tb^{3+} is 330 nm when performed in a fluorescence spectrometer, which can be strongly absorbed and scattered. Therefore the sampling volume of the light should be considered in an experimental set-up, since excitation of the nanoparticles may not occur homogeneously throughout the sample. Furthermore, CeO_2 is a known antimicrobial and therefore

effects of the CeO_2 on bacterial growth should be considered.[222] Provided these aspects are considered measurements performed in Paper III demonstrate the potential for successful application of this inorganic ratiometric optical sensor for the detection of hydrogen peroxide in complex biological environments.

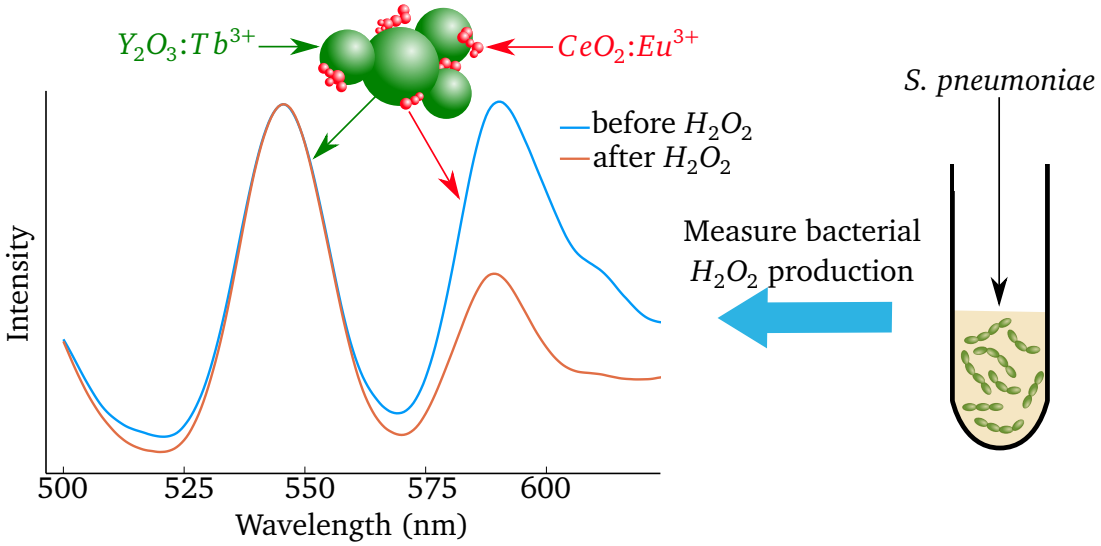

Figure 12: Schematic of the robust ratiometric sensor response developed in Paper III hydrogen peroxide sensitive red-emitting CeO_2:Eu^{3+} is combined with reference green-emitting Y_2O_3:Tb^{3+}. The luminescence of the CeO_2:Eu^{3+} decreases with increasing hydrogen peroxide concentrations whereas the Y_2O_3:Tb^{3+} maintains stable emission thereby providing a ratiometric sensor response. This sensor was then applied for the measurement of hydrogen peroxide production by *S. pneumoniae*.

Paper IV: Ammonia sensing by silver nanoparticles for point of care diagnostic applications

Paper IV describes the results obtained to date on the development of a silver nanoparticle enabled ammonia sensing assay. Dispersed silver nanoparticles display strong plasmonic extinction, observable by the naked eye as a yellow colour due to the extinction of light in the 400 nm region. Upon addition of a source of hypochlorite ions (ClO^-) such as NaOCl oxidative dissolution of the silver nanoparticles can occur in a stoichiometric fashion and therefore the extinction becomes attenuated. However, ammonia readily reacts with ClO^- and can therefore prevent the dissolution of the silver nanoparticles. In this way by adding a constant amount of ClO^- the ammonia concentration can be determined from the silver nanoparticle extinction: in high ammonia concentrations, little change to the silver nanoparticle extinction is observed whereas in low ammonia concentrations a strong decrease in silver nanoparticle extinction is

observed (summarised in Figure 13).

An important consideration is also the colloidal stability of the silver nanoparticle system and the ability for the measurement to be performed in solutions of different ionic strengths. Therefore in order to improve their colloidal stability, the silver nanoparticles are coated with a thin silica layer by using an FSP coating reactor. This allows for the successful measurement of ammonia concentrations in isotonic phosphate-buffered saline. By adjusting the concentration of ClO^- the sensing range can be adjusted. However, ClO^- is a reactive species and therefore the presence of easily oxidised species, such as can be found in proteins or serum, interferes with the ability of the assay to detect ammonia.

In order to allow for detection from these complex biological fluids a selective membrane is applied, this nafion perfluorosulfonic acid membrane allows the selective transport of small positively charged ions across it. The nafion membrane therefore allows for the selective separation of the positively charged ammonium ion (NH_4^+) from a biological fluid into a controlled sensing environment. This enabled the sensor to detect ammonia concentrations at levels relevant for human hyperammonaemia determination from PBS with concentrations of bovine serum albumin typically found in serum. Measurement time is strongly influenced by the separation process of the nafion membrane, occurring over 20 minutes to allow sufficient ammonia transfer. With subsequent ammonia determination in approximately 7 minutes. Therefore total measurement time approaches 30 minutes, a factor which further optimisation will aim to reduce.

In order to further develop this system for ease of use, the silver nanoparticles were collected as thin coatings on glass-fibre filter paper. The silver nanoparticle coated filter paper was then cut into thin strips ($\approx$ 1.3 mm wide and 10 mm long) and used to measure ammonia concentrations in a dip-stick style assay by inserting the end of the strip into the liquid containing ammonia and ClO^-. The wicking properties of the glass-fibre filter caused the liquid to travel up the strip and in low ammonia concentrations, the ClO^- dissolved the silver nanoparticles and removed the characteristic colour.

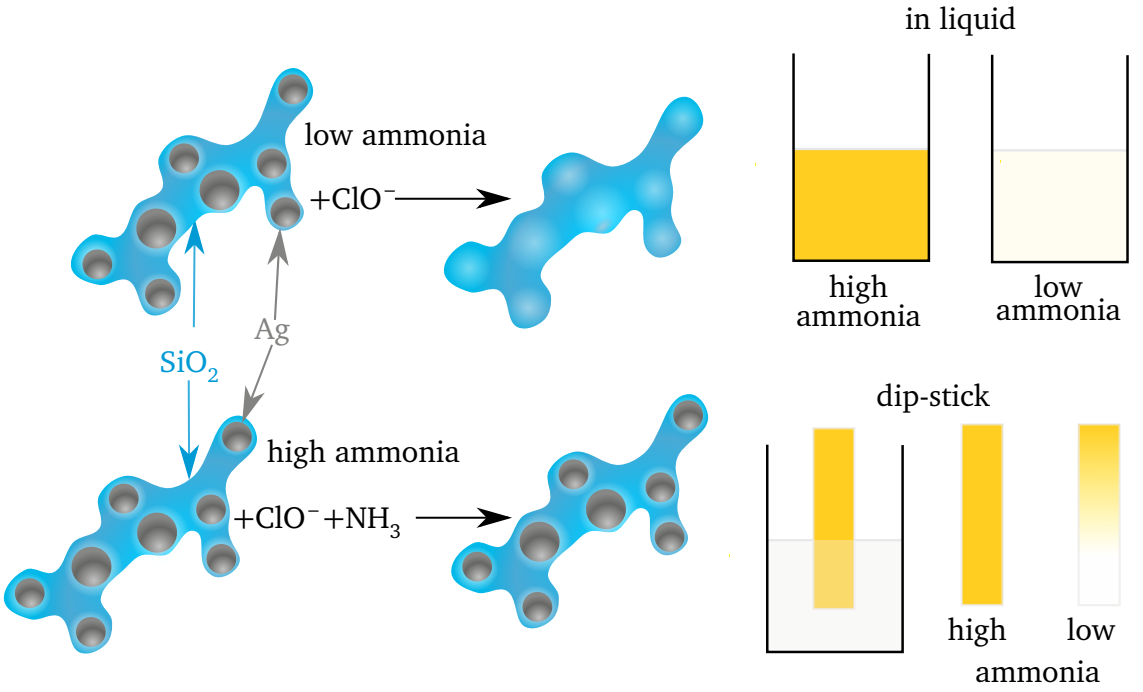

Figure 13: Summary of the work described in Paper IV where silver nanoaggregates with a silica spacer were synthesised. Upon addition of ClO^- the silver nanoparticles are dissolved removing the strong yellow colour in dispersion or as coatings on filter paper. In the presence of ammonia, the reaction between ammonia and ClO^- reduces the dissolution of the silver and therefore no colour change is observed. This was performed both in solution as a colloidal suspension and also as a deposited coating on filter paper thereby allowing for a simplified measurement procedure without the requirement of nanoparticle dispersion.

6 Conclusions

Over the course of the work described in this thesis inorganic nanomaterials have been applied and developed for four biomedical applications including both anti-biofilm treatment and bioanalyte detection. Plasmonic silver-based nanomaterials were harnessed for their photothermal properties with the development of a facile synthetic procedure to optimise their near-IR optical activity. This was achieved by the addition of varying quantities of silica which fixed primary silver nanoparticles at varying characteristic distances to one another and therefore could tune the inter-particle plasmonic coupling to improve near-IR extinction and photothermal properties. Implant mimicking coatings of these photothermal nanomaterials were then prepared and demonstrated for the effective eradication of biofilms of *S. aureus* and *E. coli*.

The acidic microenvironment of biofilms was also studied by the developed luminescent CaP:Eu^{3+} pH-sensitive surface. Coatings of CaP:Eu^{3+} were deposited onto silicon substrates and the pH dependence of their luminescence was investigated. The luminescence emission of CaP:Eu^{3+} occurred centred at two major wavelengths 590 and 614 nm the ratio between these two emissions exhibited pH dependence with a decrease of the 614 nm peak with decreasing pH. This ratiometric change was related to a decrease in carbonate content of the CaP:Eu^{3+} coatings at lower pH and thereby a decrease in the symmetry dependent peak at 614 nm, whereas the symmetry independent peak at 590 nm remained relatively stable. These coatings were then applied for the determination of interfacial biofilm pH of *E. coli*, *K. pneumoniae* and *P. aeruginosa* biofilms grown on the CaP:Eu^{3+} surfaces. *E. coli* and *K. pneumoniae* were found to develop highly acidic microenvironments.

Measurement of bacterial hydrogen peroxide production was also achieved by the development of a ratiometric luminescent sensor. CeO_2:Eu^{3+} had previously been developed as a hydrogen peroxide sensor with good limits of detection, however, the reliance on luminescence decrease of a single peak causes some limitations for application in complex biological environments. Here this sensor was further developed by

synthesising CeO_2:Eu^{3+}/Y_2O_3:Tb^{3+} which allowed for the use of small hydrogen peroxide sensitive CeO_2:Eu^{3+} with red emission (590 nm) with a stable hydrogen peroxide Y_2O_3:Tb^{3+} green reference emission (550 nm). This was applied for the measurement of hydrogen peroxide production by *S. pneumoniae*.

Finally, a silver nanoparticle-based plasmonic ammonia sensor was developed. This relied on the dual reactivity of ClO^- towards both silver nanoparticle dissolution and reaction with ammonia. In low ammonia concentrations, the plasmonic silver was dissolved causing a strong decrease in absorbance whereas as ammonia concentrations increased the amount of remaining plasmonic silver also increased and therefore less change in absorbance was observed. This was demonstrated for the detection of ammonia at levels corresponding to hyperammonemia from simulated serum. This assay was also adapted to a paper-based format thereby avoiding the necessity of forming a colloidal dispersion and improving ease of use.

7 Future perspectives

Over the course of the work presented in this thesis, additional avenues of investigation have presented themselves. Although the photothermal coatings developed in Paper I presented good plasmonic performance some additional potential improvements can be considered. An obvious concern is the effect of high local temperatures on human tissues in proximity to the implanted device. The specificity of this treatment approach is mainly achieved by localisation of the photothermal effect, with the intention of treating biofilms formed directly on the photothermal surface in this case. Photothermal plasmonic structures produce high temperatures in their immediate vicinity, therefore the distance between the biofilm to be treated and the photothermal nanoparticles could be important and was not optimised in Paper I with a comparatively thick approximately 6 μm top PDMS layer. By reducing the thickness of this top PDMS layer the temperatures experienced by the biofilm formed directly on the device surface for a given illumination intensity could be increased therefore potentially reducing the temperature increase in the human tissue surrounding the device and improving specificity.

An additional modification of potential interest could be the investigation of a thermally released antibiotic on the surface of the coating. Thus upon irradiation and photothermal action, the temperature increase not only has a direct action on the bacteria but also could cause the release of the antibiotic with additional antibacterial action. Such combined antibiotic/thermal action has been shown to even lead to synergistic antibacterial action.[223] Finally, the dielectric constant of the material used as the spacer between silver nanoparticles is likely to also play a significant role in the spectral properties of the silver nanoaggregates. Currently, silica with a refractive index close to 1.46 is used, however, an investigation of the spectral shift induced by the use of other materials with higher dielectric constants such as TiO_2 could provide yet further improved near-IR characteristics.

Presently the developed photothermal system has only been tested in a proof-of-concept

setting. In order to demonstrate a viable application for use as a coating for implanted medical devices, much further testing would be required. As a first step both sufficient temperature evolution at safe lasers doses through animal tissue should be demonstrated. Subsequently, an optimisation of temperatures providing antibacterial action without causing harmful tissue damage should be performed. Upon evaluation of these results, the decision could be made on the feasibility of further studies for clinical translation and final application.

The pH-sensitive surface for biofilm microenvironment pH determination developed in Paper II also has the potential for further optimisation. Although not presented in the publication early experiments showed some size dependence on the pH sensitivity range of the sensor. In the finally developed coating, only nanoparticles synthesised with one flame condition and therefore size range were used, therefore further experiments to explore the benefit of using multiple size ranges in order to broaden the range of pH sensitivity could be of interest. The initial plan as described in 5 was to use a ratiometric system similar to Paper III with a pH-sensitive emission and a reference pH-independent emission from a different nanoparticle. This design was abandoned when the intrinsic ratiometric nature of the CaP:Eu^{3+} was discovered. However, the use of this sensing mechanism with a defined reference and sensing phase could provide a system in which different lanthanide ions could be used and therefore the emission and excitation wavelengths could be altered. It could therefore be interesting to investigate the synthesis of CaP or other pH-sensitive nanoparticles with Nd^{3+} or other near-IR emitting lanthanide ions to develop a near-IR pH-sensitive surface.

The robust luminescent hydrogen peroxide sensor described in Paper III also has the potential to be applied for the near-IR detection of hydrogen peroxide. A key aspect of the sensing mechanism of this sensor is changes to the charge transfer band of the lattice which therefore changes the luminescence emission intensity. However, EPR data presented in Paper III also indicated oxidation of Eu^{2+} to Eu^{3+}. By harnessing this change in the oxidation state of the lanthanide ion there could be potential for a near-IR hydrogen peroxide sensor as luminescence emission typically occurs from the (III) oxidation state. For instance, Tm can exist in both the (II) and (III) oxidation states and exhibits emission from the Tm^{3+} state in the 800 nm range.

The silver nanoparticle ammonia sensor developed in Paper IV is still a manuscript and actively undergoing further investigations. Currently, separation of ammonia from biological samples must be performed prior to application of the ClO^- due to the reactivity of ClO^- with components expected to be found in blood or serum such as proteins. This significantly increases the time required for the measurement and the

complexity. Further developments are ongoing to combine both the ammonia detection and the separation into a single paper-based step. Moreover, although samples of both whole blood and serum from sheep have been tested they were found to have high baseline ammonia levels and are therefore poorly suitable for validation of the developed sensor. An immediate next step is therefore the evaluation of the sensor with healthy fresh human blood.

8 Acknowledgements

I'm very grateful to many people for their contributions to making these past few years as fun and fruitful as they have been. I may forget some people and, although not much consolation, I would reassure you that I am also quite likely grateful to you.

I think it only fair that I start with **Georgios A. Sotiriou** or as he is more usually known "George", my main supervisor. I have learnt a lot from you over the course of my PhD studies and I appreciate the supportive attitude which you have had. If I needed advice then you helped but you have also given me much freedom to develop. I also really appreciate the opportunities you have provided for the supervision of students. I leave the disproportionately large A. as a memento to the eagle-eyed nature with which you hunt down typos and inconsistencies!

My co-supervisor **Birgitta Henriques-Normark**, a wealth of knowledge and always able to cut through information to find the core of the issue and provide insightful feedback. My projects and development have benefited greatly from your expertise.

Students I have supervised, thank you all for your contributions to both the research and my personal development.

Isaac Changhun Yun and **Nicole Shuzhi Zhou** it has been a few years now! We started out at about the same time and learnt the FSP reactor together, it was nice to have such cheerful and optimistic colleagues, I wish you both all the best!

Justina Venckute Larsson One of the first students I supervised and certainly the longest lasting as you have been working in our lab alongside your studies for almost 4 years now. A dedicated, smart and talented scientist, it has been my pleasure to work with you.

Athina Eleftheraki You joined the "photothermal project" for a summer in the early stages, a dedicated scientist good luck with your PhD.

Apostolos Zaganiaris the eclectic erasmus student, you were a fun and vibrant addition

to the lab and only seemed to suffer slightly under the mountains of agar plates with which you worked.

Mariam Shahata You explored a new "twist" to the photothermal project, another dedicated scientist whose work is much appreciated.

Ossian Mathieu a talented high-school student who joined for a summer, this guy can code!

Anshika Maheshwari You started as a master's student but you have evolved into a fully fledged PhD student in our group. I was already impressed by your broad nano knowledge and certainty during your master's project. This person can outwit anybody and I'm pretty certain could win a staredown against a goose.

Yael del Carmen Suárez López Master's student in our lab, also highly talented and now pursuing a PhD in Uppsala. I look forward to seeing the lofty heights to which you climb.

Vaida Railaite You joined for the summer and worked incredibly hard. I think you provided a semester's worth of data in a month. Excellent, thorough scientist.

Stefanie Dietl Currently a master's project student, an optimistic and happy addition. I hope I am still finding enough time for you in spite of this thesis!

Other members of the Sotirioulab who have made the time memorable, fruitful and fun:

Jill Ziesmer A determined hard-working and helpful PhD student with thorough science. Also a fun office mate who gives as good as she gets. Has the name tag "boss-lady" on her desk, probably accurate.

Felix Geissel We have shared much of our PhD journey together. I'm impressed with your translation from beer to running, swimming and cycling. Also too good at table football. Good luck with your future!

Vasiliki Tsikourkitoudi Our first postdoc, you have battled with calcium phosphate with determination and come out on top, in itself quite a feat. I would also never dare to steal a pen from you, the ground trembles at the mere thought.

Eleni Bletsa A kind professional scientist and could write a book on catalysis from memory.

Haipeng Li A fun, modest guy with good sense of humour and excellent hard-working scientist. Always happy to discuss science - very approachable and knowledgeable.

The larger BHN group have accepted us warmly and shared both knowledge and good times:

Edmund Loh, my mentor and friend. I have greatly appreciated the many chats we have had over the years discussing both academic topics but also everything else from boat propellers to oil paintings.

Kim Vestö A special Finn, I think he's running away from something but I'm not sure what. I greatly appreciate you taking me for my weekly exercise rounds on your lab runs. Making up for the lost calories with pizza was also a nice way of completing the week.

Jens Karlsson A welcoming happy face and gesture to be greeted with in the morning. You have an endless appetite for board games and a fantastic ability to generate fun. Always up for a discussion, whatever the topic, and especially over a beer. Another dedicated member of the running crew.

Francesco Righetti the photoshop wiz and tiramisu master. A smart scientist knowledgeable in a broad range of topics and interested in everything. I had a lot of fun going hiking with you. I think after Kim you are probably also the most dedicated runner.

Hannes Eichner The strict German PhD student who speaks his mind. Also a fun and caring individual who does rigorous, well-planned science and apparently can write good grant applications!

John Boss always able to provide an alternative view or a glimpse at the situation from another's perspective. A balancing force in any discussion.

Pedro Henriques A late addition, we'll find you an NMR somewhere. If you keep improving the way you have been maybe one day you will be better than me at table football.

Sarp Bamyaci I feel like we click, a fun guy who will respond to silliness with yet more silliness.

Marie-Stéphanie Aschtgen Many fun interactions at the coffee machine and you have taken my jokes and responded with wit.

The new postdoc gang **Meztlli Gaytan**, **Rebecca Dookie** and **Anandi Narayana Moorthy**. Fun additions to the lab and all approachable, knowledgeable and happy to help.

Genevieve Gariss I'm still impressed by your insistent acceleration at the slightest signs of a hill on our runs.

Anuj Pathak You took our jokes with grace, the kindly lab uncle with tasty snacks to share.

Sigrún Thórsdóttir A vibrant character who will stand her own knowledgeable and independent. Always happy to chat and help.

Maria Carlson Cutting through bureaucratic issues, you have on several occasions saved me from filling out forms. I hate forms, so I am exceptionally grateful.

Katrin Pütsep I enjoyed surprising you with the Estonian, a cheerful realist and always up for a chat.

Mikael Rhen An encyclopedia of bacteriology with many fun stories.

Staffan Normark Always helping to put the research in context and suggesting new ideas.

So many other have added their unique characters to my PhD time: **Ana-Rita Narciso**, **Priyanka Nannapaneni**, **Susan Farmand**, **Karin Blomqvist**, **Karina Hentrich**, **Vicky Sender**, **Sandra Muschiol**, **Elisabeth Reithuber**, **Vitor Oliviera**, **Mario Codemo**, **Christian Spoerry**, **Federico Iovino** and **Karthik Subramanian**

Outside of the lab there has also been much support:

I discovered the MESAICOS hockey club later than I should have. It has been a lot of fun, a great way to unwind and friendly people to play hockey with and have a beer or two with afterwards.

Dearest **Mum**, always able to provide a relaxing place to go unwind and eat nice food. Zacky is also a big bonus. Presumably you have also contributed in some way to who I am today. I present to you another tome for your dusty bookshelves.

Lovely **Olivia Luige**, my partner and eternal source of joy. You have supported me and helped me in all aspects.

References

[1] **Karsten Wegner and Sotiris E. Pratsinis**. Scale-up of nanoparticle synthesis in diffusion flame reactors. *Chemical Engineering Science*, 58(20):pages 4581–4589 (2003). doi:10.1016/j.ces.2003.07.010.

[2] **Pedro Viana Baptista**. Nanodiagnostics: Leaving the research lab to enter the clinics? *Diagnosis*, 1(4):pages 305–309 (2014). doi:10.1515/dx-2014-0055.

[3] **Sofia Bisso and Jean-Christophe Leroux**. Nanopharmaceuticals: A focus on their clinical translatability. *International Journal of Pharmaceutics*, 578:page 119098 (2020). doi:10.1016/j.ijpharm.2020.119098.

[4] **Michel Vert, Yoshiharu Doi, Karl-Heinz Hellwich,** *et al.* Terminology for biorelated polymers and applications (IUPAC Recommendations 2012). *Pure and Applied Chemistry*, 84(2):pages 377–410 (2012). doi:10.1351/PAC-REC-10-12-04.

[5] **Jayasmita Jana, Mainak Ganguly, and Tarasankar Pal**. Enlightening surface plasmon resonance effect of metal nanoparticles for practical spectroscopic application. *RSC Advances*, 6(89):pages 86174–86211 (2016). doi:10.1039/C6RA14173K.

[6] **Oliver S. Thomas and Wilfried Weber**. Overcoming Physiological Barriers to Nanoparticle Delivery—Are We There Yet? *Frontiers in Bioengineering and Biotechnology*, 7:page 415 (2019). doi:10.3389/fbioe.2019.00415.

[7] **Jaeyun Kim, Yuanzhe Piao, and Taeghwan Hyeon**. Multifunctional nanostructured materials for multimodal imaging, and simultaneous imaging and therapy. *Chem. Soc. Rev.*, 38(2):pages 372–390 (2009). doi:10.1039/B709883A.

[8] **Baran Sumer and Jinming Gao**. Theranostic nanomedicine for cancer. *Nanomedicine*, 3(2):pages 137–140 (2008). doi:10.2217/17435889.3.2.137.

[9] **Alberto F. Monegro, Vijayadershan Muppidi, and Hariharan Regunath**. Hospital Acquired Infections. In *StatPearls*. StatPearls Publishing, Treasure Island (FL) (2022).

[10] **Christopher JL Murray, Kevin Shunji Ikuta, Fablina Sharara,** *et al.* Global burden of bacterial antimicrobial resistance in 2019: A systematic analysis. *The Lancet*, 399(10325):pages 629–655 (2022). doi:10.1016/S0140-6736(21)02724-0.

[11] **Hans-Curt Flemming, Jost Wingender, Ulrich Szewzyk, Peter Steinberg, Scott A Rice, and Staffan Kjelleberg**. Biofilms: An emergent form of bacterial life. *Nature Reviews Microbiology*, 14(9):pages 563–575 (2016). doi:10.1038/nrmicro.2016.94.

[12] **Anthony D. Verderosa, Makrina Totsika, and Kathryn E. Fairfull-Smith**. Bacterial Biofilm Eradication Agents: A Current Review. *Frontiers in Chemistry*, 7:page 824 (2019). doi:10.3389/fchem.2019.00824.

[13] **David J. Stickler**. Bacterial biofilms in patients with indwelling urinary catheters. *Nature Clinical Practice Urology*, 5(11):pages 598–608 (2008). doi:10.1038/ncpuro1231.

[14] **Ute Römling and Carlos Balsalobre**. Biofilm infections, their resilience to therapy and innovative treatment strategies. *Journal of Internal Medicine*, 272(6):pages 541–561 (2012). doi:10.1111/joim.12004.

[15] **Carla Renata Arciola, Davide Campoccia, Pietro Speziale, Lucio Montanaro, and John William Costerton**. Biofilm formation in Staphylococcus implant infections. A review of molecular mechanisms and implications for biofilm-resistant materials. *Biomaterials*, 33(26):pages 5967–5982 (2012). doi:10.1016/j.biomaterials.2012.05.031.

[16] **Songze Wu, Botao Zhang, Yi Liu, Xinkun Suo, and Hua Li**. Influence of surface topography on bacterial adhesion: A review (Review). *Biointerphases*, 13(6):page 060801 (2018). doi:10.1116/1.5054057.

[17] **Xi Li, Biao Wu, Hao Chen, Kaihui Nan, Yingying Jin, Lin Sun, and Bailiang Wang**. Recent developments in smart antibacterial surfaces to inhibit biofilm formation and bacterial infections. *Journal of Materials Chemistry B*, 6(26):pages 4274–4292 (2018). doi:10.1039/C8TB01245H.

[18] **Kirby R. Lattwein, Himanshu Shekhar, Joop J.P. Kouijzer, Willem J.B. van Wamel, Christy K. Holland, and Klazina Kooiman**. Sonobactericide: An Emerging Treatment Strategy for Bacterial Infections. *Ultrasound in Medicine & Biology*, 46(2):pages 193–215 (2020). doi:10.1016/j.ultrasmedbio.2019.09.011.

[19] **Yunguang Zhang, Siyu Zhang, Zihan Zhang,** *et al.* Recent Progress on NIR-II Photothermal Therapy. *Frontiers in Chemistry*, 9:page 728066 (2021). doi:10.3389/fchem.2021.728066.

[20] **Junxian Hou, Zhongliang Liu, Yu Zhou, Wenwen Chen, Yanxia Li, and Lixia Sang**. An experimental study of pH distributions within an electricity-producing biofilm by using pH microelectrode. *Electrochimica Acta*, 251:pages 187–194 (2017). doi:10.1016/j.electacta.2017.08.101.

[21] **Stephanie Fulaz, Dishon Hiebner, Caio H. N. Barros, Henry Devlin, Stefania Vitale, Laura Quinn, and Eoin Casey**. Ratiometric Imaging of the in Situ pH Distribution of Biofilms by Use of Fluorescent Mesoporous Silica Nanosensors. *ACS Applied Materials & Interfaces*, 11(36):pages 32679–32688 (2019). doi:10.1021/acsami.9b09978.

[22] **Lavida R. K. Brooks and George I. Mias**. Streptococcus pneumoniae's Virulence and Host Immunity: Aging, Diagnostics, and Prevention. *Frontiers in Immunology*, 9:page 1366 (2018). doi:10.3389/fimmu.2018.01366.

[23] **Prashant Rai, Marcus Parrish, Ian Jun Jie Tay,** *et al. Streptococcus Pneumoniae* secretes hydrogen peroxide leading to DNA damage and apoptosis in lung cells. *Proceedings of the National Academy of Sciences*, 112(26) (2015). doi:10.1073/pnas.1424144112.

[24] **Ricardo Matias Trujillo, Daniela Estefanía Barraza, Martin Lucas Zamora, Anna Cattani-Scholz, and Rossana Elena Madrid**. Nanostructures in Hydrogen Peroxide Sensing. *Sensors*, 21(6):page 2204 (2021). doi:10.3390/s21062204.

[25] **Edwin Jin Su Lee and Jonathan C. Huang**. *Ammonia*. IntechOpen (2019). ISBN 978-1-78985-066-6. doi:10.5772/intechopen.88044.

[26] **Thomas R. Veltman, Chun J. Tsai, Natalia Gomez-Ospina, Matthew W. Kanan, and Gilbert Chu**. Point-of-Care Analysis of Blood Ammonia with a Gas-Phase Sensor. *ACS Sensors*, 5(8):pages 2415–2421 (2020). doi:10.1021/acssensors.0c00480.

[27] **Omar B. Ayyub, Adam M. Behrens, Brian T. Heligman,** *et al.* Simple and inexpensive quantification of ammonia in whole blood. *Molecular Genetics and Metabolism*, 115(2-3):pages 95–100 (2015). doi:10.1016/j.ymgme.2015.04.004.

[28] **Robert Goggs, Sergio Serrano, Balazs Szladovits, Iain Keir, Ryan Ong, and Dez Hughes**. Clinical investigation of a point-of-care blood ammonia analyzer. *Veterinary Clinical Pathology*, 37(2):pages 198–206 (2008). doi:10.1111/j.1939-165X.2008.00024.x.

[29] **Jian Ma, Peicong Li, Kunning Lin, Zhaoying Chen, Nengwang Chen, Kewei Liao, and Dongxing Yuan**. Optimization of a salinity-interference-free indophenol method for the determination of ammonium in natural waters using o-phenylphenol. *Talanta*, 179:pages 608–614 (2018). doi:10.1016/j.talanta.2017.11.069.

[30] **Lutz Mädler, Hendrik K. Kammler, Roger Mueller, and Sotiris E. Pratsinis**. Controlled synthesis of nanostructured particles by flame spray pyrolysis. *Journal of Aerosol Science*, 33(2):pages 369–389 (2002). doi:10.1016/S0021-8502(01)00159-8.

[31] **Florian Meierhofer and Udo Fritsching**. Synthesis of Metal Oxide Nanoparticles in Flame Sprays: Review on Process Technology, Modeling, and Diagnostics. *Energy & Fuels*, 35(7):pages 5495–5537 (2021). doi:10.1021/acs.energyfuels.0c04054.

[32] **Mohammad Malekzadeh and Mark T. Swihart**. Vapor-phase production of nanomaterials. *Chemical Society Reviews*, 50(12):pages 7132–7249 (2021). doi:10.1039/D0CS01212B.

[33] **Robert N. Grass and Wendelin J. Stark**. Gas phase synthesis of fcc-cobalt nanoparticles. *Journal of Materials Chemistry*, 16(19):pages 1825–1830 (2006). doi:10.1039/B601013J.

[34] **Catia Contado**. Nanomaterials in consumer products: A challenging analytical problem. *Frontiers in Chemistry*, 3 (2015). doi:10.3389/fchem.2015.00048.

[35] **Zarith Asyikin Abdul Aziz, Hasmida Mohd-Nasir, Akil Ahmad,** *et al.* Role of Nanotechnology for Design and Development of Cosmeceutical: Application in Makeup and Skin Care. *Frontiers in Chemistry*, 7 (2019). doi:10.3389/fchem.2019.00739.

[36] **Liliane Bokobza**. Natural Rubber Nanocomposites: A Review. *Nanomaterials*, 9(1):page 12 (2018). doi:10.3390/nano9010012.

[37] **Cong-cong Jiang, Yan-ke Cao, Gui-yong Xiao, Rui-fu Zhu, and Yu-peng Lu**. A review on the application of inorganic nanoparticles in chemical surface coatings on metallic substrates. *RSC Advances*, 7(13):pages 7531–7539 (2017). doi:10.1039/C6RA25841G.

[38] **David Julian McClements and Hang Xiao**. Is nano safe in foods? Establishing the factors impacting the gastrointestinal fate and toxicity of organic and inorganic food-grade nanoparticles. *npj Science of Food*, 1(1):page 6 (2017). doi:10.1038/s41538-017-0005-1.

[39] **Phillip M. Potter, Jana Navratilova, Kim R. Rogers, and Souhail R. Al-Abed**. Transformation of silver nanoparticle consumer products during simulated usage and disposal. *Environmental Science: Nano*, 6(2):pages 592–598 (2019). doi:10.1039/C8EN00958A.

[40] **Nicolle S. Tulve, Aleksandr B. Stefaniak, Marina E. Vance,** *et al.* Characterization of silver nanoparticles in selected consumer products and its relevance for predicting children's potential exposures. *International Journal of Hygiene and Environmental Health*, 218(3):pages 345–357 (2015). doi:10.1016/j.ijheh.2015.02.002.

[41] **Matthieu Germain, Fanny Caputo, Su Metcalfe,** *et al.* Delivering the power of nanomedicine to patients today. *Journal of Controlled Release*, 326:pages 164–171 (2020). doi:10.1016/j.jconrel.2020.07.007.

[42] **Jianqiao Liu, Jia Liu, Shokouh Attarilar,** *et al.* Nano-Modified Titanium Implant Materials: A Way Toward Improved Antibacterial Properties. *Frontiers in Bioengineering and Biotechnology*, 8 (2020). doi:10.3389/fbioe.2020.576969.

[43] **David Roe, Balu Karandikar, Nathan Bonn-Savage, Bruce Gibbins, and Jean-Baptiste Roullet**. Antimicrobial surface functionalization of plastic catheters by silver nanoparticles. *Journal of Antimicrobial Chemotherapy*, 61(4):pages 869–876 (2008). doi:10.1093/jac/dkn034.

[44] **Loke Kok Foong, Mohammad Mehdi Foroughi, Armita Forutan Mirhosseini,** *et al.* Applications of nano-materials in diverse dentistry regimes. *RSC Advances*, 10(26):pages 15430–15460 (2020). doi:10.1039/D0RA00762E.

[45] **Amit Kumar, Sungi Kim, and Jwa Min Nam**. Plasmonically Engineered Nanoprobes for Biomedical Applications. *Journal of the American Chemical Society*, 138(44):pages 14509–14525 (2016). doi:10.1021/jacs.6b09451.

[46] **Joanna Dulińska-Litewka, Agnieszka Łazarczyk, Przemysław Hałubiec, Oskar Szafrański, Karolina Karnas, and Anna Karewicz**. Superparamagnetic Iron Oxide Nanoparticles—Current and Prospective Medical Applications. *Materials*, 12(4):page 617 (2019). doi:10.3390/ma12040617.

[47] **Lyndia C. Wu, Yanrong Zhang, Gary Steinberg,** *et al.* A Review of Magnetic Particle Imaging and Perspectives on Neuroimaging. *American Journal of Neuroradiology*, 40(2):pages 206–212 (2019). doi:10.3174/ajnr.A5896.

[48] **Jean Claude G. Bünzli**. Lanthanide light for biology and medical diagnosis. *Journal of Luminescence*, 170:pages 866–878 (2016). doi:10.1016/j.jlumin.2015.07.033.

[49] **Andrew M Smith, Gang Ruan, Matthew N Rhyner, and Shuming Nie**. Engineering Luminescent Quantum Dots for In Vivo Molecular and Cellular Imaging. *Annals of Biomedical Engineering*, 34(1):pages 3–14 (2006). doi:10.1007/s10439-005-9000-9.

[50] **Michael J. Mitchell, Margaret M. Billingsley, Rebecca M. Haley, Marissa E. Wechsler, Nicholas A. Peppas, and Robert Langer**. Engineering precision nanoparticles for drug delivery. *Nature Reviews Drug Discovery*, 20(2):pages 101–124 (2021). doi:10.1038/s41573-020-0090-8.

[51] **Dan Huang, Bin He, and Peng Mi**. Calcium phosphate nanocarriers for drug delivery to tumors: Imaging, therapy and theranostics. *Biomaterials Science*, 7(10):pages 3942–3960 (2019). doi:10.1039/C9BM00831D.

[52] **Karel Ulbrich, Kateřina Holá, Vladimir Šubr, Aristides Bakandritsos, Jiří Tuček, and Radek Zbořil**. Targeted Drug Delivery with Polymers and Magnetic Nanoparticles: Covalent and Noncovalent Approaches, Release Control, and Clinical Studies. *Chemical Reviews*, 116(9):pages 5338–5431 (2016). doi:10.1021/acs.chemrev.5b00589.

[53] **Vasiliki Tsikourkitoudi, Jens Karlsson, Padryk Merkl, Edmund Loh, Birgitta Henriques-Normark, and Georgios A. Sotiriou**. Flame-Made Calcium Phosphate Nanoparticles with High Drug Loading for Delivery of Biologics. *Molecules*, 25(7):page 1747 (2020). doi:10.3390/molecules25071747.

[54] **Elvin Blanco, Haifa Shen, and Mauro Ferrari**. Principles of nanoparticle design for overcoming biological barriers to drug delivery. *Nature Biotechnology*, 33(9):pages 941–951 (2015). doi:10.1038/nbt.3330.

[55] **Pedro Baptista, Eulália Pereira, Peter Eaton,** *et al.* Gold nanoparticles for the development of clinical diagnosis methods. *Analytical and Bioanalytical Chemistry*, 391(3):pages 943–950 (2008). doi:10.1007/s00216-007-1768-z.

[56] **Kimimichi Obata, Osamu Segawa, Mitsuru Yakabe,** *et al.* Development of a novel method for operating magnetic particles, Magtration Technology, and its use for automating nucleic acid purification. *Journal of Bioscience and Bioengineering*, 91(5):pages 500–503 (2001). doi:10.1016/S1389-1723(01)80280-2.

[57] **Tamar Walker, Sandrea Dumadag, Christine Jiyoun Lee, Seung Heon Lee, Jeffrey M. Bender, Jennifer Cupo Abbott, and Rosemary C. She**. Clinical Impact of Laboratory Implementation of Verigene BC-GN Microarray-Based Assay for Detection of Gram-Negative Bacteria in Positive Blood Cultures. *Journal of Clinical Microbiology*, 54(7):pages 1789–1796 (2016). doi:10.1128/JCM.00376-16.

[58] **Jan van den Broek, Sebastian Abegg, Sotiris E. Pratsinis, and Andreas T. Güntner**. Highly selective detection of methanol over ethanol by a handheld gas sensor. *Nature Communications*, 10(1):page 4220 (2019). doi:10.1038/s41467-019-12223-4.

[59] **Eduardo A. Coronado, Ezequiel R. Encina, and Fernando D. Stefani**. Optical properties of metallic nanoparticles: Manipulating light, heat and forces at the nanoscale. *Nanoscale*, 3(10):page 4042 (2011). doi:10.1039/c1nr10788g.

[60] **Huakang Yu, Yusi Peng, Yong Yang, and Zhi-Yuan Li**. Plasmon-enhanced light–matter interactions and applications. *npj Computational Materials*, 5(1):page 45 (2019). doi:10.1038/s41524-019-0184-1.

[61] **Gururaj V. Naik, Jeremy L. Schroeder, Xingjie Ni, Alexander V. Kildishev, Timothy D. Sands, and Alexandra Boltasseva**. Titanium nitride as a plasmonic material for visible and near-infrared wavelengths. *Optical Materials Express*, 2(4):pages 478–489 (2012). doi:10.1364/OME.2.000478.

[62] **Benjamin J. Wiley, Sang Hyuk Im, Zhi-Yuan Li, Joeseph McLellan, Andrew Siekkinen, and Younan Xia**. Maneuvering the Surface Plasmon Resonance of Silver Nanostructures through Shape-Controlled Synthesis. *The Journal of Physical Chemistry B*, 110(32):pages 15666–15675 (2006). doi:10.1021/jp0608628.

[63] **Kyeong-Seok Lee and Mostafa A. El-Sayed**. Gold and Silver Nanoparticles in Sensing and Imaging: Sensitivity of Plasmon Response to Size, Shape, and Metal Composition. *The Journal of Physical Chemistry B*, 110(39):pages 19220–19225 (2006). doi:10.1021/jp062536y.

[64] **Tennyson L. Doane and Clemens Burda**. The unique role of nanoparticles in nanomedicine: Imaging, drug delivery and therapy. *Chemical Society Reviews*, 41(7):pages 2885–2911 (2012). doi:10.1039/c2cs15260f.

[65] **Judith Langer, Dorleta Jimenez de Aberasturi, Javier Aizpurua,** *et al.* Present and Future of Surface-Enhanced Raman Scattering. *ACS Nano*, 14(1):pages 28–117 (2020). doi:10.1021/acsnano.9b04224.

[66] **Jian-Feng Li, Chao-Yu Li, and Ricardo F. Aroca**. Plasmon-enhanced fluorescence spectroscopy. *Chemical Society Reviews*, 46(13):pages 3962–3979 (2017). doi:10.1039/C7CS00169J.

[67] **Ana María Ibarra-Ruiz, Diana C. Rodríguez Burbano, and John A. Capobianco**. Photoluminescent nanoplatforms in biomedical applications. *Advances in Physics: X*, 1(2):pages 194–225 (2016). doi:10.1080/23746149.2016.1165629.

[68] **Leah Bergman and Jeanne L. McHale**, editors. *Handbook of Luminescent Semiconductor Materials*. CRC Press, Boca Raton (2012). ISBN 978-0-429-19344-6. doi:10.1201/b11201.

[69] **Feng Wang, Debapriya Banerjee, Yongsheng Liu, Xueyuan Chen, and Xiaogang Liu**. Upconversion nanoparticles in biological labeling, imaging, and therapy. *The Analyst*, 135(8):page 1839 (2010). doi:10.1039/c0an00144a.

[70] **Mônica A. Cotta**. Quantum Dots and Their Applications: What Lies Ahead? *ACS Applied Nano Materials*, 3(6):pages 4920–4924 (2020). doi:10.1021/acsanm.0c01386.

[71] **F. Pelayo García de Arquer, Dmitri V. Talapin, Victor I. Klimov, Yasuhiko Arakawa, Manfred Bayer, and Edward H. Sargent**. Semiconductor quantum dots: Technological progress and future challenges. *Science*, 373(6555):page eaaz8541 (2021). doi:10.1126/science.aaz8541.

[72] **Chunyan Zhu, Zhao Chen, Shuai Gao,** *et al.* Recent advances in non-toxic quantum dots and their biomedical applications. *Progress in Natural Science: Materials International*, 29(6):pages 628–640 (2019). doi:10.1016/j.pnsc.2019.11.007.

[73] **Santosh K. Gupta, B. Rajeshwari, S. N. Achary, S. J. Patwe, A. K. Tyagi, V. Natarajan, and R. M. Kadam**. Europium Luminescence as a Structural Probe: Structure-Dependent Changes in Eu^{3+}-Substituted $Th(C_2O_4)_2{\cdot}xH_2O$ (x = 6, 2, and 0). *European Journal of Inorganic Chemistry*, 2015(26):pages 4429–4436 (2015). doi:10.1002/ejic.201500623.

[74] **Peter A. Tanner**. Some misconceptions concerning the electronic spectra of tripositive europium and cerium. *Chemical Society Reviews*, 42(12):page 5090 (2013). doi:10.1039/c3cs60033e.

[75] **Koen Binnemans**. Interpretation of europium(III) spectra. *Coordination Chemistry Reviews*, 295:pages 1–45 (2015). doi:10.1016/j.ccr.2015.02.015.

[76] **Yong Il Park, Kang Taek Lee, Yung Doug Suh, and Taeghwan Hyeon**. Upconverting nanoparticles: A versatile platform for wide-field two-photon microscopy and multimodal in vivo imaging. *Chemical Society Reviews*, 44(6):pages 1302–1317 (2015). doi:10.1039/C4CS00173G.

[77] **Evgenii L. Guryev, Anita S. Smyshlyaeva, Natalia Y. Shilyagina,** *et al.* UCNP-based Photoluminescent Nanomedicines for Targeted Imaging and Theranostics of Cancer. *Molecules*, 25(18):page 4302 (2020). doi:10.3390/molecules25184302.

[78] **Ok-Hee Kim, Shin-Woo Ha, Jae Il Kim, and Jin-Kyu Lee**. Excellent Photostability of Phosphorescent Nanoparticles and Their Application as a Color Converter in Light Emitting Diodes. *ACS Nano*, 4(6):pages 3397–3405 (2010). doi:10.1021/nn100139e.

[79] **Federico Iovino, Padryk Merkl, Anastasia Spyrogianni, Birgitta Henriques-Normark, and Georgios A. Sotiriou**. Silica-coated phosphorescent nanoprobes for selective cell targeting and dynamic bioimaging of pathogen–host cell interactions. *Chemical Communications*, 56(51):pages 6989–6992 (2020). doi:10.1039/D0CC00329H.

[80] **Ukrae Cho and James K. Chen**. Lanthanide-Based Optical Probes of Biological Systems. *Cell Chemical Biology*, 27(8):pages 921–936 (2020). doi:10.1016/j.chembiol.2020.07.009.

[81] **Huaxin Tan, Taoyu Wang, Yaru Shao, Cuiyun Yu, and Lidan Hu**. Crucial Breakthrough of Functional Persistent Luminescence Materials for Biomedical and Information Technological Applications. *Frontiers in Chemistry*, 7 (2019). doi:10.3389/fchem.2019.00387.

[82] **Daniel Jaque and Fiorenzo Vetrone**. Luminescence nanothermometry. *Nanoscale*, 4(15):pages 4301–4326 (2012). doi:10.1039/C2NR30764B.

[83] **Jon R. Askim, Morteza Mahmoudi, and Kenneth S. Suslick**. Optical sensor arrays for chemical sensing: The optoelectronic nose. *Chemical Society Reviews*, 42(22):page 8649 (2013). doi:10.1039/c3cs60179j.

[84] **Xiaolin Huang, Jibin Song, Bryant C. Yung, Xiaohua Huang, Yonghua Xiong, and Xiaoyuan Chen**. Ratiometric optical nanoprobes enable accurate molecular detection and imaging. *Chemical Society reviews*, 47(8):pages 2873–2920 (2018). doi:10.1039/C7CS00612H.

[85] **Yan Feng, Jinghui Cheng, Li Zhou, Xiangge Zhou, and Haifeng Xiang**. Ratiometric optical oxygen sensing: A review in respect of material design. *Analyst*, 137(21):pages 4885–4901 (2012). doi:10.1039/C2AN35907C.

[86] **Jeffrey N. Anker, W. Paige Hall, Olga Lyandres, Nilam C. Shah, Jing Zhao, and Richard P. Van Duyne**. Biosensing with plasmonic nanosensors. *Nature Materials*, 7(6):pages 442–453 (2008). doi:10.1038/nmat2162.

[87] **Roberto de la Rica and Molly M. Stevens**. Plasmonic ELISA for the ultrasensitive detection of disease biomarkers with the naked eye. *Nature Nanotechnology*, 7(12):pages 821–824 (2012). doi:10.1038/nnano.2012.186.

[88] **Henryk Szmacinski and Joseph R. Lakowicz**. Fluorescence lifetime-based sensing and imaging. *Sensors and Actuators B: Chemical*, 29(1):pages 16–24 (1995). doi:10.1016/0925-4005(95)01658-9.

[89] **Wey Yang Teoh, Rose Amal, and Lutz Mädler**. Flame spray pyrolysis: An enabling technology for nanoparticles design and fabrication. *Nanoscale*, 2(8):page 1324 (2010). doi:10.1039/c0nr00017e.

[90] **David Ensor**, editor. *Aerosol Science and Technology: History and Reviews*. RTI Press, first edition (2011). ISBN 978-1-934831-01-4. doi:10.3768/rtipress.2011.bk.0003.1109.

[91] **Reto Strobel and Sotiris E. Pratsinis**. Flame aerosol synthesis of smart nanostructured materials. *Journal of Materials Chemistry*, 17(45):page 4743 (2007). doi:10.1039/b711652g.

[92] **Gary L. Messing, Shi-Chang Zhang, and Gopal V. Jayanthi**. Ceramic powder synthesis by spray pyrolysis. *Journal of the American Ceramic Society*, 76(11):pages 2707–2726 (1993). doi:10.1111/j.1151-2916.1993.tb04007.x.

[93] **Lutz Mädler, Wendelin J. Stark, and Sotiris E. Pratsinis**. Flame-made ceria nanoparticles. *Journal of Materials Research*, 17(6):pages 1356–1362 (2002). doi:10.1557/JMR.2002.0202.

[94] **Heiko Schulz, Lutz Mädler, Reto Strobel, Rainer Jossen, Sotiris E. Pratsinis, and Tue Johannessen**. Independent control of metal cluster and ceramic particle characteristics during one-step synthesis of Pt/TiO_2. *Journal of Materials Research*, 20(9):pages 2568–2577 (2005). doi:10.1557/jmr.2005.0319.

[95] **Lizoel Buss, Florian Meierhofer, Pedro Bianchi Neto, Henry França Meier, Udo Fritsching, and Dirceu Noriler**. Impact of co-flow on the spray flame behaviour applied to nanoparticle synthesis. *The Canadian Journal of Chemical Engineering*, 97(2):pages 604–615 (2019). doi:10.1002/cjce.23386.

[96] **S. Grimm, M. Schultz, S. Barth, and R. Muller**. Flame pyrolysis – a preparation route for ultrafine pure γ-Fe_2O_3 powders and the control of their particle size and properties. *Journal of Materials Science*, 32(4):pages 1083–1092 (1997). doi:10.1023/A:1018598927041.

[97] **Adrian Camenzind, Reto Strobel, Frank Krumeich, and Sotiris E. Pratsinis**. Luminescence and crystallinity of flame-made Y_2O_3:Eu^{3+} nanoparticles. *Advanced Powder Technology*, 18(1):pages 5–22 (2007). doi:10.1163/156855207779768142.

[98] **Lutz Mädler, Albert Roessler, Sotiris E. Pratsinis, Thorsten Sahm, Aleksander Gurlo, Nicolae Barsan, and Udo Weimar**. Direct formation of highly porous gas-sensing films by in situ thermophoretic deposition of flame-made Pt/SnO_2 nanoparticles. *Sensors and Actuators B: Chemical*, 114(1):pages 283–295 (2006). doi:10.1016/j.snb.2005.05.014.

[99] **Antonio Tricoli, Markus Graf, and Sotiris E. Pratsinis**. Optimal doping for enhanced SnO_2 sensitivity and thermal stability. *Advanced Functional Materials*, 18(13):pages 1969–1976 (2008). doi:10.1002/adfm.200700784.

[100] **Sheldon Kay Friedlander**. *Smoke, Dust, and Haze: Fundamentals of Aerosol Dynamics*. Oxford University Press (2000). ISBN 978-0-19-512999-1.

[101] **Gary Nichols, Stephen Byard, Mark J. Bloxham,** *et al.* A review of the terms agglomerate and aggregate with a recommendation for nomenclature used in powder and particle characterization. *Journal of Pharmaceutical Sciences*, 91(10):pages 2103–2109 (2002). doi:10.1002/jps.10191.

[102] **Arto J. Gröhn, Sotiris E. Pratsinis, Antoni Sánchez-Ferrer, Raffaele Mezzenga, and Karsten Wegner**. Scale-up of nanoparticle synthesis by flame spray pyrolysis: The high-temperature particle residence time. *Industrial & Engineering Chemistry Research*, 53(26):pages 10734–10742 (2014). doi:10.1021/ie501709s.

[103] **Florian Meierhofer, Lutz Mädler, and Udo Fritsching**. Nanoparticle evolution in flame spray pyrolysis—Process design via experimental and computational analysis. *AIChE Journal*, 66(2):page e16885 (2020). doi:10.1002/aic.16885.

[104] **Alexandra Teleki, Martin C. Heine, Frank Krumeich, M. Kamal Akhtar, and Sotiris E. Pratsinis**. In situ coating of flame-made TiO_2 particles with nanothin SiO_2 films. *Langmuir*, 24(21):pages 12553–12558 (2008). doi:10.1021/la801630z.

[105] **Young Joon Jang, Cynthia Simer, and Taein Ohm**. Comparison of zinc oxide nanoparticles and its nano-crystalline particles on the photocatalytic degradation of methylene blue. *Materials Research Bulletin*, 41(1):pages 67–77 (2006). doi:10.1016/j.materresbull.2005.07.038.

[106] **Toivo T. Kodas and Mark J. Hampden-Smith**. *Aerosol Processing of Materials*. Wiley-VCH, New York (1999). ISBN 978-0-471-24669-5.

[107] **Haipeng Li, Christopher D. Rosebrock, Norbert Riefler, Thomas Wriedt, and Lutz Mädler**. Experimental investigation on microexplosion of single isolated burning droplets containing titanium tetraisopropoxide for nanoparticle production. *Proceedings of the Combustion Institute*, 36(1):pages 1011–1018 (2017). doi:10.1016/j.proci.2016.09.017.

[108] **Christopher D. Rosebrock, Thomas Wriedt, Lutz Mädler, and Karsten Wegner**. The role of microexplosions in flame spray synthesis for homogeneous nanopowders from low-cost metal precursors. *AIChE Journal*, 62(2):pages 381–391 (2016). doi:10.1002/aic.15056.

[109] **Georgios A. Sotiriou, Gion Diego Etterlin, Anastasia Spyrogianni, Frank Krumeich, Jean-Christophe Leroux, and Sotiris E. Pratsinis**. Plasmonic biocompatible silver–gold alloyed nanoparticles. *Chemical Communications*, 50(88):pages 13559–13562 (2014). doi:10.1039/C4CC05297H.

[110] **Wendelin J. Stark, Lutz Mädler, Marek Maciejewski, Sotiris E. Pratsinis, and Alfons Baiker**. Flame synthesis of nanocrystalline ceria–zirconia: Effect of carrier liquid. *Chemical Communications*, (5):pages 588–589 (2003). doi:10.1039/b211831a.

[111] **Henrike K. Grossmann, Tim Grieb, Florian Meierhofer,** *et al.* Nanoscale mixing during double-flame spray synthesis of heterostructured nanoparticles. *Journal of Nanoparticle Research*, 17(4):page 174 (2015). doi:10.1007/s11051-015-2975-8.

[112] **Reto Strobel, Lutz Mädler, Marco Piacentini, Marek Maciejewski, Alfons Baiker, and Sotiris E. Pratsinis**. Two-Nozzle Flame Synthesis of $Pt/Ba/Al_2O_3$ for NO_x Storage. *Chemistry of Materials*, 18(10):pages 2532–2537 (2006). doi:10.1021/cm0600529.

[113] **Georgios A. Sotiriou, Takumi Sannomiya, Alexandra Teleki, Frank Krumeich, Janos Vörös, and Sotiris E. Pratsinis**. Non-toxic dry-coated nanosilver for plasmonic biosensors. *Advanced Functional Materials*, 20(24):pages 4250–4257 (2010). doi:10.1002/adfm.201000985.

[114] **Christoph O. Blattmann, Georgios A. Sotiriou, and Sotiris E. Pratsinis**. Rapid synthesis of flexible conductive polymer nanocomposite films. *Nanotechnology*, 26(12):page 125601 (2015). doi:10.1088/0957-4484/26/12/125601.

[115] **Georgios A. Sotiriou, Christoph O. Blattmann, and Sotiris E. Pratsinis**. Flexible, multifunctional, magnetically actuated nanocomposite films. *Advanced Functional Materials*, 23(1):pages 34–41 (2013). doi:10.1002/adfm.201201371.

[116] **Antonio Tricoli, Markus Graf, Felix Mayer, Stéphane Kuühne, Andreas Hierlemann, and Sotiris E. Pratsinis**. Micropatterning layers by flame aerosol deposition-annealing. *Advanced Materials*, 20(16):pages 3005–3010 (2008). doi:10.1002/adma.200701844.

[117] **Noushin Nasiri, Shayanti Mukherjee, Anitha Panneerselvan, David R. Nisbet, and Antonio Tricoli**. Optimally hierarchical nanostructured hydroxyapatite coatings for superior prosthesis biointegration. *ACS Applied Materials & Interfaces*, 10(29):pages 24840–24849 (2018). doi:10.1021/acsami.8b08029.

[118] **Christopher JL Murray, Kevin Shunji Ikuta, Fablina Sharara,** *et al.* Global burden of bacterial antimicrobial resistance in 2019: A systematic analysis. *The Lancet*, 399(10325):pages 629–655 (2022). doi:10.1016/S0140-6736(21)02724-0.

[119] **Theo Vos, Stephen S Lim, Cristiana Abbafati,** *et al.* Global burden of 369 diseases and injuries in 204 countries and territories, 1990–2019: A systematic analysis for the Global Burden of Disease Study 2019. *The Lancet*, 396(10258):pages 1204–1222 (2020). doi:10.1016/S0140-6736(20)30925-9.

[120] **Jim O'Neill**. Tackling drug-resistant infections globally: Final report and recommendations. Report, Government of the United Kingdom (2016).

[121] **Avantika Mann, Kiran Nehra, J.S. Rana, and Twinkle Dahiya**. Antibiotic resistance in agriculture: Perspectives on upcoming strategies to overcome upsurge in resistance. *Current Research in Microbial Sciences*, 2:page 100030 (2021). doi:10.1016/j.crmicr.2021.100030.

[122] **Ziad A Memish, S Venkatesh, and Atef M Shibl**. Impact of travel on international spread of antimicrobial resistance. *International Journal of Antimicrobial Agents*, 21(2):pages 135–142 (2003). doi:10.1016/S0924-8579(02)00363-1.

[123] **Michael T. Madigan, Kelly S. Bender, Daniel H. Buckley, W. Matthew Sattley, and David Allan Stahl**. *Brock Biology of Microorganisms*. Pearson, NY, NY, fifteenth edition edition (2018). ISBN 978-0-13-426192-8.

[124] **Patrick R. Murray, Ken S. Rosenthal, and Michael A. Pfaller**. *Medical Microbiology*. Mosby/Elsevier, Philadelphia, 6th ed edition (2009). ISBN 978-0-323-05470-6.

[125] **Brenda A. Wilson and Abigail A. Salyers**, editors. *Bacterial Pathogenesis: A Molecular Approach*. ASM Press, Washington, DC, 3rd ed edition (2011). ISBN 978-1-55581-418-2.

[126] **Elisa T. Granato, Thomas A. Meiller-Legrand, and Kevin R. Foster**. The Evolution and Ecology of Bacterial Warfare. *Current Biology*, 29(11):pages R521–R537 (2019). doi:10.1016/j.cub.2019.04.024.

[127] **Yvon Michel-Briand and Christine Baysse**. The pyocins of Pseudomonas aeruginosa. *Biochimie*, 84(5):pages 499–510 (2002). doi:10.1016/S0300-9084(02)01422-0.

[128] **Aishwarya K. Korgaonkar and Marvin Whiteley**. *Pseudomonas Aeruginosa* Enhances Production of an Antimicrobial in Response to *N* -Acetylglucosamine and Peptidoglycan. *Journal of Bacteriology*, 193(4):pages 909–917 (2011). doi:10.1128/JB.01175-10.

[129] **Gili Regev-Yochay, Krzysztof Trzciński, Claudette M. Thompson, Richard Malley, and Marc Lipsitch**. Interference between Streptococcus pneumoniae and Staphylococcus aureus: In Vitro Hydrogen Peroxide-Mediated Killing by Streptococcus pneumoniae. *Journal of Bacteriology*, 188(13):pages 4996–5001 (2006). doi:10.1128/JB.00317-06.

[130] **Saskia F. Erttmann and Nelson O. Gekara**. Hydrogen peroxide release by bacteria suppresses inflammasome-dependent innate immunity. *Nature Communications*, 10(1):page 3493 (2019). doi:10.1038/s41467-019-11169-x.

[131] **John W. Costerton, Gill G. Geesey, and Kuo J. Cheng**. How bacteria stick. *Scientific American*, 238(1):pages 86–95 (1978). doi:10.1038/scientificamerican0178-86.

[132] **Tom J. Battin, Katharina Besemer, Mia M. Bengtsson, Anna M. Romani, and Aaron I. Packmann**. The ecology and biogeochemistry of stream biofilms. *Nature Reviews Microbiology*, 14(4):pages 251–263 (2016). doi:10.1038/nrmicro.2016.15.

[133] **Francesca Di Pippo, Luciana Di Gregorio, Roberta Congestri, Valter Tandoi, and Sabrina Rossetti**. Biofilm growth and control in cooling water industrial systems. *FEMS Microbiology Ecology*, 94(5):page fiy044 (2018). doi:10.1093/femsec/fiy044.

[134] **Laura K. Jennings, Kelly M. Storek, Hannah E. Ledvina,** *et al.* Pel is a cationic exopolysaccharide that cross-links extracellular DNA in the *Pseudomonas aeruginosa*

biofilm matrix. *Proceedings of the National Academy of Sciences*, 112(36):pages 11353–11358 (2015). doi:10.1073/pnas.1503058112.

[135] **Cyril Guilhen, Christiane Forestier, and Damien Balestrino**. Biofilm dispersal: Multiple elaborate strategies for dissemination of bacteria with unique properties. *Molecular Microbiology*, 105(2):pages 188–210 (2017). doi:10.1111/mmi.13698.

[136] **Joao B. Xavier and Kevin R. Foster**. Cooperation and conflict in microbial biofilms. *Proceedings of the National Academy of Sciences*, 104(3):pages 876–881 (2007). doi:10.1073/pnas.0607651104.

[137] **Mette Burmølle, Jeremy S. Webb, Dhana Rao, Lars H. Hansen, Søren J. Sørensen, and Staffan Kjelleberg**. Enhanced biofilm formation and increased resistance to antimicrobial agents and bacterial invasion are caused by synergistic interactions in multispecies biofilms. *Applied and Environmental Microbiology*, 72(6):pages 3916–3923 (2006). doi:10.1128/AEM.03022-05.

[138] **Thomas K. Wood, Stephen J. Knabel, and Brian W. Kwan**. Bacterial persister cell formation and dormancy. *Applied and Environmental Microbiology*, 79(23):pages 7116–7121 (2013). doi:10.1128/AEM.02636-13.

[139] **Melanie G. Brading, Jana Jass, and Hilary M. Lappin-Scott**. Dynamics of bacterial biofilm formation. In **Hilary M. Lappin-Scott and J. William Costerton**, editors, *Microbial Biofilms*, Biotechnology Research, pages 46–63. Cambridge University Press, Cambridge (1995). ISBN 978-0-521-54212-8. doi:10.1017/CBO9780511525353.004.

[140] **Sebastian Schlafer, Merete K. Raarup, Rikke L. Meyer, Duncan S. Sutherland, Irene Dige, Jens R. Nyengaard, and Bente Nyvad**. pH landscapes in a novel five-species model of early dental biofilm. *PLOS ONE*, 6(9):page e25299 (2011). doi:10.1371/journal.pone.0025299.

[141] **Daddi S. Oubekka, Romain Briandet, Marie-Pierre Fontaine-Aupart, and Karine Steenkeste**. Correlative Time-Resolved Fluorescence Microscopy To Assess Antibiotic Diffusion-Reaction in Biofilms. *Antimicrobial Agents and Chemotherapy*, 56(6):pages 3349–3358 (2012). doi:10.1128/AAC.00216-12.

[142] **Joe J. Harrison, Howard Ceri, and Raymond J. Turner**. Multimetal resistance and tolerance in microbial biofilms. *Nature Reviews Microbiology*, 5(12):pages 928–938 (2007). doi:10.1038/nrmicro1774.

[143] **Christoph A. Fux, John W. Costerton, Philip S. Stewart, and Paul Stoodley**. Survival strategies of infectious biofilms. *Trends in Microbiology*, 13(1):pages 34–40 (2005). doi:10.1016/j.tim.2004.11.010.

[144] **Thien-Fah Mah**. Biofilm-specific antibiotic resistance. *Future Microbiology*, 7(9):pages 1061–1072 (2012). doi:10.2217/fmb.12.76.

[145] **Howard Ceri, Merle E. Olson, Carol Stremick, R. R. Read, D. Morck, and A. Buret**. The Calgary biofilm device: New technology for rapid determination of antibiotic susceptibilities of bacterial biofilms. *Journal of Clinical Microbiology*, 37(6):pages 1771–1776 (1999). doi:10.1128/JCM.37.6.1771-1776.1999.

[146] **Yuan Chen, Yujie Gao, Yue Chen, Liu Liu, Anchun Mo, and Qiang Peng**. Nanomaterials-based photothermal therapy and its potentials in antibacterial treatment. *Journal of Controlled Release*, 328:pages 251–262 (2020). doi:10.1016/j.jconrel.2020.08.055.

[147] **Fei Zhao, Youhong Guo, Xingyi Zhou, Wen Shi, and Guihua Yu**. Materials for solar-powered water evaporation. *Nature Reviews Materials*, 5(5):pages 388–401 (2020). doi:10.1038/s41578-020-0182-4.

[148] **Erica M. Knavel and Christopher L. Brace**. Tumor ablation: Common modalities and general practices. *Techniques in Vascular and Interventional Radiology*, 16(4):pages 192–200 (2013). doi:10.1053/j.tvir.2013.08.002.

[149] **Xiaomo Xu, Xiangmei Liu, Lei Tan,** *et al.* Controlled-temperature photothermal and oxidative bacteria killing and acceleration of wound healing by polydopamine-assisted Au-hydroxyapatite nanorods. *Acta Biomaterialia*, 77:pages 352–364 (2018). doi:10.1016/j.actbio.2018.07.030.

[150] **Xingshu Li, Jonathan F. Lovell, Juyoung Yoon, and Xiaoyuan Chen**. Clinical development and potential of photothermal and photodynamic therapies for cancer. *Nature Reviews Clinical Oncology*, 17(11):pages 657–674 (2020). doi:10.1038/s41571-020-0410-2.

[151] **Yufei Wang, Hong-Min Meng, and Zhaohui Li**. Near-infrared inorganic nanomaterial-based nanosystems for photothermal therapy. *Nanoscale*, 13(19):pages 8751–8772 (2021). doi:10.1039/D1NR00323B.

[152] **Moritz Friebel, Jürgen Helfmann, Uwe J. Netz, and Martina C. Meinke**. Influence of oxygen saturation on the optical scattering properties of human red blood cells in the spectral range 250 to 2000 nm. *Journal of Biomedical Optics*, 14(3):page 034001 (2009). doi:10.1117/1.3127200.

[153] **Ralph Weissleder**. A clearer vision for in vivo imaging. *Nature Biotechnology*, 19(4):pages 316–317 (2001). doi:10.1038/86684.

[154] **Andrew M. Smith, Michael C. Mancini, and Shuming Nie**. Second window for in vivo imaging. *Nature Nanotechnology*, 4(11):pages 710–711 (2009). doi:10.1038/nnano.2009.326.

[155] **Cheng Xu and Kanyi Pu**. Second near-infrared photothermal materials for combinational nanotheranostics. *Chemical Society Reviews*, 50(2):pages 1111–1137 (2021). doi:10.1039/D0CS00664E.

[156] **R. R. Anderson and J. A. Parrish**. The optics of human skin. *The Journal of Investigative Dermatology*, 77(1):pages 13–19 (1981). doi:10.1111/1523-1747.ep12479191.

[157] **Yan Zhang, Danxia Li, Jinshan Tan, Zhishang Chang, Xiangyong Liu, Weishuai Ma, and Yuanhong Xu**. Near-Infrared regulated nanozymatic/photothermal/photodynamic triple-therapy for combating multidrug-resistant bacterial infections via oxygen-vacancy molybdenum trioxide nanodots. *Small*, 17(1):page 2005739 (2021). doi:10.1002/smll.202005739.

[158] **Stanley S. Chou, Bryan Kaehr, Jaemyung Kim,** *et al.* Chemically exfoliated MoS_2 as near-infrared photothermal agents. *Angewandte Chemie (International Ed. in English)*, 52(15):pages 4160–4164 (2013). doi:10.1002/anie.201209229.

[159] **Fan Jiang, Binbin Ding, Shuang Liang,** *et al.* Intelligent MoS_2-CuO heterostructures with multiplexed imaging and remarkably enhanced antitumor efficacy via synergetic photothermal therapy/ chemodynamic therapy/ immunotherapy. *Biomaterials*, 268:page 120545 (2021). doi:10.1016/j.biomaterials.2020.120545.

[160] **Zhiyin Xiao, Chaoting Xu, Xiaohong Jiang,** *et al.* Hydrophilic bismuth sulfur nanoflower superstructures with an improved photothermal efficiency for ablation of cancer cells. *Nano Research*, 9(7):pages 1934–1947 (2016). doi:10.1007/s12274-016-1085-y.

[161] **Zhuoqian Lv, Sijia He, Youfu Wang, and Xinyuan Zhu**. Noble metal nanomaterials for NIR-triggered photothermal therapy in cancer. *Advanced Healthcare Materials*, 10(6):page 2001806 (2021). doi:10.1002/adhm.202001806.

[162] **Jeremy B. Vines, Jee-Hyun Yoon, Na-Eun Ryu, Dong-Jin Lim, and Hansoo Park**. Gold Nanoparticles for Photothermal Cancer Therapy. *Frontiers in Chemistry*, 7 (2019). doi:10.3389/fchem.2019.00167.

[163] **Alexander Pyatenko, Munehiro Yamaguchi, and Masaaki Suzuki**. Synthesis of spherical silver nanoparticles with controllable sizes in aqueous solutions. *The Journal of Physical Chemistry C*, 111(22):pages 7910–7917 (2007). doi:10.1021/jp071080x.

[164] **Christina Greulich, Dieter Braun, Alexander Peetsch, Jörg Diendorf, Bettina Siebers, Matthias Epple, and Manfred Köller**. The toxic effect of silver ions and silver nanoparticles towards bacteria and human cells occurs in the same concentration range. *RSC Advances*, 2(17):page 6981 (2012). doi:10.1039/c2ra20684f.

[165] **Steven D. Perrault and Warren C. W. Chan**. Synthesis and surface modification of highly monodispersed, spherical gold nanoparticles of 50-200 nm. *Journal of the American Chemical Society*, 131(47):pages 17042–17043 (2009). doi:10.1021/ja907069u.

[166] **Pascal M. Gschwend, Simona Conti, Andres Kaech, Caroline Maake, and Sotiris E. Pratsinis**. Silica-coated TiN particles for killing cancer cells. *ACS applied materials & interfaces*, 11(25):pages 22550–22560 (2019). doi:10.1021/acsami.9b07239.

[167] **Corey Radloff and Naomi J. Halas**. Plasmonic properties of concentric nanoshells. *Nano Letters*, 4(7):pages 1323–1327 (2004). doi:10.1021/nl049597x.

[168] **Silvia Barbosa, Amit Agrawal, Laura Rodríguez-Lorenzo,** *et al.* Tuning size and sensing properties in colloidal gold nanostars. *Langmuir*, 26(18):pages 14943–14950 (2010). doi:10.1021/la102559e.

[169] **Hsin-Lun Wu, Chun-Hong Kuo, and Michael H. Huang**. Seed-Mediated Synthesis of Gold Nanocrystals with Systematic Shape Evolution from Cubic to Trisoctahedral and Rhombic Dodecahedral Structures. *Langmuir*, 26(14):pages 12307–12313 (2010). doi:10.1021/la1015065.

[170] **Zhen-Wen Lin, Yu-Chi Tsao, Min-Yi Yang, and Michael H. Huang**. Seed-Mediated Growth of Silver Nanocubes in Aqueous Solution with Tunable Size and Their Conversion to Au Nanocages with Efficient Photothermal Property. *Chemistry – A European Journal*, 22(7):pages 2326–2332 (2016). doi:10.1002/chem.201504303.

[171] **M. Shanthil, Reshmi Thomas, Rotti S. Swathi, and K. George Thomas**. Ag@SiO_2 core–shell nanostructures: Distance-dependent plasmon coupling and SERS investigation. *The Journal of Physical Chemistry Letters*, 3(11):pages 1459–1464 (2012). doi:10.1021/jz3004014.

[172] **Kyeong-Seok Lee and Mostafa A. El-Sayed**. Dependence of the enhanced optical scattering efficiency relative to that of absorption for gold metal nanorods on aspect ratio, size, end-cap shape, and medium refractive index. *The Journal of Physical Chemistry B*, 109(43):pages 20331–20338 (2005). doi:10.1021/jp054385p.

[173] **Ardeshir R. Rastinehad, Harry Anastos, Ethan Wajswol,** *et al.* Gold nanoshell-localized photothermal ablation of prostate tumors in a clinical pilot device study. *Proceedings of the National Academy of Sciences*, 116(37):pages 18590–18596 (2019). doi:10.1073/pnas.1906929116.

[174] **Constantinos Moularas, Yiannis Georgiou, Katarzyna Adamska, and Yiannis Deligiannakis**. Thermoplasmonic Heat Generation Efficiency by Nonmonodisperse Core–Shell Ag^0@SiO_2 Nanoparticle Ensemble. *The Journal of Physical Chemistry C*, 123(36):pages 22499–22510 (2019). doi:10.1021/acs.jpcc.9b06532.

[175] **Georgios A. Sotiriou, Fabian Starsich, Athanasia Dasargyri,** *et al.* Photothermal killing of cancer cells by the controlled plasmonic coupling of silica-coated Au/Fe_2O_3 nanoaggregates. *Advanced Functional Materials*, 24(19):pages 2818–2827 (2014). doi:10.1002/adfm.201303416.

[176] **Orawan Khantamat, Chien-Hung Li, Fei Yu, Andrew C. Jamison, Wei-Chuan Shih, Chengzhi Cai, and T. Randall Lee**. Gold Nanoshell-Decorated Silicone Surfaces for the Near-Infrared (NIR) Photothermal Destruction of the Pathogenic Bacterium E. faecalis. *ACS Applied Materials & Interfaces*, 7(7):pages 3981–3993 (2015). doi:10.1021/am506516r.

[177] **Agnese D'Agostino, Angelo Taglietti, Roberto Desando,** *et al.* Bulk Surfaces Coated with Triangular Silver Nanoplates: Antibacterial Action Based on Silver Release and Photo-Thermal Effect. *Nanomaterials*, 7(1):page 7 (2017). doi:10.3390/nano7010007.

[178] **Agnese D'Agostino, Angelo Taglietti, Pietro Grisoli, Giacomo Dacarro, Lucia Cucca, Maddalena Patrini, and Piersandro Pallavicini**. Seed mediated growth of silver nanoplates on glass: Exploiting the bimodal antibacterial effect by near IR photothermal action and Ag^+ release. *RSC Advances*, 6(74):pages 70414–70423 (2016). doi:10.1039/C6RA11608F.

[179] **Weijun Fang, Hanyuan Zhang, Xin Wang,** *et al.* Facile synthesis of tunable plasmonic silver core/magnetic Fe_3O_4 shell nanoparticles for rapid capture and effective photothermal ablation of bacterial pathogens. *New Journal of Chemistry*, 41(18):pages 10155–10164 (2017). doi:10.1039/C7NJ02071F.

[180] **Egija Zaura, Mark J. Buijs, and Jacob M. ten Cate**. The Effects of the Solubility of Artificial Fissures on Plaque pH. *Journal of Dental Research*, 81(8):pages 567–571 (2002). doi:10.1177/154405910208100813.

[181] **Christiane von Ohle, Armin Gieseke, Laura Nistico, Eva Maria Decker, Dirk deBeer, and Paul Stoodley**. Real-Time Microsensor Measurement of Local Metabolic Activities in *Ex Vivo* Dental Biofilms Exposed to Sucrose and Treated with Chlorhexidine. *Applied and Environmental Microbiology*, 76(7):pages 2326–2334 (2010). doi:10.1128/AEM.02090-09.

[182] **Sebastian Schlafer, Vibeke Baelum, and Irene Dige**. Improved pH-ratiometry for the three-dimensional mapping of pH microenvironments in biofilms under flow conditions. *Journal of Microbiological Methods*, 152:pages 194–200 (2018). doi:10.1016/j.mimet.2018.08.007.

[183] **Gabriela Hidalgo, Andrew Burns, Erik Herz, Anthony G. Hay, Paul L. Houston, Ulrich Wiesner, and Leonard W. Lion**. Functional Tomographic Fluorescence Imaging of pH Microenvironments in Microbial Biofilms by Use of Silica Nanoparticle Sensors. *Applied and Environmental Microbiology*, 75(23):pages 7426–7435 (2009). doi:10.1128/AEM.01220-09.

[184] **Stephanie Fulaz, Dishon Hiebner, Caio H. N. Barros, Henry Devlin, Stefania Vitale, Laura Quinn, and Eoin Casey**. Ratiometric Imaging of the in Situ pH Distribution of Biofilms by Use of Fluorescent Mesoporous Silica Nanosensors. *ACS Applied Materials & Interfaces*, 11(36):pages 32679–32688 (2019). doi:10.1021/acsami.9b09978.

[185] **Victoria Albright, Iryna Zhuk, Yuhao Wang,** *et al.* Self-defensive antibiotic-loaded layer-by-layer coatings: Imaging of localized bacterial acidification and pH-triggering of antibiotic release. *Acta Biomaterialia*, 61:pages 66–74 (2017). doi:10.1016/j.actbio.2017.08.012.

[186] **Barry Halliwell, Marie Veronique Clement, and Lee Hua Long**. Hydrogen peroxide in the human body. *FEBS Letters*, 486(1):pages 10–13 (2000). doi:10.1016/S0014-5793(00)02197-9.

[187] **Marcel Zamocky, Paul G. Furtmüller, and Christian Obinger**. Evolution of catalases from bacteria to humans. *Antioxidants & Redox Signaling*, 10(9):pages 1527–1548 (2008). doi:10.1089/ars.2008.2046.

[188] **James R. Stone and Suping Yang**. Hydrogen peroxide: A signaling messenger. *Antioxidants & Redox Signaling*, 8(3-4):pages 243–270 (2006). doi:10.1089/ars.2006.8.243.

[189] **Elizabeth A. Veal, Alison M. Day, and Brian A. Morgan**. Hydrogen peroxide sensing and signaling. *Molecular Cell*, 26(1):pages 1–14 (2007). doi:10.1016/j.molcel.2007.03.016.

[190] **Barbara Spellerberg, Diana R. Cundell, Jens Sandros, Barbara J. Pearce, Ilona Idänpään-Heikkilä, Carsten Rosenow, and Robert H. Masure**. Pyruvate oxidase, as a determinant of virulence in Streptococcus pneumoniae. *Molecular Microbiology*, 19(4):pages 803–813 (1996). doi:10.1046/j.1365-2958.1996.425954.x.

[191] **Anna Syk, Martin Norman, Jenny Fernebro,** *et al.* Emergence of hypervirulent mutants resistant to early clearance during systemic serotype 1 pneumococcal infection in mice and humans. *The Journal of Infectious Diseases*, 210(1):pages 4–13 (2014). doi:10.1093/infdis/jiu038.

[192] **Ana M. Azevedo, D. Miguel F. Prazeres, Joaquim M. S. Cabral, and Luís P. Fonseca**. Ethanol biosensors based on alcohol oxidase. *Biosensors and Bioelectronics*, 21(2):pages 235–247 (2005). doi:10.1016/j.bios.2004.09.030.

[193] **Mei Hu, Jing Tian, Hao-Ting Lu, Li-Xing Weng, and Lian-Hui Wang**. H_2O_2-sensitive quantum dots for the label-free detection of glucose. *Talanta*, 82(3):pages 997–1002 (2010). doi:10.1016/j.talanta.2010.06.005.

[194] **Vinay Patel, Peter Kruse, and Ponnambalam R. Selvaganapathy**. Solid state sensors for hydrogen peroxide detection. *Biosensors*, 11(1):page 9 (2020). doi:10.3390/bios11010009.

[195] **Shafeeque G. Ansari, Zubaida A. Ansari, Rizwan Wahab, Young-Soon Kim, Gilson Khang, and Hyung-Shik Shin**. Glucose sensor based on nano-baskets of tin oxide

templated in porous alumina by plasma enhanced CVD. *Biosensors and Bioelectronics*, 23(12):pages 1838–1842 (2008). doi:10.1016/j.bios.2008.02.022.

[196] **Tatiana A. Sergeyeva, Nickolay V. Lavrik, Alexandre E. Rachkov, Zoya I. Kazantseva, Sergey A. Piletsky, and Anna V. El'skaya**. Hydrogen peroxide – sensitive enzyme sensor based on phthalocyanine thin film. *Analytica Chimica Acta*, 391(3):pages 289–297 (1999). doi:10.1016/S0003-2670(99)00203-2.

[197] **Rafiq Ahmad, Nirmalya Tripathy, Jin-Ho Park, and Yoon-Bong Hahn**. A comprehensive biosensor integrated with a ZnO nanorod FET array for selective detection of glucose, cholesterol and urea. *Chemical Communications*, 51(60):pages 11968–11971 (2015). doi:10.1039/C5CC03656A.

[198] **Jipei Yuan, Weiwei Guo, Jianyuan Yin, and Erkang Wang**. Glutathione-capped CdTe quantum dots for the sensitive detection of glucose. *Talanta*, 77(5):pages 1858–1863 (2009). doi:10.1016/j.talanta.2008.10.032.

[199] **Gangbing Zhu, Dongyan Huang, Lirong Liu, Yinhui Yi, Yuntao Wu, and Yongqiang Huang**. One-step green preparation of N-doped silicon quantum dots for the on-off fluorescent determination of hydrogen peroxide. *Analytical Letters*, 53(11):pages 1834–1849 (2020). doi:10.1080/00032719.2020.1720222.

[200] **Biwu Liu, Ziyi Sun, Po-Jung Jimmy Huang, and Juewen Liu**. Hydrogen peroxide displacing DNA from nanoceria: Mechanism and detection of glucose in serum. *Journal of the American Chemical Society*, 137(3):pages 1290–1295 (2015). doi:10.1021/ja511444e.

[201] **Changjian Lv, Weihua Di, Zhihe Liu, Kezhi Zheng, and Weiping Qin**. Luminescent $CePO_4$:Tb colloids for H_2O_2 and glucose sensing. *Analyst*, 139(18):pages 4547–4555 (2014). doi:10.1039/C4AN00952E.

[202] **Anna Pratsinis, Georgios A. Kelesidis, Stefanie Zuercher,** *et al.* Enzyme-mimetic antioxidant luminescent nanoparticles for highly sensitive hydrogen peroxide biosensing. *ACS Nano*, 11(12):pages 12210–12218 (2017). doi:10.1021/acsnano.7b05518.

[203] **Amit Kumar, Suresh Babu, Ajay Singh Karakoti, Alfons Schulte, and Sudipta Seal**. Luminescence properties of europium-doped cerium oxide nanoparticles: Role of vacancy and oxidation states. *Langmuir*, 25(18):pages 10998–11007 (2009). doi:10.1021/la901298q.

[204] **Jean-Daniel Cafun, Kristina O. Kvashnina, Eudald Casals, Victor F. Puntes, and Pieter Glatzel**. Absence of Ce^{3+} Sites in Chemically Active Colloidal Ceria Nanoparticles. *ACS Nano*, 7(12):pages 10726–10732 (2013). doi:10.1021/nn403542p.

[205] **Yan-Jie Wang, Hao Dong, Guang-Ming Lyu,** *et al.* Engineering the defect state and reducibility of ceria based nanoparticles for improved anti-oxidation performance. *Nanoscale*, 7(33):pages 13981–13990 (2015). doi:10.1039/C5NR02588E.

[206] **Werner Lang, T.M. Blöck, and Rolf Zander**. Solubility of NH_3 and apparent pK of NH_4^+ in human plasma, isotonic salt solutions and water at 37°C. *Clinica Chimica Acta*, 273(1):pages 43–58 (1998). doi:10.1016/S0009-8981(98)00019-9.

[207] **Valerie Walker**. Chapter Three - Ammonia Metabolism and Hyperammonemic Disorders. In **Gregory S. Makowski**, editor, *Advances in Clinical Chemistry*, volume 67, pages 73–150. Elsevier (2014). doi:10.1016/bs.acc.2014.09.002.

[208] **Manuel Romero-Gómez, María Jover, J. Jorge Galán, and A. Ruiz**. Gut ammonia production and its modulation. *Metabolic Brain Disease*, 24(1):pages 147–157 (2009). doi:10.1007/s11011-008-9124-3.

[209] **Hendrik Vilstrup, Piero Amodio, Jasmohan Bajaj,** *et al.* Hepatic encephalopathy in chronic liver disease: 2014 Practice Guideline by the American Association for the Study Of Liver Diseases and the European Association for the Study of the Liver. *Hepatology*, 60(2):pages 715–735 (2014). doi:10.1002/hep.27210.

[210] **Arthur J. L. Cooper and Barry R. Freed**. Metabolism of [^{13}N]ammonia in rat lung. *Neurochemistry International*, 47(1-2):pages 103–118 (2005). doi:10.1016/j.neuint.2005.04.013.

[211] **Wen Chen, Satu Laiho, Olavi Vaittinen,** *et al.* Biochemical pathways of breath ammonia (NH_3) generation in patients with end-stage renal disease undergoing hemodialysis. *Journal of Breath Research*, 10(3):page 036011 (2016). doi:2020031810370636.

[212] **Antonio Tricoli and Giovanni Neri**. Miniaturized Bio-and Chemical-Sensors for Point-of-Care Monitoring of Chronic Kidney Diseases. *Sensors*, 18(4):page 942 (2018). doi:10.3390/s18040942.

[213] **Azarmidokht Sheini**. A paper-based device for the colorimetric determination of ammonia and carbon dioxide using thiomalic acid and maltol functionalized silver nanoparticles: Application to the enzymatic determination of urea in saliva and blood. *Microchimica Acta*, 187(10):page 565 (2020). doi:10.1007/s00604-020-04553-8.

[214] **Niamh T. Brannelly and Anthony J. Killard**. An electrochemical sensor device for measuring blood ammonia at the point of care. *Talanta*, 167:pages 296–301 (2017). doi:10.1016/j.talanta.2017.02.025.

[215] **Anastasia Spyrogianni, Charlotte Gourmel, Leopold Hofmann, Jessica Marbach, and Jean Christophe Leroux**. Optimization of an ammonia assay based on transmembrane pH-gradient polymersomes. *Scientific Reports 2021 11:1*, 11(1):pages 1–15 (2021). doi:10.1038/s41598-021-01137-1.

[216] **Philip L. Searle**. The berthelot or indophenol reaction and its use in the analytical chemistry of nitrogen: A review. *Analyst*, 109(5):pages 549–568 (1984). doi:10.1039/AN9840900549.

[217] **Thomas Thersleff, Serhiy Budnyk, Larissa Drangai, and Adam Slabon**. Dissecting complex nanoparticle heterostructures via multimodal data fusion with aberration-corrected STEM spectroscopy. *Ultramicroscopy*, 219:page 113116 (2020). doi:10.1016/j.ultramic.2020.113116.

[218] **José Morán, Andrés Fuentes, Fengshan Liu, and Jérôme Yon**. FracVAL: An improved tunable algorithm of cluster–cluster aggregation for generation of fractal structures formed by polydisperse primary particles. *Computer Physics Communications*, 239:pages 225–237 (2019). doi:10.1016/j.cpc.2019.01.015.

[219] **Baptiste Auguié**. CDA: Coupled dipole approximation with R and C++ (2012). doi:10.5281/zenodo.60310.

[220] **Baptiste Auguié, José Lorenzo Alonso-Gómez, Andrés Guerrero-Martínez, and Luis M. Liz-Marzán**. Fingers crossed: Optical activity of a chiral dimer of plasmonic nanorods. *Journal of Physical Chemistry Letters*, 2(8):pages 846–851 (2011). doi:10.1021/jz200279x.

[221] **Ryan C Hunter and Terry J Beveridge**. Application of a pH-Sensitive Fluoroprobe (C-SNARF-4) for pH Microenvironment Analysis in Pseudomonas aeruginosa Biofilms. *Applied and Environmental Microbiology*, 71(5):pages 2501–2510 (2005). doi:10.1128/AEM.71.5.2501-2510.2005.

[222] **Manlin Qi, Wen Li, Xufeng Zheng,** *et al.* Cerium and its oxidant-based nanomaterials for antibacterial applications: A state-of-the-art review. *Frontiers in Materials*, 7 (2020). doi:10.3389/fmats.2020.00213.

[223] **Erica B. Ricker and Eric Nuxoll**. Synergistic effects of heat and antibiotics on Pseudomonas aeruginosa biofilms. *Biofouling*, 33(10):pages 855–866 (2017). doi:10.1080/08927014.2017.1381688.